# KAPOSIN B-MEDIATED MECHANORESPONSIVE SIGNALLING CONTROLS PROCESSING BODY DISASSEMBLY

by

Elizabeth L. Castle

Submitted in partial fulfillment of the requirements
for the degree of Master of Science

at

Dalhousie University
Halifax, Nova Scotia
August 2019

TABLE OF CONTENTS

## LIST OF TABLES

## LIST OF FIGURES

**ABSTRACT**

Kaposin B (KapB) is a viral protein that induces the formation of actin stress fibres (SFs) and promotes stabilization of inflammatory and angiogenic mRNAs by disassembling processing bodies (PBs). PBs are ribonucleoprotein granules that control mRNA post-transcriptional expression. The canonical cytoskeletal regulatory GTPase, RhoA, is required for both KapB-mediated phenotypes – the formation of SFs and PB disassembly. I investigated signalling controlling SF formation, bundling and contractility in the mechanism of KapB-induced PB disassembly. Knockdown of RhoA-effectors known to coordinate SF formation restored PBs in KapB-expressing cells. Inhibition of actomyosin contractility also restored PBs, while inducing contraction disassembled PBs. Since SFs mediate mechanotransduction, YAP was investigated and shown to mediate PB disassembly in the context of KapB and other mechanical forces, including shear stress. Using a viral protein, my research identified and dissected a novel mechanoresponsive pathway controlling PB turnover and the concomitant stability of inflammatory and angiogenic transcripts.

## LIST OF ABBREVIATIONS USED

| | |
|---|---|
| AIDS | Acquired Immunodeficiency Syndrome |
| ANKRD1 | Ankryn repeat domain 1 |
| ANOVA | Analysis of Variance |
| ARE | AU-rich element |
| ATP | Adenosine triphosphate |
| BCBL | Body Cavity Based Lymphoma |
| bp | Base Pairs |
| BSA | Bovine Serum Albumin |
| BSD | Blasticidin |
| CMDI | Cellular Microscopy Digital Imaging |
| cP | Centipoise |
| $CO_2$ | Carbon Dioxide |
| CTGF | Connective tissue growth factor |
| CYR61 | Cysteine-rich angiogenic inducer 61 |
| DCP | Decapping protein |
| DMEM | Dulbecco's Modified Eagle Medium |
| DNA | Deoxyribonucleic Acid |
| DR | Direct repeats |
| DTT | Dithiothreitol |
| EDTA | Ethylenediaminetetraacetic acid |
| EBM | Endothelial base medium |
| ECM | Extracellular matrix |
| EGM | Endothelial growth medium |
| EGR | Early growth response |
| EV | Empty Vector |
| FBS | Fetal Bovine Serum |
| g | Gravity |
| G-actin | Globular actin |
| GFP | Green fluorescent protein |
| GM-CSF | Granulocyte |
| gPCR | G-protein coupled receptor |
| F-actin | Filamentous actin |
| h | Hours |
| Hedls | Human enhancer of decapping large subunit |
| HI | Heat inactivated |
| HIV | Human immunodeficiency virus |
| HRP | Horseradish peroxidase |
| Hsp | Heat shock protein |
| HUVEC | Human umbilical vein endothelial cells |
| IL | Interleukin |
| ICAM | intracellular adhesion molecule |
| IFN | Interferon |

| | |
|---|---|
| Kap | Kaposin |
| KS | Kaposi's Sarcoma |
| KSHV | Kaposi' sarcoma-associated herpesvirus |
| LANA | Latency-associated nuclear antigen |
| LATS | Large tumour suppressor |
| LimK | Lim kinase |
| LPA | Lysophosphatidic acid |
| Lsm | Like-Sm |
| mDia | Mammalian diaphanous proteins |
| MEM | Minimal Essential Media |
| mg | milligram |
| miRNA | microRNA |
| MK2 | Mitogen-activated protein kinase-activated protein kinase 2 |
| mL | milliliter |
| MLC | Myosin light chain |
| MLCK | Myosin light chain kinase |
| mM | millimolar |
| MMP | Matrix metalloproteinase |
| mRNA | Messenger RNA |
| MST | Mammalian STE20 -like kinase |
| MyoVa | Myosin Va |
| NFkB | Nuclear factor kappa-light-chain-enhancer of activated B cells |
| NMII | Non-muscle myosin II |
| ORF | Open Reading Frame |
| PBS | Phosphate Buffered Saline |
| PBs | Processing bodies |
| PEI | Polyethlenimine |
| PROX1 | Prospero homeobox protein 1 |
| PSQ | Penicillin streptomycin L-glutamine |
| Puro | Puromycin |
| PVDF | Polyvinylidene fluoride |
| qPCR | Quantitative Polymerase Chain Reaction |
| RNA | Ribonucleic acid |
| RNP | Ribonucleoprotein |
| ROCK | Rho-associated coiled-coil kinase |
| RT | Room temperature |
| RUNX | Runt-related transcription factor 1 |
| shRNA | Short hairpin ribonucleic acid |
| SF | Stress fibres |
| SRF | Serum-response factor |
| STAT | Signal |
| TAZ | Transcriptional Co-activator with PDZ Domain |
| TBS-T | Tris-buffered saline with tween-20 |
| TBX | T-box transcription factor |
| TEAD | TEA-domain transcription factor |
| TGF | Transforming growth factor |

| | |
|---|---|
| TNF | Tumour necrosis factor |
| TTP | Tristetraprolin |
| μL | microliter |
| UTR | Untranslated region |
| V | Volts |
| VEGF | Vascular endothelial growth factor |
| vFLIP | viral |
| WGA | Wheat germ agglutinin |
| YAP | Yes-associated protein |

**ACKNOWLEDGEMENTS**

There is a mountain of people to thank for making my experience an incredible one. First and foremost, thank you to Jenn who has been the a fantastic supervisor. Her support extends from just helpful advice and excitement about the science being conducted, to enabling her students to grow and develop within the scientific community. Her compassion and insight makes working with her a rich and valuable experience. A big thank you to all those at Dalhousie and the University of Calgary that have been great peers and friends throughout the entire process, especially Gill, Grant, Kathleen, Carolyn, Mariel, Eric and Quin. And finally thank you to my parents, sister and to Tim for the amazing love and support. You all made this possible.

# CHAPTER 1: INTRODUCTION

## 1.1 Kaposi's Sarcoma (KS)

Kaposi's sarcoma (KS) is a highly proliferative and inflammatory endothelial cell neoplasm that commonly occurs in immunosuppressed individuals (reviewed in Mesri, Cesarman, and Boshoff (2010) and Antman and Chang (2000)). It was first described in 1872 by Moritz Kaposi as "idiopathic multipigmented sarcomas of the skin" of unknown cause in men of Mediterranean descent (Braun 1982). Originally, this disease was thought to be restricted to populations in the Mediterranean and Sub-Saharan Africa; however, this changed at the end of the 20$^{th}$ century, which saw an epidemic of acquired immunodeficiency syndrome (AIDS)-associated KS (Friedman-Kien 1981; Cook-Mozaffari et al. 1998). This precipitated the search for and eventual discovery of Kaposi's sarcoma-associated herpesvirus (KSHV), or human herpesvirus-8 (HHV-8), in 1994 (Chang et al. 1994). KSHV is now recognized as the etiologic cause of KS, and is associated with two other B-cell lymphoproliferative disorders: multicentric Castleman's disease and primary effusion lymphoma (Chang et al. 1994; Cesarman et al. 1995; Soulier et al. 1995).

The seroprevalence of KSHV varies geographically, with seropositivity at >50% in Africa, between 10-25% in the Mediterranean and <10% in non-endemic areas in Asia, Europe and North America (Minhas and Wood 2014; Yan et al. 2019). Transmission of KSHV has been confirmed to occur through saliva and blood routes (Boldogh et al. 1996; Hladik et al. 2006); however, sexual transmission of KSHV is still debated (Yan et al. 2019). The disease state of KS is classified into four main forms (Mesri, Cesarman, and Boshoff 2010): (1) classical KS, which primarily affects men of Mediterranean and Eastern European descent, (2) endemic KS, which occurs in Eastern and Central African populations, (3) AIDS-associated KS, which is related to immune suppression from human-immunodeficiency virus (HIV) infection, and (4) iatrogenic KS, which is associated with immune suppression related to transplantation. KS lesions present as patches, plaques, nodules or tumours, depending on the disease stage (Mesri, Cesarman, and Boshoff 2010). In the context of immunosuppression, these lesions can progress into disseminated KS in the skin, lymph nodes and visceral organs, which is associated with high morbidity and mortality (Mesri, Cesarman, and Boshoff 2010). The cells in these

lesions are highly-proliferative, elongated cells of endothelial origin that are infected with KSHV. These cells, known as spindle cells, form aberrant, slit-like blood vessels that leak red blood cells and hemosiderin, giving the lesions a characteristic red-purple colour (Mesri, Cesarman, and Boshoff 2010). Within the lesion, there is a high amount of inflammatory infiltrate, with elevated levels of cytokines, including interleukin-6 (IL-6) and interferon-gamma (IFNγ) (Mesri 1999).

The advent of highly-active antiretroviral therapy to treat HIV infection has significantly reduced the occurrence of AIDS-related KS in resource-rich countries (Semeere, Busakhala, and Martin 2012). However, KSHV is still a major public health concern in Sub-Saharan Africa (Mosam, Aboobaker, and Shaik 2010), and there is continued occurrence of classical and iatrogenic KS (Jakob et al. 2011). Further understanding of the viral mechanisms that induce oncogenesis is essential to limit the health impact of KSHV. Furthermore, understanding the molecular mechanisms by which the virus promotes the aberrant proliferation, as well as high levels of inflammation and angiogenesis in infected individuals, will progress our foundational understanding of the cellular systems that respond to and control these disease-associated phenotypes. KSHV provides a unique and useful tool to understand the basal cell regulation of inflammation and angiogenesis.

### 1.2 Kaposi's Sarcoma-Associated Herpesvirus (KSHV)

KSHV is a γ-herpesvirus with a linear dsDNA genome that is approximately 165 kb and encodes more than 70 open-reading frames and several non-coding RNAs (Russo et al. 1996; Arias et al. 2014). The viral capsid is icosahedral, and is made up of a complex arrangement of hexamers and pentamers of the capsid protein (Trus et al. 2002). The capsid is enveloped by a cell-derived membrane, which contains the viral glycoproteins needed for viral attachment and entry during infection of a cell (Kumar and Chandran 2016). Between the capsid and the envelope, there is a layer of tegument, which contains both host and viral proteins that are important for virion structure as well as entry, trafficking and egress (Sathish, Wang, and Yuan 2012). KSHV encodes a diverse variety of genes, including virally-encoded cytokines, host-subversion factors, replication machinery and structural genes (Arias et al. 2014). Through tight regulation of the genes

across the viral lifecycle, KSHV establishes an environment that promotes viral propagation, as well as tumour formation.

KSHV is able to infect both endothelial cells and lymphocytes, and establishes either a lytic or latent infection (Ambroziak et al. 1995; Boshoff et al. 1995). Briefly, the virus interacts with the cell through initial attachment of several KSHV glycoproteins to heparin sulfate (viral entry reviewed in Kumar and Chandran 2016). Following attachment, the interaction of KSHV glycoprotein B with $\alpha 3\beta 1$, $\alpha V\beta 3$ and $\alpha V\beta 5$ integrins mediates entry through clathrin-mediated endocytosis or macropinocytosis. The membrane of KSHV fuses with the endosomal membrane, releasing the capsid and tegument proteins into the cytoplasm, where the capsid traffics along microtubules using dynein motors to the nucleus. The viral DNA is then delivered through the nuclear pore into the nucleus where the virus will establish either the lytic lifecycle or latency (Kumar and Chandran 2016).

The lytic lifecycle is characterized by expression of most or all of the KSHV genes, replication of the viral DNA, assembly of nascent viral particles and viral egress involving budding through the nuclear and plasma membrane (Aneja and Yuan 2017). The lytic cycle is essential for lesion formation through the promotion of high levels of inflammatory and angiogenic mediators, as well as the production of new virions, which are then released to infect other cells (Mesri, Cesarman, and Boshoff 2010). However, these cells will lyse following lytic reactivation, so cannot make up the mass of a KS-associated tumour (Mesri, Cesarman, and Boshoff 2010). Accordingly, over 90% of a KS lesion is made up of cells latently infected with KSHV (Dupin et al. 2002).

### 1.2.1 KSHV Latency

The latent lifecycle of KSHV is characterized by attachment of the viral genome to the host chromatin as a circular episome and minimal expression of viral genes (reviewed in Purushothaman et al. 2016). The attachment of the viral genome to that of the host enables passive replication alongside the host DNA during cell division. The genes expressed during latency promote the principal characteristics of the KS lesion: inflammation, angiogenesis, proliferation and spindling. The latency locus of the KS genome encodes latency-associated nuclear antigen (LANA), vCyclin, viral FLICE-

inhibitory protein (vFLIP), the Kaposins, as well as a number of different microRNAs (Purushothaman et al. 2016). LANA is responsible for binding the viral DNA to the host chromatin and plays multiple roles in promoting cell proliferation, inhibition of apoptosis and suppression of lytic reactivation (reviewed in Uppal et al. 2014). vCyclin modulates the cell cycle, promoting cell proliferation (Van Dross et al. 2005). vFLIP activates NFκB, promoting cell survival and expression of pro-inflammatory cytokines (Field et al. 2003; Efklidou et al. 2008). The 12 microRNA loci within the KSHV latency locus can be processed into 18 mature microRNAs, which can regulate various cellular factors, including NFκB, and can inhibit lytic reactivation (Purushothaman et al. 2016).

The Kaposin locus encodes three different proteins, Kaposin A, B and C, in a complex, overlapping reading frame that can initiate translation at several sites (Sadler et al. 1999). The transcript is expressed at high levels in the KS lesion, implying these proteins or the transcript itself play an important role for the virus (Sadler et al. 1999). The locus is composed of two regions of 23 base-pair, GC-rich direct repeats (DR1 and DR2) upstream of the K12 open-reading frame (ORF). Kaposin A (KapA) is translated from a canonical AUG start codon and consists solely of the K12 region, which encodes a transmembrane domain (Sadler et al. 1999; Kliche et al. 2001). KapA is proposed to dysregulate cytohesin-1, a cell adhesion regulator, to induce cell transformation (Muralidhar et al. 1998; Kliche et al. 2001). Kaposin C (KapC) is in the same reading frame as KapA but initiates upstream at a CUG translation initiation site, encoding both the DR1 and DR2 repeats as well as the K12 ORF (Sadler et al. 1999). Currently, there is no known function attributed to KapC. Finally, Kaposin B (KapB) is encoded in a different reading frame from KapA and C and initiates from a CUG or GUG translation start codon. The KapB transcript includes the DR1 and DR2 repeats but not the K12 ORF. KapB is the focus of this study and its function is discussed in detail below.

### 1.3 Kaposin B (KapB)

Though the precise role of KapB in the context of viral infection is not yet clear, overexpression models have shown that it is able to induce endothelial cell spindling, increase cell migration, promote endothelial reprogramming and contribute to the KS inflammatory and angiogenic environment (McCormick and Ganem 2005; Corcoran,

Johnston, and McCormick 2015; King 2013; Wu et al. 2011). KapB expression induces spindling of endothelial cells through the formation of actin stress fibres (SFs, discussed in more detail below) (Corcoran, Johnston, and McCormick 2015). This modulation of the cytoskeleton promotes cell motility (Corcoran, Johnston, and McCormick 2015). Additionally, KapB also inhibits the expression of cellular microRNAs (mi221 and mi222) that supress cell motility, thereby promoting migration (Wu et al. 2011). Notably, promotion of endothelial cell migration contributes to angiogenesis (Lamalice, Le Boeuf, and Huot 2007).

KapB also promotes alterations to endothelial cell fate through upregulation of *PROX1* mRNA, encoding a transcription factor involved in endothelial cell reprogramming (Yoo et al. 2010). *PROX1* controls expression of genes that promote a lymphatic endothelial cell phenotype, rather than a blood endothelial cell phenotype (Hong et al. 2002). KapB-mediated stabilization of *PROX1* promotes the development of an intermediate EC phenotype – a feature of KS lesions, of which the significance is not clear.

KapB also contributes to the inflammatory and angiogenic environment in KS by upregulating transcription of and stabilizing inflammatory and angiogenic mRNAs. KapB promotes phosphorylation and activation of signal transducer and activator of transcription 3 (STAT3), which transcriptionally activates genes that promote pro-oncogenic, inflammatory and angiogenic environments (King 2013; Bakheet, Hitti, and Khabar 2017; Yu, Pardoll, and Jove 2009). KapB also promotes inflammation by mediating the disassembly of cytoplasmic RNA granules called processing bodies (PBs, discussed in more detail below), important sites of cytokine mRNA decay (Corcoran, Johnston, and McCormick 2015; McCormick and Ganem 2005). This increases mRNA stability, which corresponds to increased transcript abundance and protein levels of certain cytokines, including granulocyte-macrophage colony-stimulating factor (GM-CSF) and interleukin (IL-6) (Corcoran, Johnston, and McCormick 2015; McCormick and Ganem 2005). PB disassembly is observed during KSHV latent infection (Corcoran, Johnston, and McCormick 2015).

### 1.4 Processing Bodies (PBs)

PBs are non-membranous ribonucleoprotein (RNP) granules that act as sites of post-transcriptional RNA regulation. They were initially identified as cytoplasmic puncta in 1997 when characterizing the exoribonuclease, Xrn-1, in mice (Bashkirov et al. 1997). Subsequent studies identified additional proteins that localize to PBs, including the mRNA decapping factors, DCP1 and DCP2, and decapping coactivators, Lsm1-7 and Hedls (Ingelfinger et al. 2002; Van Dijk et al. 2002). The study of PBs over the last 15 years has revealed many associated proteins that function in various mechanisms of RNA regulation, reviewed in Parker and Sheth 2007, Luo, Na, and Slavoff 2018; and Hubstenberger et al. 2017. In mammalian cells, PBs are constitutively present in the cytoplasm of cells and are highly dynamic; they are commonly observed to change in size, number and composition in response to various stimuli, including cell cycle status and cellular stressors, such as starvation, ultraviolet light or osmotic stress (Yu et al. 2005; Yang et al. 2004; Teixeira et al. 2005).

#### 1.4.1 Structure of PBs

As an RNP granule, the structural integrity of the PB is dependent on the presence of both proteins and RNA. The proteins required for PB integrity include, but are not limited to the decapping cofactor human enhancer of decapping large subunit (Hedls, also known as EDC4) (Yu et al. 2005), and the RNA helicase DDX6/rck (Chu and Rana 2006; Coller and Parker 2005), as knockdown of these proteins leads to a loss of PBs in cells. Conversely, knockdown of proteins such as the exonuclease Xrn1 (Cougot, Babajko, and Séraphin 2004) and decapping protein DCP1 (Sheth and Parker 2003) lead to increased numbers of PBs, likely due to mRNA accumulation in the cytoplasm. RNA is also required for PB integrity, mediated through both RNA-protein and RNA-RNA interactions (Teixeira et al. 2005; Van Treeck and Parker 2018).

Within PBs, the exact localization of individual proteins has not been well-described. From electron microscopy studies, PBs are described to contain a subset of resident proteins that act as a core, including DCP1a and certain proteins that localize mostly to the periphery and act as a shell, including DDX6 (Cougot et al. 2012). RNA localization within the PB is dependent on the function of the RNA (Pitchiaya et al.

2019): PB-targeted microRNAs (miRNAs) and mRNAs are more likely to be found within the center of PBs, while PB-targeted long non-coding RNAs (lncRNAs) primarily localize to the periphery (Pitchiaya et al. 2019). Since the size of PBs, ranging from 150 to 340 nm (Cougot et al. 2012), is near to the limit of resolution of conventional light microscopy, the increased use of super resolution techniques will improve our understanding of the ultrastructure of PBs.

### 1.4.2 Function of PBs

PBs are involved in the processes of RNA surveillance, RNA interference and mRNA decay (reviewed in Eulalio, Behm-Ansmant, and Izaurralde 2007). RNA surveillance refers to the cellular mechanism regulating nonsense-mediated decay of mRNAs. Upon translation of a premature stop codon, the surveillance complex is recruited to the RNA, localizes to PBs and then recruits mRNA decay factors (Eulalio, Behm-Ansmant, and Izaurralde 2007). RNA interference inhibits the expression of transcripts targeted by a specific miRNA through translational repression or accelerated decay (reviewed in Wilson and Doudna (2013)). All proteins required for miRNAs to inhibit a given transcript can be found at PBs (Eulalio, Behm-Ansmant, and Izaurralde 2007). Finally, PBs contain all the necessary proteins to conduct mRNA decay through the removal of the 5' cap and subsequent 5' to 3' RNA decay by the exonuclease, Xrn1 (Eulalio, Behm-Ansmant, and Izaurralde 2007). Certain classes of mRNAs are constitutively targeted to PBs for decay, including mRNAs containing ARE-elements.

#### 1.4.2.1 ARE-mRNA Decay

ARE elements are *cis* elements in the 3' UTR of 22% of human mRNAs and in 25% of introns (Bakheet, Hitti, and Khabar 2017). The core element consists of an AUUUA pentamer with further enrichment of adenines and uracil surrounding the element (Bakheet, Williams, and Khabar 2006). The pentamers are often clustered with two or more elements overlapping (Bakheet, Williams, and Khabar 2006). As diagrammed in Figure 1.1, certain RNA-binding proteins, such as tristetraprolin (TTP), can bind to ARE-elements and recruit the mRNA to PBs, where the mRNA can be translationally suppressed or decayed (Franks and Lykke-Andersen 2007). Thus, the ARE elements target mRNAs for accelerated decay, making these transcripts inherently

unstable (Cougot, Babajko, and Séraphin 2004). Experimentally, the presence or absence of PBs by microscopy directly correlates with the stability of ARE-mRNAs (Corcoran, Johnston, and McCormick 2015; Vindry et al. 2017; Blanco et al. 2014).

ARE-mRNAs encode for cytokines and angiogenic factors, including IL-6, IL-8 TNF, and GM-CSF (Caput et al. 1986; Bakheet, Hitti, and Khabar 2017). The tight regulatory control exerted by the cell over this class of messages, both at the level of transcription and mRNA decay, highlights how PBs act as essential nodes of gene expression control. By enabling precise and rapid changes in mRNA levels in response to stress stimuli, PBs control the expression of many disease-associated mRNAs. Research into how KapB dysregulates PBs and ARE-mRNAs will further mechanistic understanding about how inflammation is promoted both within the KS environment as well as other inflammatory diseases.

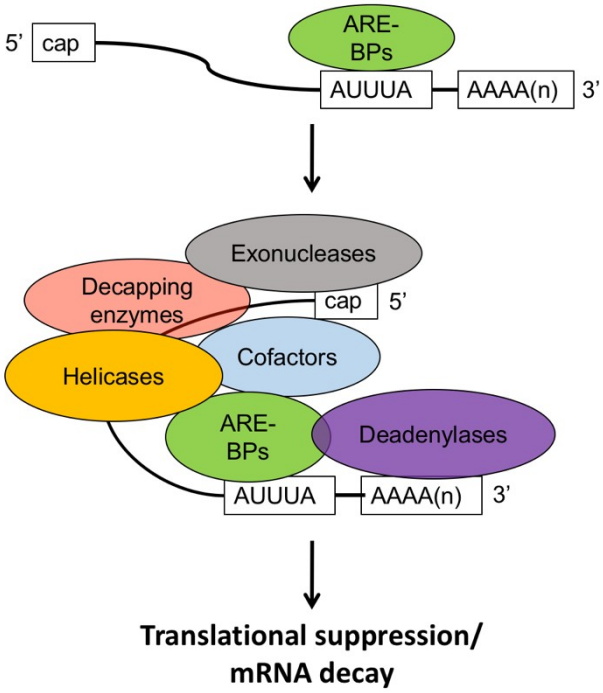


**Figure 1.1: mRNAs containing ARE-elements are recruited to PBs for translational suppression or decay.** Certain ARE-binding proteins bind the AU-rich element for recruitment to PBs. At PBs, these mRNAs are translationally supressed or decayed.

### 1.4.3 Associations of PBs with the Cytoskeleton

PBs can associate with both microtubules and actin (Aizer et al. 2008). Microtubules mediate long-range transport of PBs through actions of the molecular motors, dynein and kinesin (Aizer et al. 2008; Loschi et al. 2009). Disruption of microtubules or inhibition of dynein or kinesin movement inhibits proper assembly and disassembly of PBs (Aizer et al. 2008; Loschi et al. 2009). Aizer et al (2008) initially reported that the population of PBs associated with actin are primarily stationary. However, subsequent studies have demonstrated actin-associated movement of PBs (Lindsay and McCaffrey 2011; Steffens et al. 2014; Hamada et al. 2012). The cargo transport protein, Myosin Va (MyoVa), can bind simultaneously to resident PB proteins and actin, acting as a linker between actin and PBs (Lindsay and McCaffrey 2011). Knockdown of MyoVa causes disassembly of PBs, indicating that, similar to the observation with microtubules, PB association with actin is required to maintain proper structure (Lindsay and McCaffrey 2011). Though the current literature implicates the cytoskeleton as being an important scaffold for PBs, there are no studies that currently indicate how changes in actin structures impact PB dynamics.

### 1.4.4 Methods to Study PBs

Microscopy is the primary tool used to study PBs as it is the only currently available tool that is capable of direct visualization of cytoplasmic puncta. The presence or absence of PBs can be detected via immunofluorescent labeling of endogenous PB proteins followed by conventional light microscopy, which are commonly quantified through manual counting of endogenous PBs in cells. There are several PB-resident proteins that are established to detect endogenous PBs, discussed in Kedersha et al. (2008), including Hedls which is used in this study. This technique is the most representative of the visible PB status in a given cell, though manual quantification introduces potential observation bias and is time-intensive.

More advanced techniques, such as live-cell microscopic analysis of fluorescently-tagged PB-resident proteins, can provide real-time data on changes in the granule, which allows for improved understanding of PB movement and dynamics (Kedersha et al. 2008). However, experiments involving overexpression of aggregative proteins may not

be accurately representative of native PB behaviour. This is demonstrated with the overexpression of GFP-tagged versions of the PB-resident protein DCP1a. Several studies have indicated that overexpression of this construct can result in colocalization of the over-expressed Dcp1a with several PB proteins, including DDX6 and Hedls, and had a similar phenotypic distribution to endogenous DCP1a (Kedersha et al. 2008; Blumenthal and Ginzburg 2008; Wang et al. 2017). Further, granules formed from DCP1a overexpression behave analogously to endogenously stained DDX6, indicating potential PB-like behaviour (Takahashi et al. 2011). Blumenthal and Ginzburg (2008) examined polysome profiles with DCP1a overexpression and saw no differences in the polysome profiles, suggesting that global translation had not been affected. However, a separate study by Wang et al. (2017) found that overexpression of DCP1a-GFP supressed protein translation. These studies indicate that, though DCP1a granules often behave in the same manner as PBs, there may be functional and contextual differences. It highlights the importance of ensuring careful interpretation of results obtained from experiments employing overexpression of a given protein, and to consider the potential impact on the function under investigation.

More recently, a fluorescence-associated particle sorting technique was used to purify PBs and analyze their composition (Hubstenberger et al. 2017). This method involved using fluorescent sorting of GFP particles formed from overexpression of fluorescently-tagged versions of PB-resident proteins. Sorting of such particles resulted in a sufficiently high abundance of granules to quantify RNA-levels associated with PBs (Hubstenberger et al. 2017). The analysis of RNA present in PBs informs on the functional status of visible PBs by revealing which transcripts are targeted to PBs under a given experimental condition. However, since this technique used an overexpression model, the cautions described above must be considered. Furthermore, this method was only presented in unstressed HEK 293T cells, so must be verified to be responsive to various conditions known to alter PBs.

Beyond conventional light microscopy, electron microscopy has been the primary method used to understand PB higher-level structure (Cougot et al. 2012). In the future, advances in super-resolution microscopy techniques will enable a more complete understanding of these structures. These techniques provide structural insight to the

composition and organization of a PB, but are not useful tools for the wide-scale study of population-based changes in PBs due to the laborious preparation involved in these techniques.

Finally, there are many techniques that can be used to probe the functional status of PBs, including luciferase-based assays that monitor stability of mRNA populations with AREs (Corcoran, Khaperskyy, and McCormick 2011), but these do not visualize PBs directly. Since my work focused on the presence and absence of PBs in cell populations, the most feasible and economical approach was to employ conventional light microscopy. However, to avoid the laborious and subjective limitations inherent in manual quantification of PBs, a quantitative approach to image analysis was developed, which minimizes error associated with manual PB counts. This technique uses the freeware CellProfiler (Kamentsky et al. 2011) to quantify PBs, and is described in the results section below.

### 1.5 Stress Fibres (SFs)

During the process of actin polymerization, the monomeric form of actin, globular actin (G-actin), aggregates in groups of three subunits or more to nucleate an actin filament, which extends via addition of further G-actin monomers through ATP-dependent polymerization (reviewed in Pollard 2016). Filamentous actin (F-actin) can form many different structures by branching and bundling to form actin networks; these structures include SFs, lamellipodia and filipodia, but also function to generally maintain cell structure in the cortex of the cell, called cortical actin (Pollard 2016). The bundling of 10 to 30 actin filaments forms a SF (Cramer, Siebert, and Mitchison 1997). SFs are defined as ordered cytoskeletal structures composed of bundled actin filaments with periodic distribution of actin-crosslinking proteins and non-muscle myosin II (NMII) (Small et al. 1998). α-actinin is the primary crosslinking protein that facilitates the bundling of actin filaments (Lazarides and Burridge 1975; Pellegrin and Mellor 2007). Often, NMII is incorporated into the filaments, which results in a contractile structure (Katoh et al. 1998; Tan et al. 2003). Both α-actinin and NMII are discussed in detail in section 1.5.3 below.

SF formation, and consequently actin polymerization and bundling, is responsive to many environmental cues that function to promote cell motility and resist mechanical forces (reviewed in Tojkander, Gateva, and Lappalainen 2012). SFs can anchor at focal adhesions, which are cellular structures that mediate the connection between the cytoskeleton and extracellular matrix-binding proteins, called integrins (reviewed in Burridge and Wittchen 2013, Ridley and Hall 1992). In endothelial cells, SFs can also localize to cell-cell junctions, known as adherens junctions, to mediate cell-cell adhesion (Millán et al. 2010; Efimova and Svitkina 2018). Incorporation of NMII into actin bundles forms an actomyosin structure which enables them to be contractile (Tan et al. 2003). The ability of SFs to provide stability via anchoring, in addition to being contractile structures, enables them to act as tension-generating structures in the cell; a critical feature for cellular response to external environment and cell motility (Zaidel-bar, Zhenhuan, and Luxenburg 2015; Burridge and Wittchen 2013).

### 1.5.1 Types of SFs

The term "stress fibre" is used to describe a variety of bundled actin structures. Within this group, different types of SFs exhibit distinct mechanisms of formation and diverse associations with the extracellular matrix (ECM) (Small et al. 1998; Hotulainen and Lappalainen 2006). As shown in Figure 1.2, the main types of SFs include ventral SFs, dorsal SFs and transverse arcs (Small et al. 1998). Ventral SFs are attached at both termini to the extracellular matrix (ECM) through focal adhesions, and contain NMII, which imparts a contractile phenotype (Hotulainen and Lappalainen 2006; Small et al. 1998). Generally, these structures occur on the ventral side of the cell, closest to the ECM. Dorsal SFs are also connected through focal adhesions to the ECM, but only at a single terminus and project upwards, away from the ECM into the cell (Heath and Dunn 1978). Dorsal SFs are not associated with NMII and, thus, are not contractile (Burnette et al. 2014). Finally, transverse arcs are not adherent to the ECM at either end, but, rather, connect to the dorsal side of dorsal SFs (Heath 1983). These SFs contain both α-actinin and NMII, and have been suggested to mediate contractile forces through the attachment to dorsal SFs and thus, to the ECM (Burnette et al. 2014; Hotulainen and Lappalainen 2006). The functional significance of each SF subtype is not well-understood, though in

migrating cells, dorsal SFs are thought to be important in the leading edge of the cell, while ventral SFs contract to move the trailing edge (Vallenius 2013).

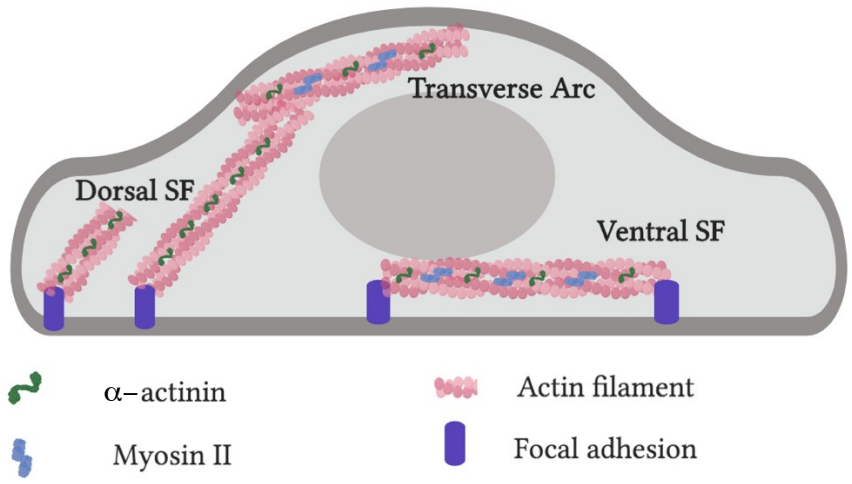


**Figure 1.2: Types of SFs in adherent cells.**
Dorsal SFs are attached to focal adhesions at one terminus, contain α-actinin but not NMII, and often attach to transverse arcs the dorsal side of the cell. Transverse arcs are not attached to focal adhesions, contain α-actinin and NMII and can promote contractile force through connections with dorsal SFs. Ventral SFs are attached at both termini by focal adhesions and contain both α-actinin and NMII. Illustration made with: https://app.biorender.com/.

### 1.5.2 Signalling Regulating SF Formation

The formation of SFs is mediated by the Rho-GTPase, RhoA, through the activation of actin polymerization, inhibition of actin severing/depolymerization, and promotion of fibre contractility (Figure 1.3) (Tojkander, Gateva, and Lappalainen 2012). It has been well described that RhoA activates the formin mammalian diaphanous protein 1 (mDia1), which binds the actin-polymerizing protein, profilin, and promotes the elongation of actin filaments (Watanabe et al. 1997; Watanabe et al. 1999). Additionally, RhoA binds and activates the kinase Rho-associated coiled-coil kinase (ROCK) (Amano et al. 1997), which can then phosphorylate Lim kinase (LimK) (Ohashi et al. 2000). LimK can, in turn, phosphorylate and inactivate cofilin, an actin-severing protein, thereby promoting actin stability (Moriyama, Iida, and Yahara 1996). Active ROCK promotes actin fibre contractility by both directly phosphorylating a component of NMII, myosin light chain (MLC), as well as its upstream regulator, MLC-phosphatase, inhibiting the phosphatase and preventing dephosphorylation of MLC (Amano et al. 1996; Kimura et al. 1996). Both mDia1 and ROCK act in concert to form the elongated actin filaments that are organized, stable and contractile (Watanabe et al. 1999).

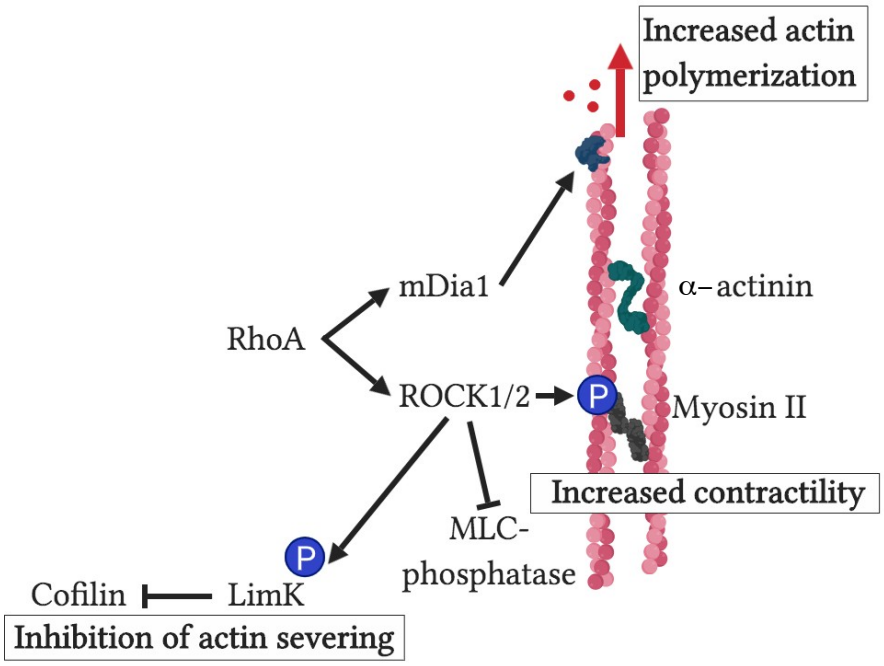


**Figure 1.3: RhoA controls SF formation through increased actin polymerization, increased actomyosin contractility and inhibition of actin severing.** RhoA activates mDia1 and ROCK. mDia1 promotes actin polymerization, elongating the actin fibres. ROCK phosphorylates LimK, MLC-phosphatase and MLC, a component of myosin II. Phosphorylated LimK is active, and then phosphorylates and inactivates cofilin, preventing actin severing and thus promoting actin stability. Phosphorylation of MLC induces contraction. Phosphorylation of MLC-phosphatase prevents dephosphorylation of MLC, promoting actomyosin contractility. Illustration made with: https://app.biorender.com/.

While it is known that the formation of SFs requires RhoA and its effectors, different subtypes of SFs (mentioned above) are formed through distinct mechanisms (Hotulainen and Lappalainen 2006). Dorsal SF are typically formed through mDia1-mediated actin polymerization, which initiates from nascent focal adhesions (Hotulainen and Lappalainen 2006). Conversely, transverse arcs are formed through the joining of short actin bundles, which originate at the lamellipodia and are transported by centripetal flow toward the cell center (Hotulainen and Lappalainen 2006). Since lamellipodia are formed through activity of the RhoGTPase, Rac, and its effector, Arp2/3, transverse arc formation is also dependent on other actin-modulating pathways (Hotulainen and Lappalainen 2006; Burridge and Wennerberg 2004). Finally, ventral SF form through the joining of dorsal SFs with transverse arcs, creating a continuous contractile actin filament with focal adhesions at both ends. Thus, formation of this subtype of actin SF filament is dependent on both previously described SF formation pathways (Hotulainen and Lappalainen 2006).

Additionally, the recruitment of α-actinin and NMII is also dependent on SF type (Hotulainen and Lappalainen 2006). Dorsal SFs recruit α-actinin as they are being formed, but NMII is not recruited until the fibres are several micrometers long or are attached to transverse arcs. At this point, NMII is inserted between sites of α-actinin bundling to form the characteristic, periodic pattern of these two proteins on SFs (Hotulainen and Lappalainen 2006). In transverse arcs, the smaller actin structures that join to form the arcs already contain α-actinin and NMII, and the periodic pattern of the two form from end to end joining of the filaments to form the transverse arc (Hotulainen and Lappalainen 2006). Importantly, NMII-mediated contractility and α–actinin bundling are required for the formation of organized SF (Hotulainen and Lappalainen 2006; Chrzanowska-Wodnicka 2004; Senger et al. 2019). Once formed the structures are very stable regardless of SF type (Hotulainen and Lappalainen 2006). While the disassembly of SFs is less well-studied, it has been shown that SFs disassemble during mitosis, when cells lose the ability to adhere to their substrate and when RhoA is inhibited (Burridge and Wittchen 2013).

### 1.5.3 Key Proteins in SF Formation and Structure

Several key proteins involved in SF formation (Rho-effectors, mDia and ROCK) and SF structure (α-actinin and MLC) are discussed in detail below.

#### 1.5.3.1 Mammalian Diaphanous Proteins (mDia)

The mDia proteins are well-described to direct the location and timing of actin polymerization (reviewed in Chesarone, Dupage, and Goode (2010)). They bind both profilin and the barbed, or fast-growing, end of F-actin filaments to promote actin polymerization at a given filament (Li and Higgs 2003; Watanabe et al. 1997). The mDia proteins can also bind to RhoA via GTPase-interacting domains (Maiti et al. 2012). Such binding releases the auto-inhibitory conformation of inactive mDia, exposing the formin homology domains that dimerize and are able to bind profilin (Maiti et al. 2012). There are three isoforms of mDia: mDia1 (DIAPH1), mDia2 (DIAPH3) and mDia3 (DIAPH2), which each play very different roles in the cellular coordination of actin polymerization. mDia1 is the most well-studied of the formins; along with its role in SF formation, it is also implicated in focal adhesion formation and maintenance (Hotulainen and Lappalainen 2006; Yamana et al. 2006a), cell junction stabilization (Acharya et al. 2017), filipodia and lamellipodia formation (Goh et al. 2012; Isogai et al. 2015), maintenance of cortical tension during mitosis (Nishimura et al. 2019), and microtubule stabilization (Ishizaki et al. 2001; Qu et al. 2017). mDia2 plays a role in formation of filipodia and lamellipodia (Yang et al. 2007; Gupton et al. 2007; Schirenbeck et al. 2005), and is also required for cytokinesis (Watanabe et al. 2013, 2008). Finally, mDia3 is required for chromosome alignment during mitosis (Cheng et al. 2011; Yasuda et al. 2004).

#### 1.5.3.2 Rho-Associated Coiled-Coil Kinase (ROCK)

ROCK is a serine-threonine kinase that phosphorylates a wide variety of targets (reviewed in Julian and Olson 2014). It participates in a diverse range of cell processes, including SF formation, cell division, senescence, apoptosis and autophagy (Julian and Olson 2014). The structure of the ROCK protein consists of an N-terminal kinase domain, followed by a coiled-coil containing the Rho-binding domain and at the C-terminus, an autoinhibitory domain (Julian and Olson 2014). There are two isoforms of ROCK: ROCK1 and 2, which regulate different processes, but can also act redundantly (Kümper et al. 2016; Julian and Olson 2014). ROCK1 mediates SF formation and focal

adhesion assembly (Yoneda et al. 2007), and plays a role in autophagy (Gurkar et al. 2013). ROCK2 has also been implicated in SF formation and stability (Yoneda, Multhaupt, and Couchman 2005; Shi et al. 2013), as well as focal adhesion maturation, endocytosis and phagocytosis (Yoneda et al. 2007). In regards to SF formation, both ROCK1 and ROCK2 can phosphorylate MLC to promote actomyosin contractility, though only ROCK2 is thought to maintain actin fibre stability through phosphorylation of LimK (Yoneda, Multhaupt, and Couchman 2005; Shi et al. 2013). Most work involving ROCK does not distinguish the two isoforms, so the various roles of each isoform are still being discerned.

#### 1.5.3.3 α-actinin

A wide variety of proteins are involved in the bundling of F-actin, but the primary protein that bundles actin filaments in SFs is α-actinin (Lazarides and Burridge 1975; Pellegrin and Mellor 2007). The basic structure of α-actinin is comprised of an actin-binding domain and a rod-domain, which can homodimerize in an antiparallel arrangement, enabling the simultaneous binding to two separate actin filaments (Sjöblom, Salmazo, and Djinović-Carugo 2008; Ylänne et al. 2001). There are four isoforms of α-actinin: α-actinin-2 and 3 are primarily found in muscle cells, while α-actinin-1 and 4 are found in non-muscle cells (Lazarides and Burridge 1975). Much of the formative research on this protein has been performed in muscle cells, showing that, in addition to actin binding, α-actinin has a wide-array of binding partners that function in cell adhesion (Sjöblom, Salmazo, and Djinović-Carugo 2008). Newer research has since expanded our understanding of α-actinin in non-muscle cells, which has shown that α-actinin can both bind actin fibres in a periodic pattern and promote their assembly, as well as function in focal adhesion regulation (Laukaitis et al. 2001; Burnette et al. 2014; Peterson et al. 2004; Edlund, Lotano, and Otey 2001; Lazarides and Burridge 1975; Choi et al. 2008; Kovac 2010). Several studies examining localization of the isoforms converge on the idea that α-actinin-1 shows a higher association with SFs in the cell, while α-actinin-4 is found more diffusely in the cytoplasm and nucleus but can occasionally be found on dorsal SFs (Honda et al. 1998; Nikolopoulos et al. 2000; Kovac 2010). Notably, though α-actinin-4 can localize to dorsal SFs, only α-actinin-1 is required for dorsal SF formation (Kovac

2010). Both isoforms can localize to focal adhesions, though play different roles: α-actinin-1 is required for focal adhesion maturation, while α-actinin-4 suppresses maturation to promote cell motility (Kovac 2010; Fukumoto et al. 2015). Interestingly, nuclear localization of α-actinin-4 corresponds to several reports that α-actinin-4 can act as a transcriptional cofactor involved in cell proliferation and differentiation (Khurana et al. 2011; Goffart et al. 2006; Foley and Young 2014). This non-canonical role has not been reported for α-actinin-1 and may explain why α-actinin-4 is extensively linked with various cancers, reviewed in Honda (2015). The above-mentioned studies displayed many discrepancies, especially in patterns of the immunofluorescence in subcellular localization studies (Honda et al. 1998; Araki et al. 2000; Kovac 2010). These discrepancies may be due to cell type so the localization of both isoforms must be confirmed in endothelial cells, the system used in this study.

#### 1.5.3.4 Non-Muscle Myosin II (NMII)

The myosin superfamily consists of 25 classes of actin-based motors of which NMII is the largest subfamily (reviewed in Conti and Adelstein 2008). NMII has a hexameric structure consisting of two myosin heavy chains (MHC) and two pairs of myosin light chains (MLC) (Conti and Adelstein 2008). The structure has two globular heads that can bind actin and hydrolyze ATP, followed by helical tails that have the ability to multimerize with other myosin II molecules in an antiparallel arrangement (Holmes 2008). This multimerization enables the binding of multiple actin filaments to mediate contraction. The hydrolysis of ATP promotes a conformational change in the head domain that rotates the head like a lever, pulling on the actin and thereby inducing contraction (Tan et al. 2003; Holmes 2008). NMII is primarily regulated through phosphorylation of the light chain, which increases ATPase activity in the globular domain (Conti and Adelstein 2008). The primary kinases that phosphorylate MLC include ROCK (Amano et al. 1996) and calmodulin-dependent myosin light chain kinase (MLCK) (Bárány et al. 1979), while myosin light chain phosphatase mediates dephosphorylation to oppose actomyosin contractility (Morgan, Perry, and Ottaway 1976). Contractile ability through MLC is an essential process in mechanosensing of the environment and is required for cell migration, adhesion and polarity (Zaidel-bar, Zhenhuan, and Luxenburg 2015).

### 1.5.4 Methods for SF Induction Converge on RhoA Activation

SFs can be induced through both chemical and mechanical stressors. Widely-used chemical stressors include serum factors, such as lysophosphatidic acid (LPA), and various cytokines, such as tumour necrosis factor (TNF) and transforming growth factor β (TGFβ) (Ridley and Hall 1992; Hanna et al. 2001; Bakin et al. 2002). SFs can also be induced by mechanical stressors, including changes in matrix stiffness (reviewed in Lee and Kumar (2016)) and shear stress caused by fluid flow. Shear stress refers to the stress caused by hemodynamic factors; the mechanical forces in flowing blood (Davies 1995). Unidirectional shear stress from fluid flow over endothelial cells results in alignment of the cells in the direction of flow and formation of actin SFs (Noria et al. 2004). RhoA coordinates SF formation in response to all these inducers (Ridley and Hall 1992; Hanna et al. 2001; Bakin et al. 2004; Lee and Kumar 2016; Davies 1995), thus the signalling resulting from many different inputs converge on a common SF formation mechanism.

### 1.5.5 Mechanotransduction

SFs are tension-generating structures that enable conversion of mechanical cues in the external environment to changes in cellular signalling in a process called mechanotransduction. Mechanical cues can be transmitted to the cell through changes in ECM binding, stretch-activated ion channels, receptors and other cell-cell contacts (Finch-Edmondson and Sudol 2016). For example, increases in ECM type and stiffness induces conformational changes in integrin proteins (Friedland, Lee, and Boettiger 2009; Kong et al. 2009), which, in turn, induce conformational changes at focal adhesions to then promote the formation of actomyosin structures and increase cytoskeletal tension (del Rio et al. 2009; Grashoff et al. 2010; reviewed in Finch-Edmondson and Sudol 2016). The structural changes in integrins, focal adhesions and actomyosin can subsequently modulate cell signalling (Finch-Edmondson and Sudol 2016). Thus, the actin cytoskeleton and its component parts, including SFs, function as force transducers that convert extracellular mechanical inputs into intracellular biochemical signaling cascades that can impact a multitude of cell behaviours. One common outcome of mechanical signals is altered gene expression within the cell.

There are two main transcriptional activators that control gene expression changes in response to mechanical stress: serum-response factor (SRF) and yes-associated protein (YAP). SRF translocates to the nucleus with changes in cytoskeletal polymerization and regulates over 300 genes, many involved in actin dynamics, adhesions, growth and differentiation (reviewed in Chai and Tarnawski 2002). SRF activation is controlled by monomeric G-actin; increased G-actin within the cytoplasm sequesters SRF (Sotiropoulos et al. 1999). However, with inducers of actin polymerization, such as RhoA, G-actin levels are depleted and SRF translocates to the nucleus to mediate transcription (Sotiropoulos et al. 1999). Thus, mechanical changes in the cell that activate RhoA can deplete G-actin and induce SRF signalling. YAP is discussed in section 1.6.

### 1.6 Yes-Associated Protein (YAP)

One of the primary signalling molecules that mediates mechanoresponsive biological changes is the transcriptional regulator YAP (reviewed in Halder, Dupont, and Piccolo 2012). YAP is an 80 kDa protein containing many domains responsible for protein-protein interaction, including a TEA-binding domain and WW domain at the N-terminus and a PDZ-binding motif at the C-terminus (Vassilev et al. 2001; Sudol et al. 1995; Sudol 1994; Oka et al. 2010). The PDZ domain is also required for nuclear translocation of YAP (Oka et al. 2010; Shimomura et al. 2014). YAP contains a transcriptional activator domain, upstream of the PDZ domain in the C-terminus to mediate changes in transcription (Komuro et al. 2003). There are two homologues of YAP, YAP1 and 2, that are produced through alternative splicing. YAP1 only contains one WW domain, while YAP2 contains two, a difference that potentially modulates the binding partners of the two homologues (Iglesias-Bexiga et al. 2015). The difference between function of the two isoforms has not yet been well-characterized, so this study will report findings in the context of YAP in general. YAP is often reported in conjunction with its paralog, transcriptional coactivator with PDZ-binding motif (TAZ). The profiles of genes regulated by YAP and TAZ are largely overlapping but have definite differences and can be modified by various binding partners (Plouffe et al. 2018; Kim, Jang, and Bae 2018).

### 1.6.1 Function in Transcriptional Regulation

YAP and TAZ are generally known to regulate cell proliferation, differentiation, survival and migration making them important in organ development, size and tissue structure (Halder, Dupont, and Piccolo 2012). There are distinct profiles of YAP activation that are determined by various DNA-binding partners (reviewed in Kim, Jang, and Bae 2018). For instance, YAP association with the transcription factors, TEAD1-4, SMADs, TBX5, ERBB4 and RUNX1-3 promote cell growth, often in the context of organ development and tissue differentiation (Zhao et al. 2008; Varelas et al. 2010; Haskins, Nguyen, and Stern 2014; Rosenbluh et al. 2012; Jang et al. 2017). Conversely, YAP association with other transcription factors, p73 and EGR-1, promotes apoptosis (Strano et al. 2005; Downward et al. 2004; Zagurovskaya et al. 2009). The diversity of its DNA-binding partners enables YAP to fine tune transcriptional responses for a variety of different stimuli and signalling inputs.

### 1.6.2 Regulation of YAP Activation

YAP is a nucleocytoplasmic shuttling protein; its localization is regulated by phosphorylation, sequestration and degradation (reviewed in Hansen, Moroishi, and Guan (2015)). Active YAP translocates to the nucleus, where it associates with a given coactivator to mediate transcription of specific genes. Inactive YAP remains in the cytoplasm where it is typically sequestered by various binding proteins, or targeted for degradation by the proteasome or autophagy (Hansen, Moroishi, and Guan 2015). The most well-known signalling cascade controlling YAP is the Hippo pathway, originally described in *Drosophila,* but is now defined for mammalian cells as well. The basic components of this pathway include the Ste20-like kinases (MST1/2) which phosphorylate large tumour suppressor 1/2 (LATS1/2) kinase, activating it (Zhao et al. 2007). Active LATS phosphorylates YAP to promote its cytoplasmic retention by 14-3-3 proteins (Zhao et al. 2007). Serine 127 in YAP is the most potent phosphorylation site of YAP, though there are four other sites that are phosphorylated to regulate YAP activity (Zhao et al. 2007). Various upstream regulators of YAP activity have been reported; of these, only some converge on components of the Hippo pathway while others are MST1/2- or LATS1/2-independent.

As a mechanoresponsive transcription factor, YAP can respond to a variety of changes in the physical environment. This includes cell-cell contact, the regulation that first defined the Hippo pathway (Zhao et al. 2007), which is thought to be primarily mediated through intracellular junctional signalling (Boggiano and Fehon 2012). Other mechanical inputs that are known to modulate YAP include stiffness of the ECM (Dupont et al. 2011) or shear stress due to fluid flow (Lee et al. 2017; Nakajima et al. 2017; Chien et al. 2016). YAP can also be activated by biochemical signalling inputs, including changes in nutrient status and G-protein coupled receptor (GPCR) signalling (Mo et al. 2015; Yu et al. 2012). Several of the activators of YAP, including increased ECM stiffness, shear stress and GPCR signalling, also promote the formation of SFs, (Noria et al. 2004; Lee and Kumar 2016) and highlight an important intermediate mechanotransducer involved in YAP activation: the actin cytoskeleton.

#### 1.6.2.1 The Actin Cytoskeleton Controls YAP Activation

Several groups have shown that YAP activation can be directly controlled by changes in the actin cytoskeleton. Inhibition of F-actin formation through polymerization inhibitors and cell detachment prevent YAP nuclear translocation (Wada et al. 2011; Zhao et al. 2012; Das et al. 2016). Conversely, overexpression of mDia1 to promote actin fibre polymerization promotes YAP activity (Dupont et al. 2011). Furthermore, induction of SFs also induces YAP nuclear translocation and transcriptional activity (Wada et al. 2011; Dupont et al. 2011). The proteins involved in SF formation, including RhoA, ROCK and MLC, have been heavily implicated in nuclear translocation and activity of YAP (Dupont et al. 2011; Halder, Dupont, and Piccolo 2012; Yu et al. 2012; Wada et al. 2011). RhoA, ROCK and MLC modulate YAP activation upon changes in ECM stiffness through changes in cell stretch and cytoskeletal tension (Dupont et al. 2011). ROCK also modulates YAP under shear stress conditions (Lee et al. 2017). Notably, YAP can also be activated by GPCRs in a Rho-dependent manner (Yu et al. 2012). Yu et al. (2012) reported that $G_{12/13}$ and $G_{q/11}$ receptor-signalling with LPA and sphingosine-1-phosphate, known SF inducers, can induce RhoA-dependent YAP nuclear localization through inhibition of LATS. Since these reports, several studies have indicated a dependence on RhoA in YAP-mediated signalling in a variety of different contexts, indicating the

conserved actin-dependent control of YAP across systems (Yu et al. 2012; Cai et al. 2018; Dupont et al. 2011; Torrino et al. 2019; Liu et al. 2017).

The signalling events that precisely link actin cytoskeletal changes to YAP activation are unclear. Some reports suggest that LATS1/2 but not MST1/2 is required in the signalling (Wada et al. 2011; Zhao et al. 2012; Mana-Capelli et al. 2014). However, studies that varied both matrix stiffness and shear stress indicated that LATS is likely not regulating YAP activation in response to these mechanical stimuli (Dupont et al. 2011; Nakajima et al. 2017). Recently, the actin-binding protein angiomotin has been implicated in the actin-mediated regulation of YAP (Zhao et al. 2011). It has been proposed that F-actin and YAP compete for angiomotin binding as follows: when increased actin polymerization recruits more angiomotin to F-actin, the increase in unbound YAP enables it to translocate to the nucleus (Mana-Capelli et al. 2014). Nakajima et al. (2017) demonstrate that angiomotin may regulate YAP during shear stress by this mechanism. Despite the confusion regarding intermediate signaling events, it is clear that changes to actin cytoskeletal dynamics elicited by the GTPase RhoA promote YAP activation.

### 1.7 Rationale and Objectives

KapB promotes the disassembly of PBs, leading to stabilization of ARE-mRNAs which encode inflammatory and angiogenic factors (Corcoran, Johnston, and McCormick 2015). Notably, KapB-mediated activation of STAT3 upregulates mRNA with AREs like IL-6 (King 2013; Bakheet, Hitti, and Khabar 2017; Yu, Pardoll, and Jove 2009). Furthermore, *PROX1* mRNA, also upregulated by KapB, contains an AU-rich element (Yoo et al. 2010). Therefore, in order to promote a tumorigenic environment, it is hypothesized that KapB must disassemble PBs to enable increased expression of ARE-mRNA.

KapB also promotes the formation of actin SFs to elicit endothelial cell spindling (Corcoran, Johnston, and McCormick 2015). The signalling controlling actin SF formation and PB disassembly has not been uncoupled. The molecular signalling cascade required for KapB to mediate SF formation and PB disassembly is shown in Figure 1.4. KapB interacts with and activates the stress-responsive kinase, mitogen-activated protein kinase associated protein kinase 2 (MK2) (McCormick and Ganem 2005). MK2 then

phosphorylates and activates heat-shock protein 27 (hsp27) (Corcoran, Johnston, and McCormick 2015; Garcia et al. 2009), which complexes with p115RhoGEF to mediate RhoA activation (Garcia et al. 2009; Corcoran, Johnston, and McCormick 2015). Active RhoA coordinates the formation of actin SFs and it is also essential for the disassembly of PBs (Ridley and Hall 1992; Corcoran, Johnston, and McCormick 2015).

Previous studies have thoroughly described the role of RhoA in actin SF formation (Ridley and Hall 1992; Watanabe et al. 1999; Pellegrin and Mellor 2007; Schmitz et al. 2000), therefore the requirement for RhoA in KapB-mediated SF formation was unsurprising. However, the regulation of PBs by RhoA is not well described. RhoA activation was reported to mediate the formation of numerous, tiny PBs during starvation compared to the controls that had larger but less abundant PBs (Takahashi et al. 2011). RhoA is also important for PB disassembly when activated by a different KSHV protein, viral G-protein coupled receptor (vGPCR) (Corcoran et al. 2012). The reported association of PBs with the actin cytoskeleton (Aizer et al. 2008; Lindsay and McCaffrey 2011) also suggests an important role for RhoA and the actin cytoskeleton in PB dynamics. Taken together, these studies indicate that RhoA controls PB dynamics; however, no studies have investigated what signals downstream of RhoA control PBs.

In this study, I sought to address how RhoA downstream effectors, SF structure itself and resulting functional outcome of pronounced SF formation modulate PB dynamics in the context of KapB expression. To test this hypothesis, the following objectives were established:

1. Investigate whether or not RhoA downstream effector molecules required for SF formation are also required for KapB-mediated PB disassembly.
2. Determine whether bundling of F-actin into SFs and the enhanced actomyosin contractility imparted by SFs are required for KapB-mediated PB disassembly.
3. Examine if KapB mediates mechanoresponsive signalling to activate YAP and if this event is required for KapB-mediated PB disassembly.

I now show that the RhoA-effectors ROCK and mDia1 contribute to KapB-mediated PB disassembly, failing to uncouple the signalling controlling SF formation and PB disassembly. I also show that actomyosin contractility is required for PB disassembly; however, the requirement of actin-bundling for this process remains unclear. Finally, I

discovered that KapB activates the mechanoresponsive transcriptional activator YAP, and YAP is required for PB disassembly, both in the context of KapB expression and in response to other external mechanical forces known to activate YAP.

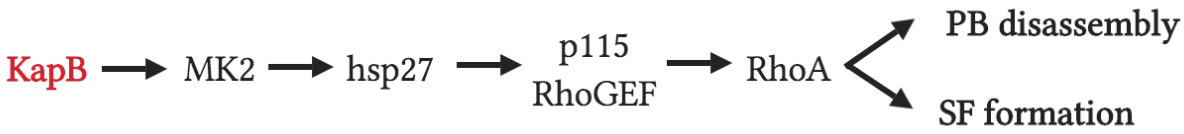


**Figure 1.4: KapB activates the MK2-hsp27-p115-Rho-GEF-RhoA axis to mediate SF formation and PB disassembly.** KapB binds and activates MK2 (McCormick and Ganem 2005), which then phosphorylates and activates hsp27 (Corcoran, Johnston, and McCormick 2015; Garcia et al. 2009). Hsp27 complexes with p115RhoGEF to mediate RhoA activation (Garcia et al. 2009; Corcoran, Johnston, and McCormick 2015). Active RhoA then coordinates the formation of actin SFs and the disassembly of PBs (Ridley and Hall 1992; Corcoran, Johnston, and McCormick 2015).

# CHAPTER 2: MATERIALS AND METHODS

## 2.1 Cell Culture

Cells were cultured in a humidified environment at 37˚C, supplemented with 5% $CO_2$ and 20% $O_2$. Human embryonic kidney 293T cells (HEK-293T, ATCC) and human cervical adenocarcinoma cells (HeLa, ATCC) were cultured in Dulbecco's Modified Eagle Medium (DMEM, Gibco) supplemented with 10% heat-inactivated fetal bovine serum (HI-FBS, Gibco), 100 U/mL penicillin, 100 $\mu$g/mL streptomycin, and 2 mM L-glutamine (1% PSQ, Gibco). Cells were passaged using 0.05% tryspin-ethylenediaminetetraacetic acid (EDTA, Gibco) at a 1:10 dilution.

Pooled human umbilical vein endothelial cells (HUVECs, Lonza) were cultured in endothelial cell growth medium 2 (EGM-2, Lonza)). EGM-2 contained endothelial cell base medium 2 (EBM-2) supplemented with 2% FBS, 0.4% human fibroblast growth factor B (hFGF-b), 0.1% vascular endothelial growth factor (VEGF), 0.1% human epithelial growth factor (hEGF), 0.1% ascorbic acid, 0.1% long arginine-3 insulin-like growth factor (R3-IGF-1), 0.1% gentamicin sulfate and amphotericin, and 0.04% hydrocortisone. For HUVEC passaging, tissue culture plates were precoated for 30 min at 37˚C with 0.1% (w/v) porcine gelatin (Sigma) in 1X sterile phosphate-buffered saline (PBS, Gibco). Following gelatin coating, cells were washed with PBS, incubated in 0.5 mL 0.05% trypsin- EDTA for 1 to 3 min, and resuspended in EBM-2. Cells were passaged in 6-well plates at a 1:3 dilution and were seeded for experiments in 12-well plates at a 1:6 dilution, unless otherwise indicated. EBM-2 media was replaced 24 h after passaging and subsequently, every 48 h. HUVECs between passage 5 and 8 were used for experiments.

## 2.2 Plasmids and Cloning

The plasmids used in this study can be found in Table 2.1. DNA stocks were prepared using the Qiagen Plasmid MiniPrep Kit (Qiagen) or Qiagen Plasmid MidiPrep Kit (Qiagen) according to the manufacturer's instructions. All constructs were sequenced using Sanger DNA sequencing by GENEWIZ or University Core DNA Services (University of Calgary).

**Table 2.1: Plasmids used in this study.**

| Plasmid Name | Use | Source | Bacterial Selection Cassette | Mammalian Selection Cassette (Lentiviral Plasmids Only) |
|---|---|---|---|---|
| pLJM-1-EV | Control vector for lentiviral expression studies | C. McCormick (Dalhousie University) | Ampicillin | Blasticidin, Puromycin |
| pLJM-1 KapB (pulmonary KS) | Lentiviral expression of KapB | C. McCormick (Dalhousie University) | Ampicillin | Blasticidin |
| pLKO-(shRNA) | Lentiviral expression of short hairpin RNAs (shRNA sequences in Table 2.3) | Cloned from: pLKO-TRC Addgene no.: 26655 | Ampicillin | Puromycin |
| pLJM-1 α–actinin1-GFP | Lentiviral expression of α-actinin1-GFP | Cloned from: pEGFP-N1 α-actinin-1, Addgene no.: 11908 | Ampicillin | Puromycin |
| pLJM-1-YAP-5SA (CA-YAP) | Lentiviral expression of constitutively active YAP | Cloned from: p2XFLAG-YAP-5SA, Donated by C. McCormick (Dalhousie University) | Ampicillin | Blasticidin |
| pcDNA3.1 | Transfection control | Invitrogen | Ampicillin | N/A |
| pcDNA3.1 KapB BCBL | Transfection of BCBL-derived KapB | C. McCormick (Dalhousie University) | Ampicillin | N/A |

| Plasmid Name | Use | Source | Bacterial Selection Cassette | Mammalian Selection Cassette (Lentiviral Plasmids Only) |
|---|---|---|---|---|
| | | | | |
| pMD2.G | Envelope protein for lentiviral production | Addgene no.: 12259 | Ampicillin | N/A |
| psPAX2 | Packaging proteins for lentiviral production | Addgene no.: 12260 | Ampicillin | N/A |

### 2.2.1 Cloning Short Hairpin RNA (shRNA) Sequences into pLKO.1

Forward and reverse shRNA sequences were selected from the TRC Library Database in the Broad Institute RNAi consortium. Details on shRNA design can be found at Addgene (2006). Sequences were chosen according to the following criteria: targeted the coding sequence, had less than 50% identity with an alternate human gene, and had a high intrinsic score, which indicated shRNA clonability and predicted knockdown performance. YAP target shRNAs in pLKO.1 were obtained from Dr. C. McCormick (Dalhousie University), prepared by S. O'Brien. The remainder of the shRNA-expressing plasmids were cloned in this study. Sequences for all shRNA oligonucleotides used for cloning are listed in Table 2.2.

Cloning of shRNAs was conducted according to the pLKO.1 protocol (Addgene 2006). Briefly, pLKO.1-TRC was digested with EcoRI-HF (New England BioLabs) and AgeI-HF (New England BioLabs) enzymes. The forward and reverse oligomers were annealed and ligated into digested pLKO.1. Colonies were screened for shRNA insertion using Sanger sequencing with the pLKO.1 sequencing primer (5' CAA GGC TGT TAG AGA GAT AAT TGG A 3').

**Table 2.2: shRNA sequences used in this study.**

| Target | Sequence (5' – 3') |
|---|---|
| Non-targeting sense | CCGGAGCACAAGCTGGAGTACAACTACTCGAGATCAA CATGAGGTCGAACACGATTTG |
| Non-targeting antisense | AATTCAAAAAGCACAAGCTGGAGTACAACTAATCAAC ATGAGGTCGAACACGATTTG |
| mDia1 sh1 sense | CCGGCCAATTCTGCTCATAGAAATTCTCGAGAATTTCT ATGAGCAGAATTGGTTTTTG |
| mDia1 sh1 antisense | AATTCAAAAACCAATTCTGCTCATAGAAATTCTCGAG AATTTCTATGAGCAGAATTGG |
| mDia1 sh2 sense | CCGGAAGATGACGTTGTTACACTTCCTCGAGGAAGTG TAACAACGTCATCTTTTTTG |
| mDia1 sh2 antisense | AATTCAAAAAAAGATGACGTTGTTACACTTCCTCGAG GAAGTGTAACAACGTCATCTT |
| mDia3 sh1 sense | AATTCAAAAAACGTTATTCTGGAGGTTAATGCTCGAG CATTAACCTCCAGAATAACGT |
| mDia3 sh1 antisense | CCGGACGTTATTCTGGAGGTTAATGCTCGAGCATTAA CCTCCAGAATAACGTTTTTTG |
| ROCK1 sh1 sense | CCGGAAGATGACGTTGTTACACTTCCTCGAGGAAGTG TAACAACGTCATCTTTTTTG |
| ROCK1 sh1 antisense | AATTCAAAAAAAGATGACGTTGTTACACTTCCTCGAG GAAGTGTAACAACGTCATCTT |
| ROCK1 sh2 sense | CCGGAAGATGACGTTGTTACACTTCCTCGAGGAAGTG TAACAACGTCATCTTTTTTG |
| ROCK1 sh2 antisense | AATTCAAAAAAAGATGACGTTGTTACACTTCCTCGAG GAAGTGTAACAACGTCATCTT |
| ROCK2 sh1 sense | CCGGCGTTGCCATATTAAGTGTCATCTCGAGATGACA CTTAATATGGCAACGTTTTTG |
| ROCK2 sh1 antisense | AATTCAAAAACGTTGCCATATTAAGTGTCATCTCGAG ATGACACTTAATATGGCAACG |

| **Target** | **Sequence (5’ – 3’)** |
|---|---|
| ROCK2 sh2 sense | CCGGGCCTTGCATATTGGTCTGGATCTCGAGATCCAG ACCAATATGCAAGGCTTTTTG |
| ROCK2 sh2 antisense | AATTCAAAAAGCCTTGCATATTGGTCTGGATCTCGAG ATCCAGACCAATATGCAAGGC |
| Cofilin sh1 sense | CCGGACGACATGAAGGTGCGTAAGTCTCGAGACTTAC GCACCTTCATGTCGTTTTTTG |
| Cofilin sh1 antisense | AATTCAAAAAACGACATGAAGGTGCGTAAGTCTCGAG ACTTACGCACCTTCATGTCGT |
| Cofilin sh2 sense | CCGGCCAGATAAGGACTGCCGCTATCTCGAGATAGCG GCAGTCCTTATCTGGTTTTTG |
| Cofilin sh2 antisense | AATTCAAAAACCAGATAAGGACTGCCGCTATCTCGAG ATAGCGGCAGTCCTTATCTGG |
| α-actinin-1 sh1 sense | CCGGACGGCGAGAGTGACCTCTAATCTCGAGATTAGA GGTCACTCTCGCCGTTTTTTG |
| α-actinin-1 sh1 antisense | AATTCAAAAAACGGCGAGAGTGACCTCTAATCTCGAG ATTAGAGGTCACTCTCGCCGT |
| α-actinin-1 sh2 sense | CCGGCCAGACCTACCACGTCAATATCTCGAGATATTG ACGTGGTAGGTCTGGTTTTTG |
| α-actinin-1 sh2 antisense | AATTCAAAAACCAGACCTACCACGTCAATATCTCGAG ATATTGACGTGGTAGGTCTGG |
| α-actinin-4 sh1 sense | CCGGGCCACACTATCGGACATCAAACTCGAGTTTGAT GTCCGATAGTGTGGCTTTTTG |
| α-actinin-4 sh1 antisense | AATTCAAAAAGCCACACTATCGGACATCAAACTCGAG TTTGATGTCCGATAGTGTGGC |
| α-actinin-4 sh2 sense | CCGGCCCGTATAAGAACGTCAATGTCTCGAGACATTG ACGTTCTTATACGGGTTTTTG |
| α-actinin-4 sh2 antisense | AATTCAAAAACCCGTATAAGAACGTCAATGTCTCGAG ACATTGACGTTCTTATACGGG |
| YAP sh1 sense | CCGGCTGGTCAGAGATACTTCTTAACTCGAGTTAAGA AGTATCTCTGACCAGTTTTTC |

| Target | Sequence (5' – 3') |
|---|---|
| | |
| YAP sh1 antisense | AATTGAAAAACTGGTCAGAGATACTTCTTAACTCGAG TTAAGAAGTATCTCTGACCAG |
| YAP sh2 sense | CCGGAAGCTTTGAGTTCTGACATCCCTCGAGGGATGT CAGAACTCAAAGCTTTTTTTC |
| YAP sh2 antisense | AATTGAAAAAAAGCTTTGAGTTCTGACATCCCTCGAG GGATGTCAGAACTCAAAGCTT |
| MyoVa sh1 sense | CCGGGCTGGTTTATGAAGGGTTAAACTCGAGTTTAAC CCTTCATAAACCAGCTTTTTG |
| MyoVa sh1 antisense | AATTCAAAAAGCTGGTTTATGAAGGGTTAAACTCGAG TTTAACCCTTCATAAACCAGC |
| MyoVa sh2 sense | CCGGGTGTCGTTCATTCGTACTATACTCGAGTATAGTA CGAATGAACGACACTTTTTG |
| MyoVa sh2 antisense | AATTCAAAAAGTGTCGTTCATTCGTACTATACTCGAGT ATAGTACGAATGAACGACAC |

### 2.3 Transfection for Lentivirus Production

HEK-293T cells at 100% confluence were passaged at a 1:4 dilution into 10-cm$^2$ tissue culture dishes to ensure a confluency of 70-80% the following day. For transfection, two solutions were prepared: (1) 500 $\mu$L Opti-mem (Gibco) with 19 $\mu$L 1 mg/mL polyethyenimine (PEI, Sigma) pH = 7.0 and (2) 500 $\mu$L of Opti-mem with 3.3 $\mu$g of target lentiviral DNA, 2 $\mu$g of psPAX2 and 1 $\mu$g of pMD2.G. The solutions were mixed by inversion and incubated at room temperature (RT) for 5 min. Solution (1) was added to solution (2), mixed by inversion and incubated for 15 min at RT. After the 15-min incubation, HEK-293T cells were washed with PBS, supplied with 4 mL serum-free DMEM and the PEI-DNA solution was added drop-wise to plated HEK-293T cells. After 5-6 h, media was replaced with antibiotic-free DMEM containing 10% FBS and 2 mM L-glutamine (Gibco). Transfected cells were incubated for 48 h at 37˚C to allow lentivirus production. The supernatant media was harvested and filtered through a 0.45 $\mu$m polyethersulfone (PES) filter (VWR) and aliquoted. Virus was stored at -80˚C until use.

### 2.4 Lentiviral Transduction of Target Cells

HUVECs were passaged as described in Section 2.1 and allowed to adhere overnight. HUVEC medium was replaced with fresh EGM-2 supplemented with 5 $\mu$g/mL hexadimethrine bromide (polybrene). Lentivirus was thawed at 37°C in a water bath and added into wells of plated HUVECs at the appropriate dilution. For pLJM-1 KapB, pLJM-1 YAP-5SA, and the pLJM-1 empty vector control, a dilution of 1:30 was used. For all pLKO-shRNA constructs and pLJM-1 α-actinin-1-GFP, a dilution of 1:10 was used. After 24 h incubation, the virus-containing EGM-2 media was removed and replaced with EGM-2 containing antibiotic selection. Transduced cells were selected with either 5 $\mu$g/mL blasticidin (Sigma) for 96 h, replacing the media and antibiotic at 48 h, or 1 $\mu$g/mL puromycin (Sigma) for 48 h. Selection markers for each plasmid are indicated in Table 2.1. Following selection, HUVEC medium was replaced with EGM-2 without antibiotic for at least 24 h recovery before further use.

### 2.5 Fluorescence Microscopy

#### 2.5.1 Immunofluorescence Staining

Cells were grown on coverslips (no. 1.5, Electron Microscopy Sciences) and following treatment, coverslips were washed with 1X PBS and fixed in freshly-prepared 4% paraformaldehyde (PFA, Electron Microscopy Sciences) in 1X PBS (137 mM NaCl, 2.7 mM KCl, 10 mM $Na_2HPO_4$, 1 mM $KH_2PO_4$) at 37°C for 10 min. Coverslips were then washed 2 times with 1X PBS prior to storage in 1X PBS at 4°C. Cells were permeabilized with 0.1% Triton-X100 (Sigma) in 1X PBS for 10 min at RT and coverslips were then washed 4 times with 1X PBS. The coverslips were blocked in 1% Human AB serum (blocking buffer, Sigma) in 1X PBS for 1 h at RT. Coverslips were then incubated with diluted primary antibody in blocking buffer overnight at 4°C in a humidified chamber or for 30 min at RT. Table 2.3 lists antibodies and staining conditions used for immunofluorescence. After primary antibody incubation, coverslips were washed 3 times in 1X PBS and incubated in fluorescently-tagged secondary antibody diluted in blocking buffer for 1 h at RT. Coverslips were washed 3 times in 1X PBS and if applicable, stained with Phalloidin-conjugated Alexa-Fluor 647 (Invitrogen, 1:100) in 1X PBS for 1.5 h. Coverslips were then washed 3 times in 1X PBS and mounted onto microscope slides

(FisherBrand) using Prolong Gold Antifade Mounting Media (Invitrogen) and allowed to cure overnight.

### 2.5.2 Immunofluorescence for CellProfiler

Immunofluorescence for CellProfiler analysis was performed as in section 2.5.1, with the following modifications: (1) Prior to treatment with Triton X-100, coverslips were stained with wheat germ agglutinin (WGA) Alexa-647 conjugate (Invitrogen, 1:400) in 1X PBS for 10 min at RT. Coverslips were washed 3 times with 1X PBS before permeabilization. (2) Following secondary antibody incubation, coverslips were washed 3 times in 1X PBS and stained with 4',6-Diamidino-2-Phenylindole (DAPI, Invitrogen, 1:10,000) in 1X PBS for 5 min. PBs were identified using immunofluorescence for Hedls, a PB-resident protein (Kedersha et al. 2008).

### 2.5.3 Microscopy

Confocal imaging was performed on the Zeiss LSM 880 Confocal Microscope (Charbonneau Microscopy Facility, University of Calgary) at the 63X oil objective. This microscope was equipped with the following lasers: a 25 mW multiline Argon 488 nm laser, a 20 mW diode-pumped solid state 561 nm laser and 5 mW 633 nm helium neon laser. Representative images in immunofluorescence panels were taken at 0.6X zoom and exported as .tiff files from the ZenBlack software (Zeiss).

CellProfiler imaging was performed on the Zeiss AxioImager Z2 (CORES facility, Dalhousie University) or Zeiss AxioObserver (Charbonneau Microscopy Facility, University of Calgary) with filtered LED illumination at the 40X oil objective. At least 7 fields of view were obtained per treatment, imaging ≥100 cells per condition. As per standard microscopy practices, exposure time (ms) was set to just below pixel saturation for the maximum dynamic range of intensity and was kept consistent across all conditions within a given experiment. Individual channel images were exported using the 'Batch Export' function from ZenBlue software (Zeiss) as .tiff files.

### 2.5.4 Quantification of Processing Bodies Using CellProfiler Analysis

CellProfiler (cellprofiler.org) is an open source software for high-content image analysis (Kamentsky et al. 2011) that I used to develop an unbiased method for quantifying changes to PB dynamics that is now a standard method in the Corcoran lab. The pipeline used for quantifying PBs was structured as follows: To detect nuclei, the DAPI image was thresholded into a binary image. In the binary image, primary objects between 30 to 200 pixels in diameter were detected and defined as nuclei. Cells were identified as secondary objects in the WGA image using a propagation function from the identified nuclei which determined the cell's outer edge. Using the parameters of a defined nucleus and cell border, the cytoplasm was then defined as a tertiary object. The Hedls channel image was enhanced using an "Enhance Speckles" function to identify distinct puncta and eliminate background staining. The cytoplasm image was then applied as a mask to the enhanced puncta image to ensure quantitation of only cytoplasmic puncta. Hedls puncta were measured in the cytoplasm of cells using a 'global thresholding with robust background adjustments' function as defined by the program. The threshold cut-off for identified Hedls puncta remained constant through all CellProfiler experiments. Puncta number per cell, intensity and locations with respect to the nucleus were measured and exported as .csv files and analyzed in RStudio. A template of the RStudio analysis pipeline is attached in Appendix A. Data was represented as fold change in Hedls puncta count per cell normalized to the vector puncta count. 'Relative Hedls Puncta/Cell (KapB/Vector)' demonstrates the KapB puncta count divided by vector puncta count, a ratio that was calculated within each treatment group for each biological replicate.

**Table 2.3: Antibodies used for immunofluorescence in this study.**

| Antibody | Source | Staining Procedure |
|---|---|---|
| Mouse α-p70 s6 kinase (detects Hedls) | Santa Cruz (Cat#:sc-8418) | 1:1000 in blocking buffer (1% Human AB in PBS), 4˚C overnight |
| Rabbit α-KapB | Gift from D. Ganem and C. McCormick | 1:1000 in blocking buffer (1% Human AB in PBS), 30 min RT |
| Mouse α-YAP | Santa Cruz (Cat#:sc-101199) | 1:1000 in blocking buffer (1% Human AB in PBS), 4˚C overnight |
| Rabbit α-YAP | Cell Signalling Technologies (Cat#:4912) | 1:100 in blocking buffer (1% Human AB in PBS), 4˚C overnight |
| Rabbit α-α-actinin-1 | Abclonal (Cat#:A1160) | 1:500 in blocking buffer (1% Human AB in PBS), 4˚C overnight |
| Mouse α-α-actinin-4 | Santa Cruz (Cat#:sc-390205) | 1:500 in blocking buffer (1% Human AB in PBS), 4˚C overnight |
| Rabbit α-DDX6 | Bethyl Labs (Cat#:A300-461A) | 1:1000 in blocking buffer (1% Human AB in PBS), 4˚C overnight |
| Alexa Fluor 555-conjugated donkey α-mouse IgG (2˚) | Invitrogen (Cat#:A31570) | 1:1000 in blocking buffer (1% Human AB in PBS), 1h RT |
| Alexa Fluor 488-conjugated chicken α-rabbit IgG (2˚) | Invitrogen (Cat#:A21441) | 1:1000 in blocking buffer (1% Human AB in PBS), 1h RT |
| Alexa Fluor 555-conjugated donkey α-rabbit IgG (2˚) | Invitrogen (Cat#:A31572) | 1:1000 in blocking buffer (1% Human AB in PBS), 1h RT |
| Alexa Fluor 488-conjugated chicken α-mouse IgG (2˚) | Invitrogen (Cat#:A21200) | 1:1000 in blocking buffer (1% Human AB in PBS), 1h RT |

## 2.6 Protein Electrophoresis and Immunoblotting

Cells were washed with PBS and lysed in 2X Laemmli buffer (20% glycerol, 4% SDS, 120 mM Tris-HCl), between 150 to 300 $\mu$L, depending on cell density. Lysates were homogenized with a 0.21-gauge needle and stored at -20˚C until further use. Once thawed, protein concentration was quantified using the DC™ protein assay (BioRad) according to the instructions of the manufacturer using serial dilutions (0 to 2.8 $\mu$g/mL) of bovine serum albumin (BSA, Sigma) in 2X Laemmli to generate a standard curve. Absorbance at 750 nm was measured on SpectraMax M2 plate reader (Molecular Devices). Following protein quantification, lysates were supplemented to contain 0.02% (w/v) bromophenol blue (Sigma) and 0.05 M dithiothreitol (DTT, Sigma) and heated at 95˚C for 5 min.

7.5 or 12% TGX Stain-Free SDS-polyacrylamide gels (BioRad) were cast according to the instructions of the manufacturer and 5 to 15 $\mu$g of total protein were subjected to SDS gel electrophoresis using 1X SDS running buffer (25 mM Tris, 192 mM Glycine, 0.1% SDS). The voltage used for electrophoresis was 100V for 15 min followed by 120 V for approximately 1.5 h or until bromophenol blue dye front was no longer present on the gel. Precision Plus Protein All Blue Prestained Protein Standards (BioRad) was used as a molecular weight marker. After electrophoresis, gels were UV-activated using the ChemiDocTouch (BioRad) Stain-Free Gel setting with automated exposure for 45 s. UV activation resulted in visualization of complexes of tryptophan and the proprietary 'trihalo compound' in the stain-free gel (BioRad), enabling visualization of the total protein levels in each lane. The protein was transferred to low-fluorescence polyvinylidene difluoride (PVDF) membranes (BioRad) on the Trans-Blot Turbo Transfer System (BioRad) according to the instructions of the manufacturer. Following transfer, total protein amounts on membranes were imaged on the ChemiDocTouch using the Stain-Free Membrane setting with automated exposure. Membranes were blocked using either 5% BSA (Sigma) in 1X TBS-T (150 nM NaCl, 10 mM Tris, pH 7.8, 0.01% Tween-20) for 1 h at RT. Primary antibody was diluted in 2.5% BSA in 1X TBS-T. Table 2.4 lists the antibodies used and the appropriate dilution for immunoblotting. Membranes were incubated in primary antibody solution overnight at 4˚C with rocking. The following day, membranes were washed 3 times for 5 min in 1X TBS-T. Membranes were

incubated with the appropriate secondary antibody, conjugated to horseradish peroxidase (HRP) for 1 h at RT. Membranes were washed 4 times for 5 min in 1X TBS-T. Clarity™ Western ECL Blotting Substrate (BioRad) was mixed at a 1:1 ratio and applied to the membrane for 5 min. Chemiluminescent signal was imaged on ChemiDocTouch Chemiluminescence setting. Band intensity was quantified using ImageLab software (BioRad), normalizing to total protein.

**Table 2.4: Antibodies used for immunoblotting in this study.**

| Antibody | Source | Dilution |
|---|---|---|
| Rabbit α-mDia1 | Cell Signalling Technologies (Cat#:5486) | 1:1000 in 2.5% BSA |
| Rabbit α-mDia3 | Cell Signalling Technologies (Cat#:5474) | 1:1000 in 2.5% BSA |
| Rabbit α-ROCK1 | Cell Signalling Technologies (Cat#:4035) | 1:1000 in 2.5% BSA |
| Rabbit α-ROCK2 | Cell Signalling Technologies (Cat#:9029) | 1:500 in 2.5% BSA |
| Rabbit α-Cofilin | Cell Signalling Technologies (Cat#:5175) | 1:1000 in 2.5% BSA |
| Rabbit α-DCP1a | Cell Signalling Technologies (Cat#:15365) | 1:500 in 2.5% BSA |
| Rabbit α-α-actinin-1 | Abclonal (Cat#:A1160) | 1:1000 in 2.5% BSA |
| Mouse α-α-actinin-4 | Santa Cruz (sc-390205) | 1:1000 in 2.5% BSA |
| Rabbit α-α-actin-HRP-linked | Cell Signalling Technologies (Cat#:12620) | 1:1000 in 2.5% BSA |
| Rabbit α-P-YAP | Cell Signalling Technologies (Cat#: 4911) | 1:1000 in 2.5% BSA |
| Rabbit α-YAP | Cell Signalling Technologies (Cat#: 4912) | 1:1000 in 2.5% BSA |
| Rabbit α-DDX6 | Bethyl Labs (Cat#:A300-461A) | 1:1000 in 2.5% BSA |
| α-Mouse IgG, HRP-linked (2˚) | Cell Signalling Technologies (Cat#: 7076) | 1:2000 to 1:4000 in 2.5% BSA |
| α-Rabbit IgG, HRP-linked (2˚) | Cell Signalling Technologies (Cat#: 7074) | 1:2000 to 1:4000 in 2.5% BSA |

## 2.7 Quantitative Reverse-Transcriptase Polymerase Chain Reaction (qRT-PCR)

Following treatment as indicated, cells were lysed in 250 $\mu$L RLT buffer and RNA was extracted using the RNeasy Plus Mini kit (Qiagen) according to the manufacturer's instructions. RNA concentration was quantified using the NanoDrop One (ThermoFisher). Complementary DNA (cDNA) was synthesized from 1 $\mu$g of total RNA using the qScript cDNA SuperMix (QuantaBio) according to the manufacturer's instructions. Real-time quantitative PCR with SsoFast EvaGreen qPCR MasterMix (BioRad) was used to quantify the fold-change in mRNA abundance in different conditions. The reaction conditions included the following: 4 $\mu$L cDNA, 5 $\mu$L SsoFast EvaGreen MasterMix (BioRad) and 1 $\mu$L of a 2 nM mixture of forward and reverse primer. All qRT-PCR primer sequences are found in Table 2.5.

The reaction conditions were as follows: 2 min at 98˚C, cycling 39X between 98˚C for 2 s and 56˚C for 5 s with a plate read after every cycle, incubation at 65˚C for 10 s, and 95˚C for 2 s. Melt curves were calculated by increasing the temperature from 75˚C to 95˚C, by increments of 0.2˚C/10 s after every run to ensure single products in each reaction. Primer efficiency was calculated on a dilution series of pooled samples prior to comparing experimental conditions. All samples were run in duplicate and average values were normalized to hypoxanthine phophoribosyltransferase-1 (HPRT-1). Relative fluorescence was quantified using CFX Connect (BioRad) to determine the cycle threshold (Ct) of each sample. The fold change between mRNA expression levels was calculated using the delta-delta Ct ($\Delta\Delta$Ct), as follows:

$\Delta$Ct = Average Ct of Target Gene – Average Ct of Control Gene

$\Delta\Delta$Ct = $\Delta$Ct Experimental Condition - $\Delta$Ct Control Condition

Fold Change = $2^{\Delta\Delta Ct}$

**Table 2.5: qRT-PCR primers used in this study.**

| Target | Forward/ Reverse | Sequence | Tm (˚C) | Reference |
|---|---|---|---|---|
| CYR61 | Forward | ATGGTCCCAGTGCTCAAAGA | 60 | (Chien et al. 2016) |
| CYR61 | Reverse | GGGCCGGTATTTCTTCACAC | 62 | (Chien et al. 2016) |
| CTGF | Forward | CAGCATGGACGTTCGTCTG | 60 | (Chien et al. 2016) |
| CTGF | Reverse | AACCACGGTTTGGTCCTTGG | 62 | (Chien et al. 2016) |
| CTGF | Forward | CCCTCGCGGCTTACCG | 56 | (Chien et al. 2016) |
| CTGF | Reverse | GGACCAGGCAGTTGGCTCT | 62 | (Chien et al. 2016) |
| ANKRD1 | Forward | ACGCCAAAGACAGAGAAGGA | 60 | (Chien et al. 2016) |
| ANKRD1 | Reverse | TTCTGCCAGTGTAGCACCAG | 52 | (Chien et al. 2016) |
| YAP | Forward | TTGGGAGATGGCAAAGACAT | 58 | (Chen et al. 2013) |
| YAP | Reverse | CGTTCATCTGGGACAGCAT | 58 | (Chen et al. 2013) |
| 18S | Forward | TTCGAACGTCTGCCCTATCAA | 62 | (Singh, 2019) |
| 18S | Reverse | GATGTGGTAGCCGTTTCTCAGG | 68 | (Singh, 2019) |
| B2M | Forward | TCGCGCTACTCTCTCTTTCT | 60 | (Singh, 2019) |

| Target | Forward/ Reverse | Sequence | Tm (˚C) | Reference |
|---|---|---|---|---|
| B2M | Reverse | TTTCCATTCTCTGCTGGATGAC | 64 | (Singh, 2019) |
| B2M | Forward | TGCTGTCTCCATGTTTGATGTA | 62 | (Singh, 2019) |
| B2M | Reverse | GACCAAGATGTTGATGTTGGATAAG | 70 | (Singh, 2019) |
| HPRT-1 | Forward | CTTTCCTTGGTCAGGCAGTATAA | 66 | (Singh, 2019) |
| HPRT-1 | Reverse | AGTCTGGCTTATATCCAACACTTC | 60 | (Singh, 2019) |
| HPRT-1 | Forward | TGGCGTCGTGATTAGTGATG | 64 | (Singh, 2019) |
| HPRT-1 | Reverse | GACGTTCAGTCCTGTCCATAAT | 68 | (Singh, 2019) |

### 2.8 Drug Treatments

The drug treatments used in this study can be found in table 2.6. All drug treatments were performed on HUVECs in EGM-2.

**Table 2.6: Drug treatments used in this study.**

| Drug | Use | Source (Cat#) | Concentration | Duration |
|---|---|---|---|---|
| Y-27623 dihydrochloride (ROCKi) | Non-isoform specific inhibition of ROCK | Sigma-Aldrich (Cat#:Y0503) | 10 $\mu$M | 4 h |
| (-)-Blebbistatin | Inhibition of MLC contractility | Sigma-Aldrich (Cat#:B0560) | 10 $\mu$M | 30 min |
| Calyculin A | Inhibition of MLC phosphatase, resulting in cell contraction | Abcam (Cat#: ab141784) | 2.5 nM, 5 nM | 20 min |
| Jasplakinolide | Aberrant polymerization of actin, decreasing monomeric G-actin | Sigma-Aldrich (Cat#:J4580) | 0.5 $\mu$M, 1 $\mu$M | 30 min |
| Latrunculin B | Inhibition of actin polymerization, increasing monomeric G-actin | Sigma-Aldrich (Cat#:L5288) | 0.1 $\mu$M | 30 min |
| Cytochalasin D | Inhibition of actin polymerization, increasing monomeric G-actin | Sigma-Aldrich (C8273) | 1 $\mu$g/mL | 30 min |

### 2.9 Filamentous and Globular Actin Fraction Separation

Following treatment, two confluent wells of HUVECs were each lysed in 100 $\mu$L prewarmed actin stabilization buffer (0.1M PIPES, pH = 6.9, 30% glycerol, 5% DMSO, 1mM MgSO4, 1mM EGTA, 1% Triton X-100, 1mM ATP, protease inhibitor) and lysates were pooled, homogenized with a 21-gauge needle and then incubated at 37˚C for 10 min. One hundred $\mu$L of lysate was subjected to centrifugation at 350xg for 5 min to remove cell debris. The supernatant was transferred into a 600 $\mu$L thick-walled centrifuge tube (Beckman) subjected to ultracentrifugation at 100,000 xg for 1 h at 37˚C using the TL-100 ultracentrifuge (Beckman), with the TLA-100-1 rotor (Beckman). In parallel, the remaining 100 $\mu$L of lysate was used to perform a DC™ protein assay according to the instructions of the manufacturer. Following ultracentrifugation, the supernatant (G-actin fraction) was removed, mixed with 25 $\mu$L 5X SDS sample buffer (0.25 M Tris-Cl, pH = 6.8, 10% SDS, 50% glycerol, 0.5 M DTT and 0.25% bromophenol blue) and heated at 95˚C for 5 min. The F-actin pellet was resuspended in 100 $\mu$L ice-cold actin depolymerization buffer (0.1 M PIPES, pH = 6.8, 1mM $MgSO_4$, 10mM $CaCl_2$, 5 $\mu$M Cytochalasin D), mixed with 25 $\mu$L 5X SDS sample buffer and heated at 95˚C for 5 min. Samples were subjected to SDS-12%PAGE and immunoblotting as in Section 2.6. Buffer recipes were obtained from Rasmussen et al. (2010) and protocol was adapted from "G-Actin / F-Actin In Vivo Assay Kit," (n.d.).

### 2.10 Transfection for KapB Expression

HeLa cells were seeded at a density of 100,000 cells/well onto coverslips in a 12-well plate. After 24 h, the following solutions were prepared per well to be transfected: (1) 62.5 $\mu$L Opti-mem was mixed with 3 $\mu$L 1 mg/mL PEI, pH = 7.0 and (2) 62.5 $\mu$L of Opti-mem was mixed with 1 $\mu$g of pcDNA3.1 KapB-BCBL or pcDNA3.1 control. The solutions were mixed by inversion and incubated at RT for 5 min. Solution (1) was added to solution (2) for a final reaction mixture volume of 125 $\mu$L, mixed by inversion and incubated for 15 min at RT. After incubation, cells were washed with PBS and supplied with 375 $\mu$L serum-free DMEM. The reaction mixture was added drop-wise to the plated HeLa cells. After 5 to 6 h, media was replaced with DMEM containing 10% FBS and 1%

PSQ. Transfected cells were incubated for 72 h and fixed for immunofluorescence as described in section 2.5.

### 2.11 Collagen-Coating for Altering Matrix Stiffness

Coverslips (no. 1.5, Electron Microscopy Sciences) in a 12-well plate were coated with a dilution series (0 to 64 $\mu$g/mL) of rat-tail collagen-1 (Gibco) in 0.02 M acetic acid for 1 h at 37˚. Coverslips were then washed 2 times with sterile PBS prior to seeding HUVECs as described in section 2.1.

### 2.12 Unidirectional Fluid Flow for Endothelial Cell Shear Stress

Unfrosted microscope slides (Cole-Parmer) were sonicated in a water bath sonicator (Cole-Parmer) containing water and 0.5% Sparkleen detergent (FisherBrand) for 15 minutes and rinsed twice with ultrapure water. Slides were sterilized with 70% isopropanol and allowed to dry in the biosafety cabinet. Slides were then fitted with a thick silicone gasket template (Specialty Manufacturing) and 400 $\mu$L 0.133 mg/mL rat-tail collagen-1 (Gibco) in 0.02 M acetic acid was added onto the slide, within the area designated by the gasket. Since slide surface area within the area bordered by the template gasket was 6.35 cm$^2$, the resulting collagen density was 8.3 $\mu$g/cm$^2$. The collagen solution was incubated on the slides for 4 h at RT then removed, and the slide was sterilized; first under UV light for 15 min and then again for 30 min with the gasket removed. Slides were washed twice with sterile PBS and placed in 10 cm$^2$ tissue culture dish for subsequent cell plating. HUVECs were trypsinized as in section 2.1 and subjected to centrifugation at 250xg for 5 min. The supernatant was removed and the pellet containing cells was resuspended in 3 mL fresh EGM-2. Of the 3 mL cell suspension, 500 $\mu$L was plated onto each slide on the area coated with collagen-1. HUVECs were allowed to adhere for 30 min and then the dishes containing the slides were supplemented with 12 mL EGM-2 to cover slides adequately. HUVECs were incubated on slides for 24 h.

Elevated EGM-2 was prepared at least 24 h prior to fluid flow as follows: 15 g dextran (Spectrum Chemical) was autoclaved in a 500 mL glass bottle. Once cooled, 500 mL EGM-2 was added to dextran for a viscosity of approximately 3 cP. Elevated EGM-2 was stored at 4˚C for at least 24 h to ensure adequate solubilization.

The following day, a stock media bottle, flow loop lid (Machine Shop, University of Calgary) with attached tubing (Masterflex & Cole-Parmer, size 14 and 16) and thin silicone gaskets (Specialty Manufacturing) for the flow chamber were autoclaved. All tubing was subsequently purged with sterile gas in a biosafety cabinet. Forty-five mL of elevated EGM-2 was added to the stock media bottle and secured with the flow loop lid. The flow loop was prepared by using tubing (Masterflex & Cole-Parmer, size 14) to attach the pulse dampener (Machine Shop, University of Calgary) to the tubing on the flow loop lid, ensuring that the outlet of the flow loop lid was connected with the inlet of the pulse dampener. The flow loop was inserted into 37°C incubator and tubing was inserted into the pump head (Masterflex) ensuring to match the tubing size to the respective pump head (size 14). The direction of fluid flow from the stock bottle and into the pulse dampener was confirmed with pump priming. Before cells were inserted into the flow loop, the pump was run to fill the pulse dampener with 15 mL of media ensuring to cover the outlet of the pulse dampener adequately. Mixed air containing 5% $CO_2$ (Praxair) was supplemented into flow loop at an 0.2 $\mu$M sterile in-line gas filter (VWR) inlet attached to the flow loop lid. Slides with seeded cells were then inserted onto the flow chamber (Specialty Manufacturing) with an autoclaved thin gasket between the slide and the chamber, clamped and attached to the flow loop following the outlet of the pulse dampener. The flow chamber was slightly elevated at the outlet to facilitate elimination of air bubbles. The pump head was then primed to send liquid through the flow chamber and eliminate any air bubbles. The rate of fluid flow was started at 0.3 L/min and doubled every 15 min to avoid sudden stress on the cells. Final flow rates of 0.6 L/min and 2.7 L/min, corresponding to shear stress rates of 2 and 10 dyn/cm$^2$, were used. Following 20 to 22 h flow, cells were removed and immediately fixed for immunofluorescence as described in section 2.5 or lysed for immunoblotting as described in section 2.6.

### 2.13 Statistical Analysis

Statistical analysis of individual CellProfiler experiments was performed in RStudio (Appendix A). Error and significance of puncta counts within a given experiment was determined using a negative binomial model, commonly used for count data with unequal variance. A single biological replicate consisted of 7 images of each treatment in

a given experiment, counting 100 to 200 cells per treatment. In order to combine biological replicates, data was represented as 'puncta count per cell normalized to vector control'. Statistical analysis of combined biological replicates was performed in GraphPad Prism 8.0 software. Significance was determined using a ratio paired t-test or repeated measures analysis of variance (ANOVA). Statistical significance was determined as $p < 0.05$.

# CHAPTER 3: RESULTS

## 3.1 CellProfiler Characterizes PB Disassembly in KapB-Expressing HUVECs

In order to effectively study PB disassembly, a quantitative microscopy approach was needed. CellProfiler is a freeware software program designed for quantitative analysis of large image sets (Kamentsky et al. 2011). This program enabled the development of an image analysis pipeline through the addition of different modules to enhance, identify and measure images. As outlined in Figure 3.1 (A), this pipeline was designed to count PBs that were stained by immunofluorescence to the PB-resident protein Hedls. The first step was identifying the DAPI-stained nucleus as a primary object through applying a threshold to the image, then converting pixels above said threshold to a binary image. Nuclei were identified from the binary image as objects between 30 and 200 pixels in diameter. The pipeline then uses the defined nucleus to apply a propagation function in the wheat-germ agglutinin (WGA) image to identify the periphery of a cell. The object of a cell was masked with the defined nucleus to define the cytoplasm of the cell, which is then applied as a mask in the Hedls channel to ensure only cytoplasmic puncta were counted. The intensities of the masked Hedls images were enhanced to avoid counts from background staining. Puncta between 1 and 6 pixels above a threshold of 0.02 intensity units were counted. This threshold was maintained between experiments. Puncta counts, intensity and distance from the nucleus were all measured and data analysis was performed in RStudio with the attached template code (Appendix A). As a proof of concept, KapB- and vector-transduced HUVECs were analyzed through the described pipeline (Figure 3.1 (B - E)). Puncta counts confirmed PB disassembly in KapB-expressing cells. Figure 3.1 (B) shows the distribution of puncta counts from a single experiment, and demonstrated that KapB-expressing cells contained very few cells with high puncta counts. Figure 3.1 (C) shows fold change in puncta counts from three independent replicates, with consistent decreases in KapB-expressing cells. KapB-expressing cells also showed decreased puncta intensity (Figure 3.1 (D)). Finally, Hedls puncta in KapB-expressing cells were on average closer to the nucleus, though this effect was not significant ($p = 0.18$) (Figure 3.1 (E)). These data confirmed that CellProfiler is an effective pipeline for PB analysis.

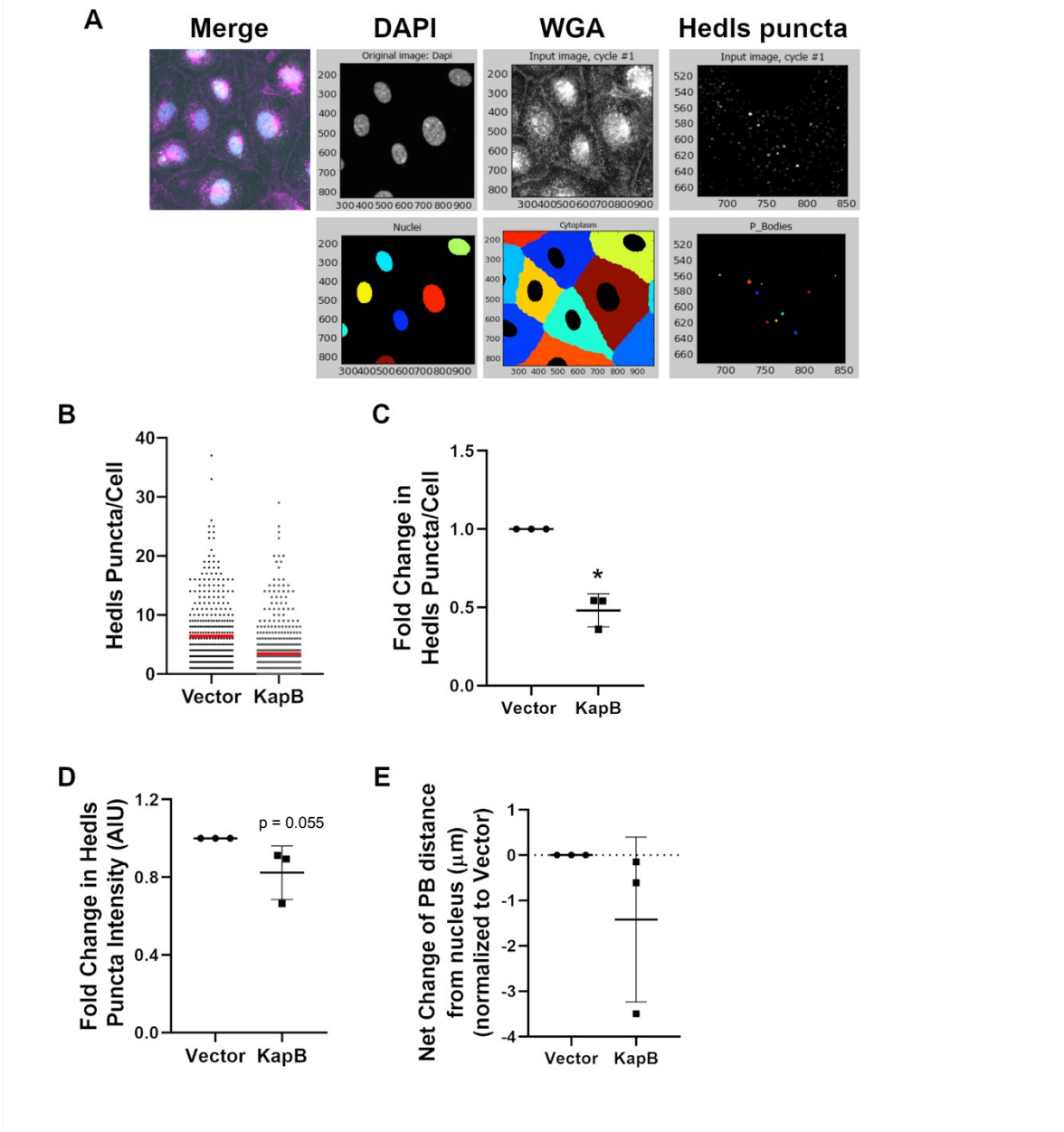


**Figure 3.1 CellProfiler pipeline accurately identifies nuclei, cytoplasm and Hedls puncta.** (A) Schematic of the pipeline identifying nuclei from the DAPI channel, cell periphery from the WGA channel and Hedls puncta from the Hedls channel. The program enables analysis of several characteristics of PB dynamics, including (B) Hedls puncta counts per cell (representative n=1, each dot represents a single cell, mean count denoted by red line) (C) fold change in mean Hedls puncta per cell, normalized to vector (D) fold change in puncta intensity, normalized to vector, and (E) puncta distance from the nucleus, calculated by setting vector puncta distance from the nucleus = 0. Analysis of CellProfiler output was performed in RStudio and GraphPad Prism. Error bars represent standard deviation. Statistics were determined using a ratio paired t-test, n=3 except in B, $p < 0.05$.

### 3.2 RhoA-Effectors and Downstream Signalling that Control Actin SF Dynamics are Required for PB Disassembly by KapB

To understand if the KapB-mediated SF formation could be uncoupled from KapB-mediated PB disassembly, the downstream effectors of RhoA known to control SF formation were interrogated for their role in PB disassembly. The effector mDia1 (gene name: *DIA1*) is a formin that contributes to actin polymerization and SF formation; mDia1 was knocked down using shRNAs in cells that expressed KapB, and the number of Hedls puncta was examined using CellProfiler (Figure 3.2). The designed shRNAs effectively reduced steady-state levels of mDia1 protein, as determined by immunoblotting for mDia1 (Figure 3.2 (A)). The knockdown of mDia1 did not eliminate SF formation (Figure 3.2 (B)) but, instead, increased elongated cells with SFs across the cell in both vector and KapB conditions. Knockdown of mDia1 increased Hedls puncta counts in both vector and KapB-expressing cells (Figure 3.2 (B, C)). Both mDia1-targeting shRNAs resulted in increased numbers of Hedls puncta per cell, with shDIA1-1 showing a much more robust effect. The difference in Hedls puncta counts between shRNAs is likely explained by knockdown efficiency, because shDIA1-1 decreased mDia1 protein level more effectively (Figure 3.2 (A)).

Importantly, to ensure that the loss of mDia1 was not increasing Hedls puncta irrespective of KapB expression but rather that mDia1 contributed specifically to KapB-mediated PB disassembly, the ratio of KapB to vector Hedls puncta per cell within each treatment was calculated (Figure 3.2 (D)). The ratio informs whether KapB is still able to disassemble Hedls puncta with the treatment applied; if the ratio is restored to ≥1, it indicates that KapB is no longer able to disassemble Hedls puncta in comparison to the vector control, thus indicating that the protein/process targeted by the treatment contributes directly to KapB-mediated Hedls puncta disassembly. Conversely, if the ratio is maintained around 0.4 to 0.6, KapB is still disassembling Hedls puncta even in the context of the treatment, indicating that though the basal level of Hedls puncta may be changed, the protein targeted is not involved in KapB-mediated Hedls puncta disassembly specifically. With mDia1 knockdown, the ratio of puncta in the treatment was restored to 1, as there is no difference between vector and KapB Hedls puncta counts in the absence of mDia1. Therefore, mDia1 contributes to KapB-mediated PB disassembly specifically.

This ratio will be reported in subsequent figures to ensure that the treatment applied changes KapB-mediated PB disassembly specifically and is not just changing global Hedls puncta counts.

To assess if other mDia isoforms that have not been implicated in SF formation play a role in KapB-mediated PB disassembly, mDia3 (gene name: DIA2) known to control chromosome alignment (Yasuda et al. 2004), was knocked down using targeted shRNAs (Figure 3.3 (A)). Unlike mDia1, mDia3 knockdown did not restore Hedls puncta counts in KapB-expressing cells and decreased puncta counts in vector cells (Figure 3.3 (B, C, D)). mDia3 knockdown resulted in elongated actin SF across the center of the cell (Figure 3.3 (B)).

Another principal RhoA-effector that mediates SF formation is ROCK (Watanabe et al. 1999). Inhibition of both isoforms of ROCK, 1 and 2, with a chemical inhibitor (Ishizaki et al. 2000) restored Hedls puncta counts in KapB-expressing cells (Figure 3.4 (A, B)). ROCK inhibition decreased Hedls puncta counts in vector cells and increased the ratio of KapB to vector Hedls puncta to greater than 1 (Figure 3.4 (A, B, C)), indicating ROCK plays a role in KapB-mediated PB disassembly specifically. Treatment with the ROCK inhibitor eliminated SFs. Cells had scalloped edges, minimal cortical actin and an apparent lack of fibre organization compared to control cells (Figure 3.4 (A)).

Both isoforms of ROCK control SF formation through modulation of actin fibre stability via cofilin inhibition and actomyosin contractility (Watanabe et al. 1999). ROCK1 primarily mediates actomyosin contractility, while ROCK2 mediates both actomyosin contractility as well as inhibition of cofilin to increase actin fibre stability (Yoneda, Multhaupt, and Couchman 2005; Shi et al. 2013). To examine the role of each ROCK isoform in the disassembly of PBs, isoform-specific shRNAs were designed. Immunoblot analysis confirmed that all shRNAs knocked down the isoforms for which they were designed (Figure 3.5 (A)). However, two shRNAs (shROCK1-1 and shROCK2-1), also increased the protein level of the non-targeted isoform, suggesting a cellular mechanism exists that is capable of compensating for ROCK1/2 loss via increased production of the alternative isoform (Figure 3.5 (A)). The other two shRNAs (shROCK1-2 and shROCK2-2) decreased protein levels of both isoforms, suggesting lower levels of specificity by these constructs (Figure 3.5 (A)). The actin phenotypes with

ROCK1/2 knockdown were varied, with shROCK1-1, shROCK1-2 and shROCK2-1 showing phenotypes similar to those observed with ROCK inhibitor treatment, resulting in primarily cortical actin and warped cell edges (Figure 3.6 (A)). An exception to this was shROCK2-2 which induced robust fibres across the center of the cell (Figure 3.6 (A)). All shRNAs restored Hedls puncta counts in KapB-expressing cells and restored the KapB:vector ratio of Hedls puncta to 1 (Figure 3.6 (A, B, C)). The most robust PB restoration was observed with strong knockdown of ROCK2 (Figure 3.6 (A, B,C)). These data support the hypothesis that ROCK participates in KapB-mediated PB disassembly.

To investigate whether ROCK and mDia1 work synergistically to disassemble Hedls puncta in KapB-expressing cells, ROCK was inhibited in the context of mDia1 knockdown to see if combinatorial inhibition further restored the PB phenotype (Figure 3.7). I used shDIA1-1 to knock down mDia1 (Figure 3.7 (A)) and in combination, treated KD cells with the ROCK1/2 inhibitor. Separate mDia1 knockdown or treatment with the ROCK inhibitor restored Hedls puncta in KapB-expressing cells, as observed previously (Figure 3.7 (B, C, D)). The combination of shDIA1-1 plus ROCK inhibitor restored Hedls puncta in KapB-expressing cells to a level that was slightly higher to mDia1 KD alone (Figure 3.7 (B, C, D)). It is unclear whether this is a significant effect.

There is a strong body of literature demonstrating that ROCK acts as a multifunctional kinase (Julian and Olson 2014), that controls many phenotypes in addition to actin dynamics. To determine if KapB-mediated PB disassembly required ROCK1/2 because of its role as an actin regulator, I explored downstream ROCK targets that modulate cytoskeletal behavior. ROCK can phosphorylate and activate LimK, which will then phosphorylate and inactivate cofilin, an actin-severing protein (Ohashi et al. 2000). To investigate the role of cofilin in KapB-mediated PB disassembly, shRNAs to knockdown cofilin expression were used (Figure 3.8 (A)). Since ROCK activation results in less cofilin activity and reduced actin severing, I hypothesized that knockdown of cofilin in KapB-expressing cells would augment KapB-mediated PB disassembly. Knockdown of cofilin resulted in elongated cells with more SFs (Figure 3.8 (B)). Excluding one outlier, cofilin-knockdown alone disassembled Hedls puncta in vector cells and augmented Hedls puncta disassembly in KapB-expressing cells (Figure 3.8 (B, C, D)). This indicates that an inhibition of cofilin activity disassembles PBs. This supports

the hypothesis that KapB is likely inactivating cofilin through ROCK-mediated signalling, and by further reducing cofilin activity, PB disassembly can be enhanced.

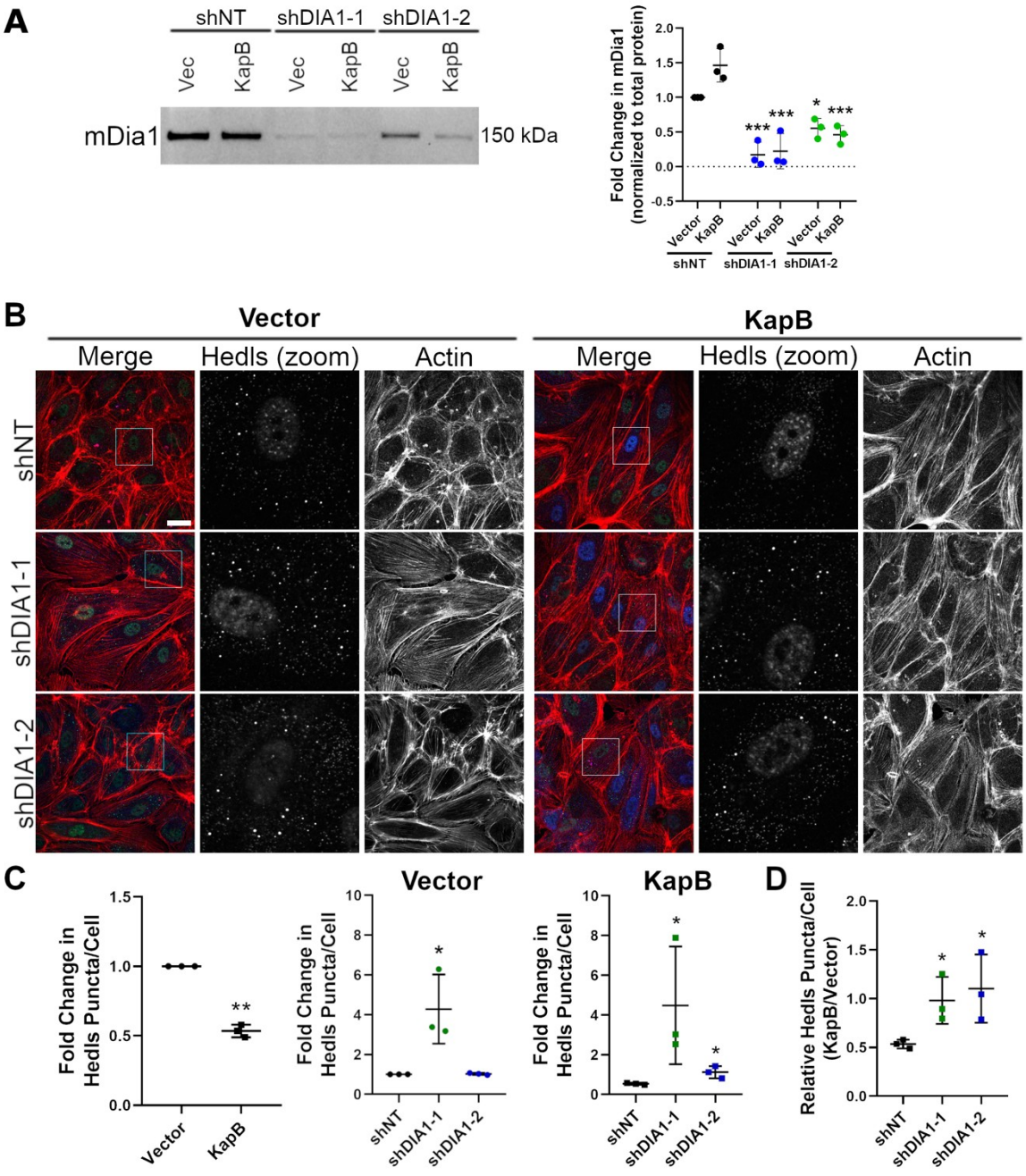
A
shNT
shDIA1-1
shDIA1-2
Vec
KapB
mDia1
150 kDa
Fold Change in mDia1 (normalized to total protein)
Vector
KapB
shNT
shDIA1-1
shDIA1-2
B
Vector
KapB
Merge
HedIs (zoom)
Actin
shNT
shDIA1-1
shDIA1-2
C
Fold Change in HedIs Puncta/Cell
Vector
KapB
shNT
shDIA1-1
shDIA1-2
D
Relative HedIs Puncta/Cell (KapB/Vector)

**Figure 3.2: Knockdown of mDia1 restores Hedls puncta in KapB-expressing cells.** HUVECs were transduced with KapB-expressing and empty vector lentivirus then selected with 5 $\mu$g/mL blasticidin. Cells were then transduced with shRNAs targeting mDia1 (shDIA1-1, shDIA1-2) or with a non-targeting (shNT) control and selected with 1 $\mu$g/mL puromycin. In parallel, cells were fixed for immunofluorescence or lysed for immunoblotting. (A) Representative blot and quantification of lysates immunoblotted using an antibody to mDia1. mDia1 protein levels in each condition were normalized to total protein (not shown). All treatments were normalized to vector NT control. (B) Representative images of cells stained for PB-resident protein Hedls (green), KapB (blue), and F-actin (red, phalloidin). Boxes indicate the area of the field of view that is shown in Hedls (zoom) panel. Scale bar represents 20 $\mu$m. (C, D) Fixed cells were stained for CellProfiler analysis as detailed in the methods. (C) The number of Hedls puncta per cell was quantified and normalized to the vector NT control. (D) CellProfiler data was used to calculate the ratio of Hedls puncta count in KapB-expressing cells versus the vector control for each treatment condition. Error bars represent standard deviation. Statistics were determined using a ratio paired t-test, n=3, $p < 0.05$.

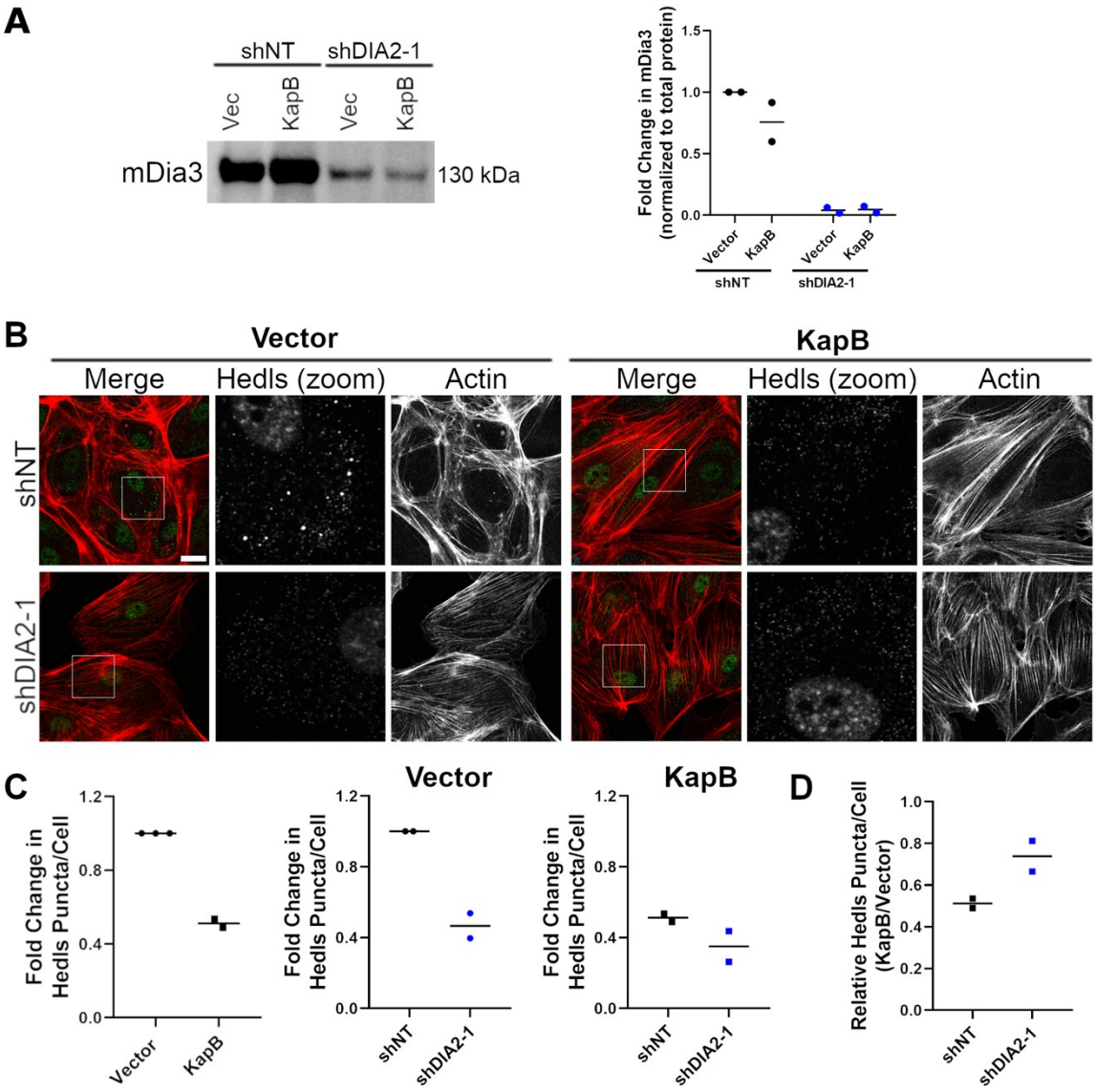
A
shNT
shDIA2-1
Vec
KapB
Vec
KapB
mDia3
130 kDa
Fold Change in mDia3 (normalized to total protein)
1.5
1.0
0.5
0.0
Vector
KapB
Vector
KapB
shNT
shDIA2-1
B
Vector
KapB
Merge
Hedls (zoom)
Actin
Merge
Hedls (zoom)
Actin
shNT
shDIA2-1
C
Fold Change in Hedls Puncta/Cell
1.2
0.8
0.4
0.0
Vector
KapB
Vector
Fold Change in Hedls Puncta/Cell
shNT
shDIA2-1
KapB
Fold Change in Hedls Puncta/Cell
shNT
shDIA2-1
D
Relative Hedls Puncta/Cell (KapB/Vector)
1.0
0.8
0.6
0.4
0.2
0.0
shNT
shDIA2-1

**Figure 3.3: Knockdown of mDia3 does not restore Hedls puncta in KapB-expressing cells.** HUVECs were transduced with KapB-expressing and empty vector lentivirus then selected with 5 $\mu$g/mL blasticidin. Cells were then transduced with shRNAs targeting mDia3 (shDIA2-1) or with a non-targeting (shNT) control and selected with 1 $\mu$g/mL puromycin. In parallel, cells were fixed for immunofluorescence or lysed for immunoblotting. (A) Representative blot and quantification of lysates immunoblotted using an antibody to mDia3. mDia3 protein levels in each condition were normalized to total protein (not shown). All treatments were normalized to vector NT control. (B) Representative images of cells stained for PB-resident protein Hedls (green), KapB (blue), and F-actin (red, phalloidin). Boxes indicate images shown in Hedls (zoom) panel. Scale bar represents 20 $\mu$m. (C, D) Fixed cells were stained for CellProfiler analysis as detailed in the methods. (C) The number of Hedls puncta per cell was quantified and normalized to the vector NT control. (D) CellProfiler data was used to calculate the ratio of Hedls puncta count in KapB-expressing cells versus the vector control for each treatment condition. CellProfiler quantification is representative of two independent experiments.

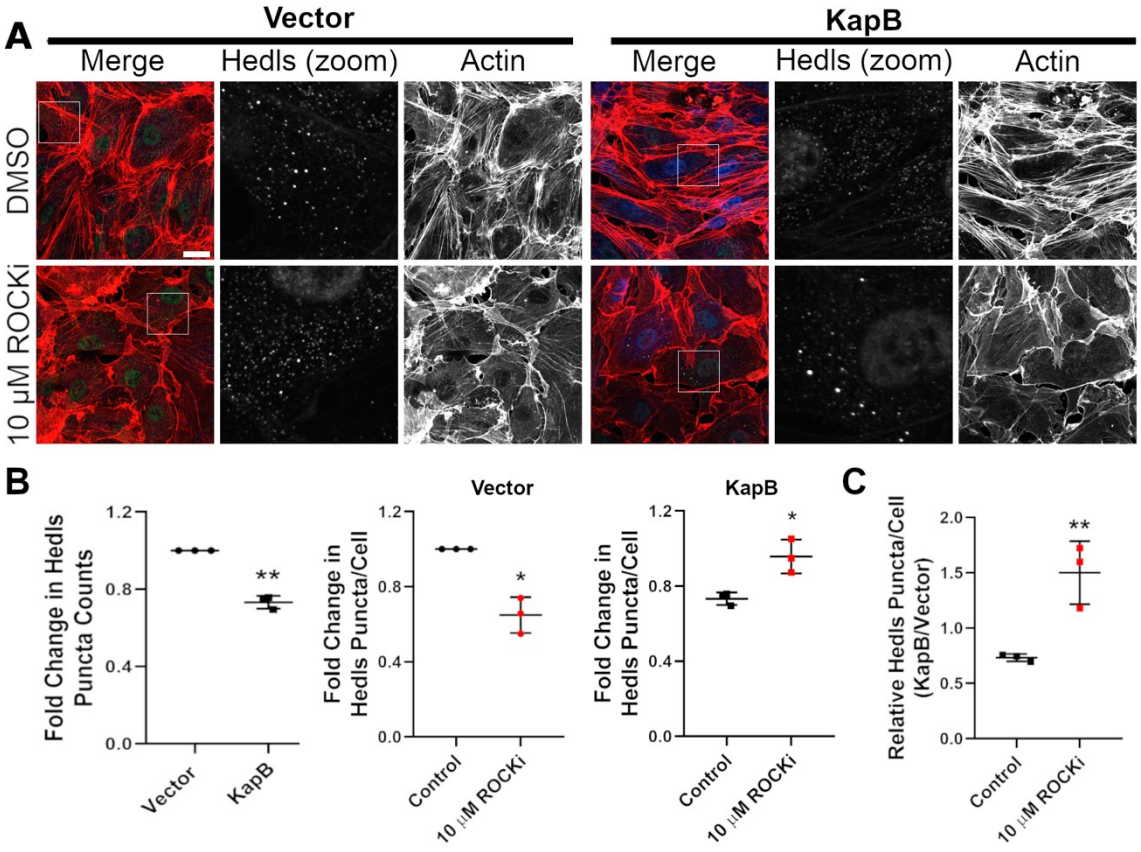


**Figure 3.4: Inhibition of ROCK isoforms restores Hedls puncta in KapB-expressing cells.** HUVECs were transduced with KapB-expressing and empty vector lentivirus and selected with 5 $\mu$g/mL blasticidin. Cells were treated with 10 ∝M Y-27632 (inhibitor of both ROCK1 and ROCK2 [ROCKi]) or water control for 4 h and fixed for immunofluorescence. (A) Representative images of cells stained for PB-resident protein Hedls (green), KapB (blue), and F-actin (red, phalloidin). Boxes indicate images shown in Hedls (zoom) panel. Scale bar represents 20 $\mu$m. (B, C) Fixed cells were stained for CellProfiler analysis as detailed in the methods. (B) The number of Hedls puncta per cell was quantified and normalized to the vector NT control. (C) CellProfiler data was used to calculate the ratio of Hedls puncta count in KapB-expressing cells versus the vector control for each treatment condition. Error bars represent standard deviation. Statistics were determined using a ratio paired t-test, n=3, $p < 0.05$.

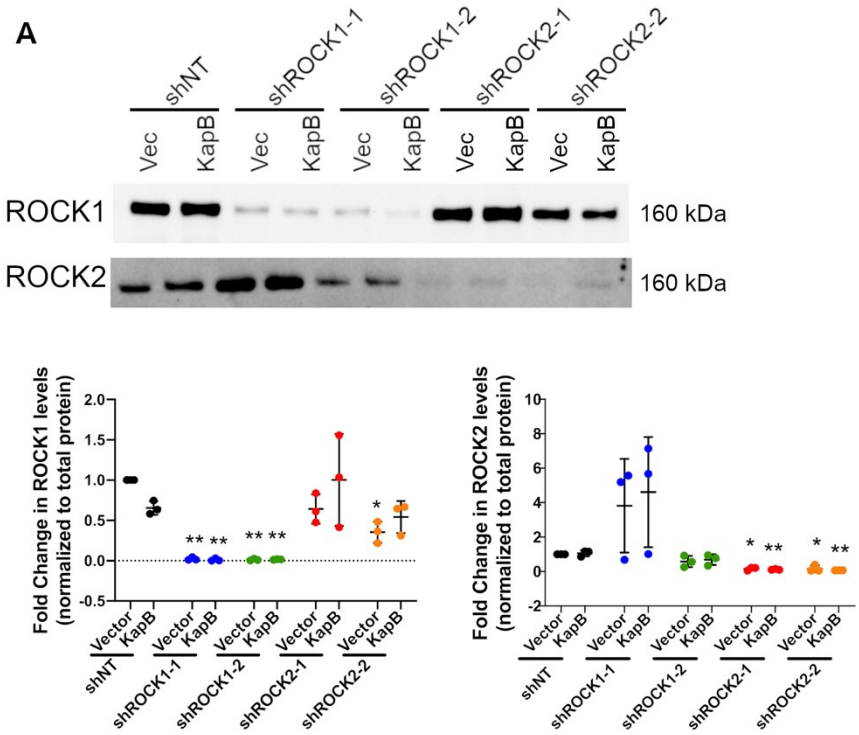


**Figure 3.5: Protein levels of ROCK1 and ROCK2 are reduced with targeted shRNAs.** HUVECs were transduced with KapB-expressing and empty vector lentivirus and selected with 5 $\mu$g/mL blasticidin. Cells were then transduced with shRNAs targeting ROCK1 and ROCK2 (shROCK1-1, shROCK1-2, shROCK2-1, shROCK2-2) or with a non-targeting (shNT) control and selected with 1 $\mu$g/mL puromycin. Cells were lysed for immunoblotting. (A) Representative blot and quantification of lysates immunoblotted using an antibody to ROCK1 or ROCK2. ROCK1/2 protein levels in each condition were normalized to total protein (not shown). All treatments were normalized to vector NT control. Error bars represent standard deviation. Statistics were determined using a ratio paired t-test, n=3, $p < 0.05$.

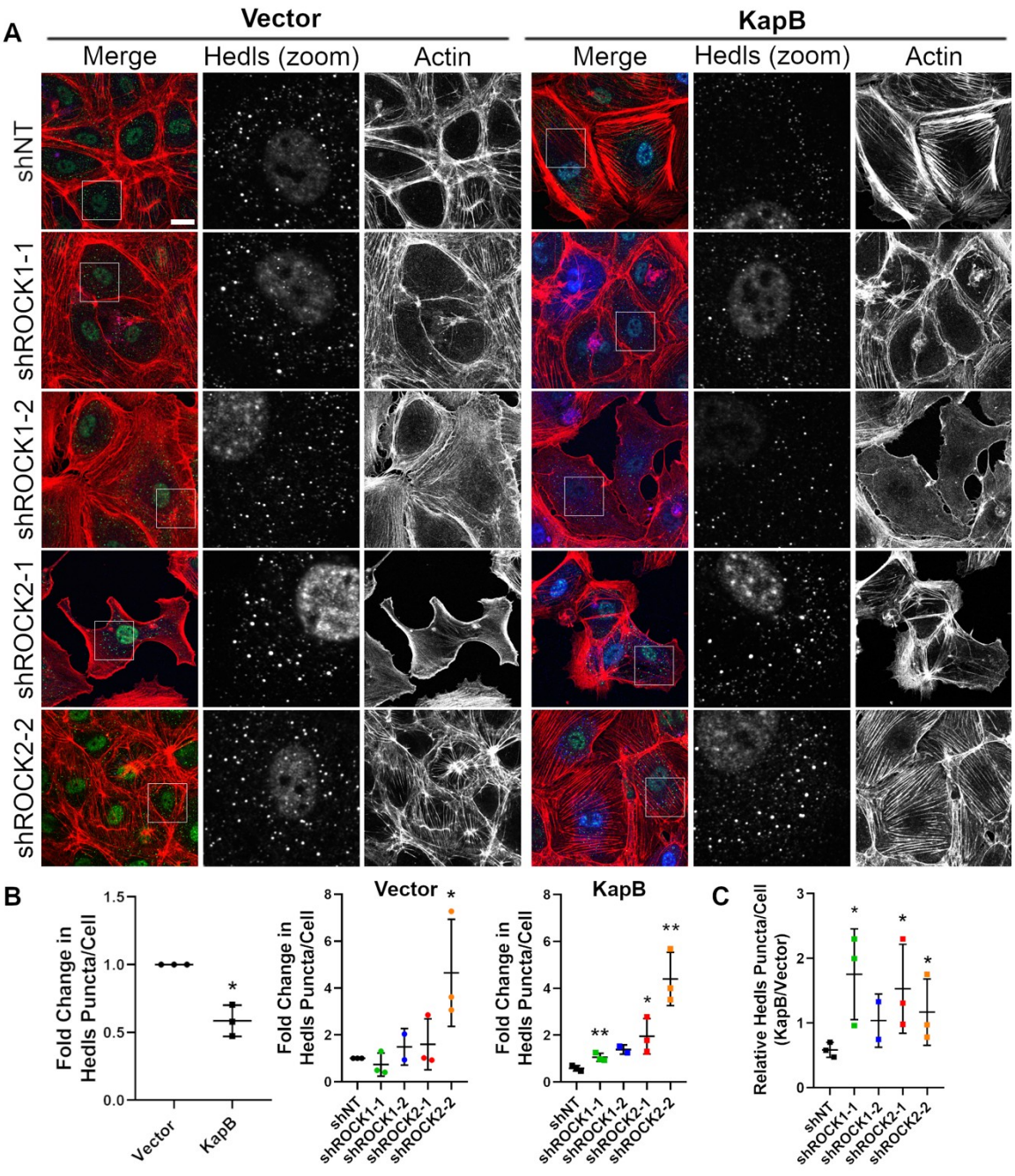
A
Vector
KapB
Merge
Hedls (zoom)
Actin
shNT
shROCK1-1
shROCK1-2
shROCK2-1
shROCK2-2
B
Fold Change in Hedls Puncta/Cell
Vector
KapB
C
Relative Hedls Puncta/Cell (KapB/Vector)

**Figure 3.6: Knockdown of ROCK1 or ROCK2 restores Hedls puncta in KapB-expressing cells.** HUVECs were transduced with KapB-expressing and empty vector lentivirus and selected with 5 $\mu$g/mL blasticidin. Cells were then transduced with shRNAs targeting ROCK1 and ROCK2 (shROCK1-1, shROCK1-2, shROCK2-1, shROCK2-2) or with a non-targeting (shNT) control and selected with 1 $\mu$g/mL puromycin. Cells were fixed for immunofluorescence. (A) Representative images of cells stained for PB-resident protein Hedls (green), KapB (blue), and F-actin (red, phalloidin). Boxes indicate images shown in Hedls (zoom) panel. Scale bar represents 20 $\mu$m. (B, C) Fixed cells were stained for CellProfiler analysis as detailed in the methods. (B) The number of Hedls puncta per cell was quantified and normalized to the vector NT control. (C) CellProfiler data was used to calculate the ratio of Hedls puncta count in KapB-expressing cells versus the vector control for each treatment condition. Error bars represent standard deviation. Statistics were determined using a ratio paired t-test, n=3, except shROCK1-2, $p < 0.05$.

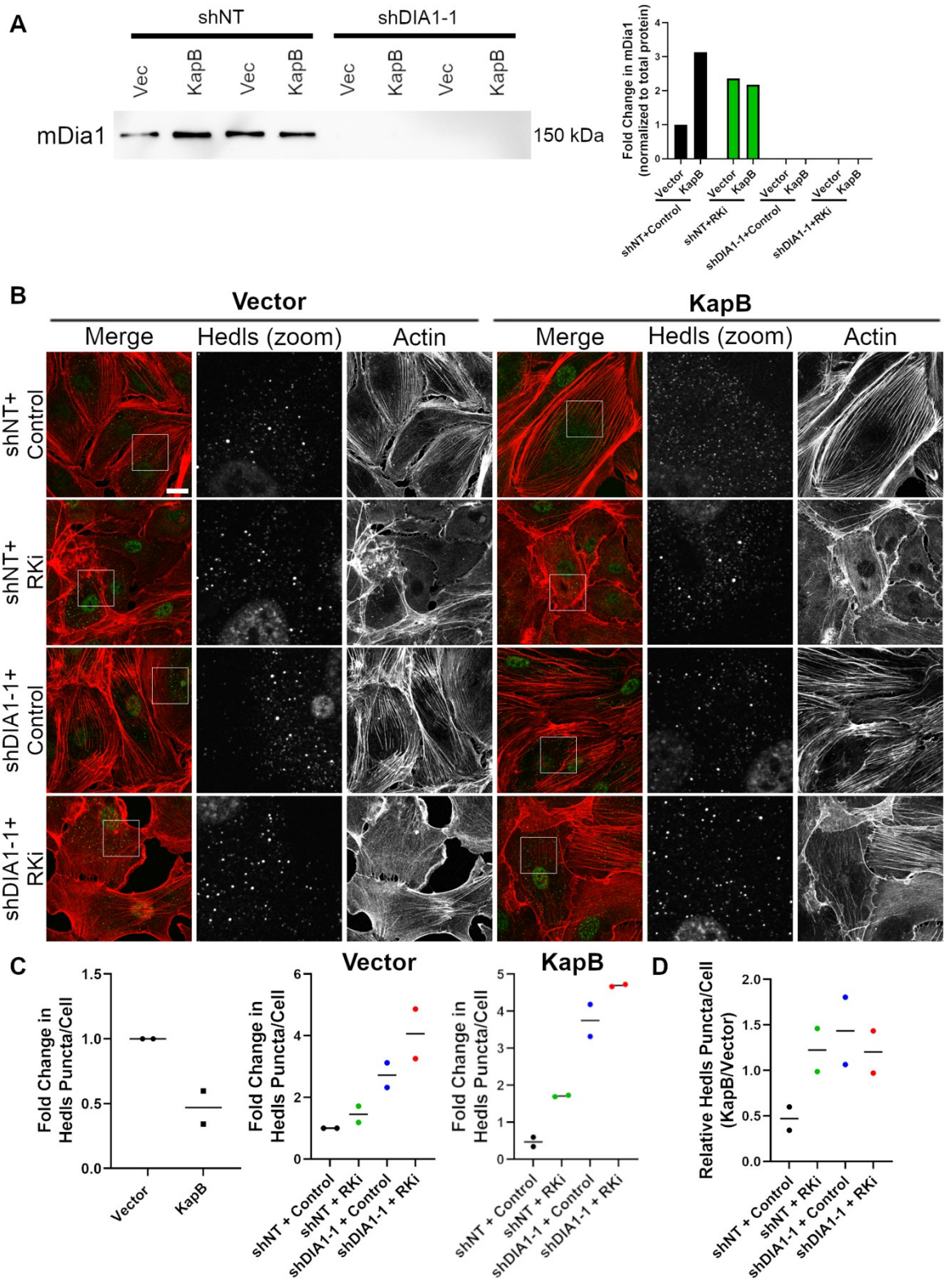
A
shNT
shDIA1-1
Vec
KapB
Vec
KapB
Vec
KapB
Vec
KapB
mDia1
150 kDa
Fold Change in mDia1 (normalized to total protein)
Vector
KapB
shNT+Control
shNT+RKi
shDIA1-1+Control
shDIA1-1+RKi
B
Vector
KapB
Merge
Hedls (zoom)
Actin
shNT+ Control
shNT+ RKi
shDIA1-1+ Control
shDIA1-1+ RKi
C
Fold Change in Hedls Puncta/Cell
Vector
KapB
shNT + Control
shNT + RKi
shDIA1-1 + Control
shDIA1-1 + RKi
D
Relative Hedls Puncta/Cell (KapB/Vector)

**Figure 3.7: Combined inhibition of mDia1 and ROCK may further enhance Hedls puncta restoration.** HUVECs were transduced with KapB-expressing and empty vector lentivirus then selected with 5 $\mu$g/mL blasticidin. Cells were then transduced with shRNAs targeting mDia1 (shDIA1-1) or with a non-targeting (shNT) control and selected with 1 $\mu$g/mL puromycin. Selected cells were treated with 10 ∝M Y-27632 (RKi) or water control for 4 h and fixed for immunofluorescence or lysed for immunoblotting. (A) Representative blot and quantification of lysates immunoblotted using an antibody to mDia1. mDia1 protein levels in each condition were normalized to total protein (not shown). All treatments were normalized to vector NT control. N=1. (B) Representative images of cells stained for PB-resident protein Hedls (green), KapB (blue), and F-actin (red, phalloidin). Boxes indicate images shown in Hedls (zoom) panel. Scale bar represents 20 $\mu$m. (C, D) Fixed cells were stained for CellProfiler analysis as detailed in the methods. (C) The number of Hedls puncta per cell was quantified and normalized to the vector NT control. (D) CellProfiler data was used to calculate the ratio of Hedls puncta count in KapB-expressing cells versus the vector control for each treatment condition. CellProfiler quantification is representative of two independent experiments.

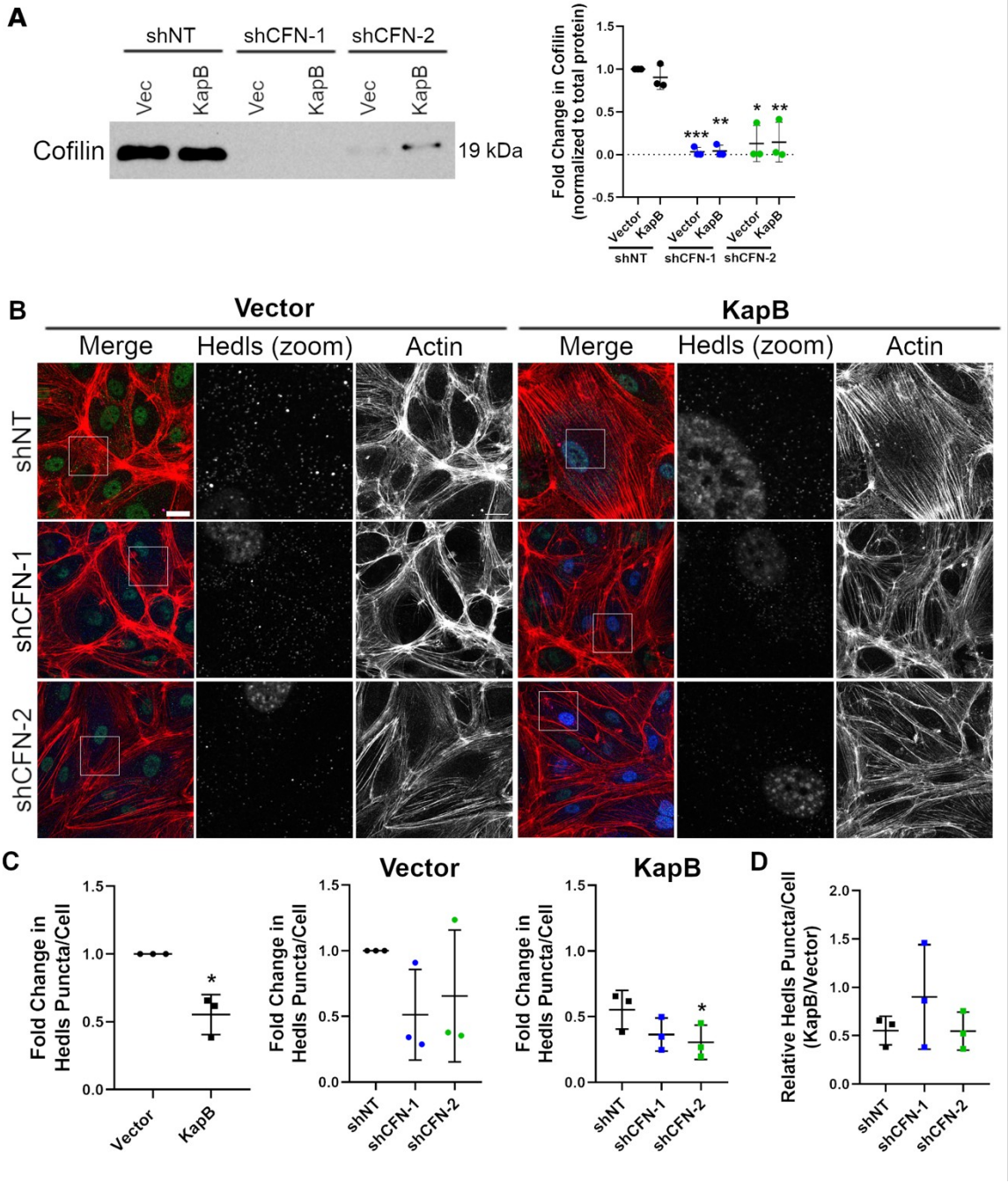
A
shNT
shCFN-1
shCFN-2
Vec
KapB
Cofilin
19 kDa
Fold Change in Cofilin (normalized to total protein)
Vector
KapB
shNT
shCFN-1
shCFN-2
B
Vector
KapB
Merge
Hedls (zoom)
Actin
shNT
shCFN-1
shCFN-2
C
Fold Change in Hedls Puncta/Cell
D
Relative Hedls Puncta/Cell (KapB/Vector)

**Figure 3.8: Knockdown of cofilin enhances KapB-mediated Hedls puncta disassembly.** HUVECs were transduced with KapB-expressing and empty vector lentivirus then selected with 5 $\mu$g/mL blasticidin. Cells were then transduced with shRNAs targeting cofilin (shCFN1-1, shCFN1-2) or with a non-targeting (shNT) control and selected with 1 $\mu$g/mL puromycin. In parallel, cells were fixed for immunofluorescence or lysed for immunoblotting. (A) Representative blot and quantification of lysates immunoblotted using an antibody to cofilin. Cofilin protein levels in each condition were normalized to total protein (not shown). All treatments were normalized to vector NT control. (B) Representative images of cells stained for PB-resident protein Hedls (green), KapB (blue), and F-actin (red, phalloidin). Boxes indicate images shown in Hedls (zoom) panel. Scale bar represents 20 $\mu$m. (C, D) Fixed cells were stained for CellProfiler analysis as detailed in the methods. (C) The number of Hedls puncta per cell was quantified and normalized to the vector NT control. (D) CellProfiler data was used to calculate the ratio of Hedls puncta count in KapB-expressing cells versus the vector control for each treatment condition. Error bars represent standard deviation. Statistics were determined using a ratio paired t-test, n=3, $p < 0.05$.

### 3.3 α-actinin-4 is Required for KapB-Mediated PB Disassembly

The signalling controlling SF formation could not be uncoupled from PB disassembly by targeting RhoA downstream effectors. As a next step, I decided to examine actin fibre bundling, an important component of SF structure, for its role in PB disassembly. α-actinin mediates the bundling of actin filaments to form SFs (Lazarides and Burridge 1975; Edlund, Lotano, and Otey 2001). Both non-muscle isoforms, α-actinin-1 and -4, were investigated. Since the localization of α-actinin-1 and α-actinin-4 is not well-defined in endothelial cells, I first confirmed the localization of both isoforms in HUVECs before investigating PB disassembly. Similar to other non-muscle cell types, α-actinin-1 was primarily localized to actin fibres and at the periphery of the cell, presumably at focal adhesions (Kovac 2010) (Figure 3.9 (A)). In contrast, α-actinin-4 could be observed tracing along the SF; however, it was largely diffuse throughout the cytoplasm and nucleus, congruent with other reports (Honda et al. 1998; Kovac 2010) (Figure 3.9 (B)).

To examine the requirement for actin bundling in KapB-mediated PB disassembly, shRNAs targeting α-actinin-1 and α-actinin-4 were used to knockdown protein levels of each isoform. All shRNAs were specific for the isoform for which they were designed (Figure 3.10 (A)). Knockdown of α-actinin-1 showed varied results, with one shRNA restoring Hedls puncta in KapB-expressing cells, while the other decreased Hedls puncta (Figure 3.11 (A, B, C)). In both α-actinin-1 knockdown conditions, cells were elongated, but only one shRNA (shACTN1-1) maintained SFs across the cell (Figure 3.11 (A)). The shRNA (shACTN1-1) that maintained SF across the cell body did not exhibit PB restoration. Knockdown of α-actinin-4 consistently restored Hedls puncta in KapB-expressing cells and cells exhibited dense SFs (Figure 3.11 (A, B, C)). In an attempt to more clearly discern the role of α-actinin-1 in PB regulation, I overexpressed α-actinin-1-GFP in HUVECs. Overexpression of α-actinin-1-GFP, in the absence of KapB, elicited disassembly of Hedls puncta (Figure 3.12 (A, B)). Taken together, the data indicate the non-muscle α-actinins can modulate PBs, though it is unclear whether α-actinin-1 contributes to KapB-mediated PB disassembly.

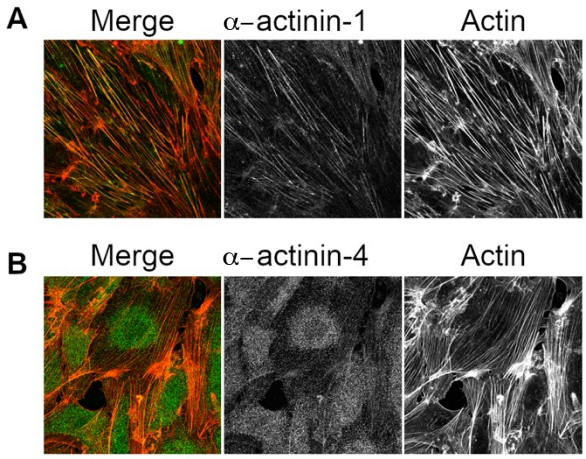


**Figure 3.9: α-actinin-1 localizes to SFs while α-actinin-4 is primarily found diffusely in the cytoplasm and nucleus.** Untreated HUVECs were fixed for immunofluorescence using antibodies to α−actinin-1 or α−actinin-4. N=1.

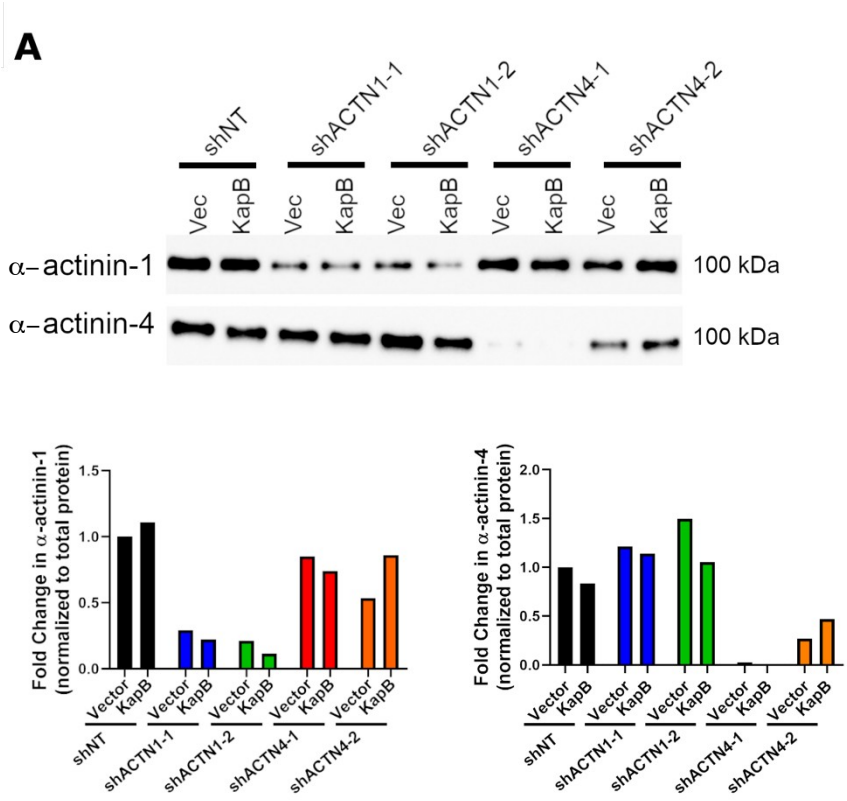


**Figure 3.10: Protein levels of α-actinin-1 and -4 are reduced using shRNAs.** HUVECs were transduced with KapB-expressing and empty vector lentivirus and selected with 5 $\mu$g/mL blasticidin. Cells were then transduced with shRNAs targeting ACTN1 and ACTN4 (shACTN1-1, shACTN1-2, shACTN4-1, shACTN4-2) or with a non-targeting (shNT) control and selected with 1 $\mu$g/mL puromycin. Cells were lysed for immunoblotting. (A) Representative blot and quantification of lysates immunoblotted using an antibody to α-actinin-1 or α-actinin-4. α-actinin-1 and α-actinin-4 protein levels in each condition were normalized to total protein (not shown). All treatments were normalized to vector NT control. N=1.

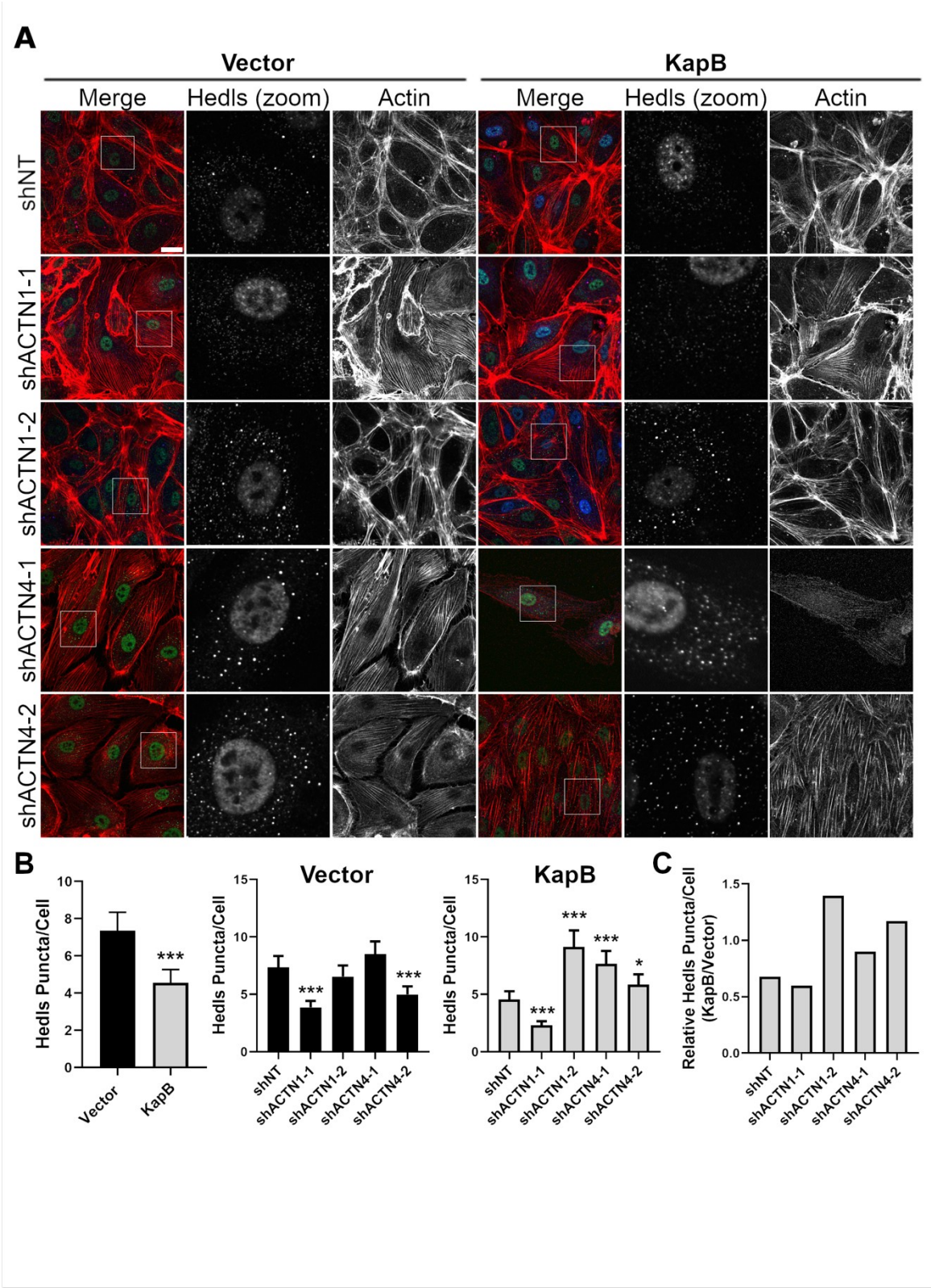
A
Vector
KapB
Merge
Hedls (zoom)
Actin
shNT
shACTN1-1
shACTN1-2
shACTN4-1
shACTN4-2
B
Hedls Puncta/Cell
Vector
KapB
shNT
shACTN1-1
shACTN1-2
shACTN4-1
shACTN4-2
C
Relative Hedls Puncta/Cell (KapB/Vector)

**Figure 3.11: Knockdown of α-actinin-4 restores Hedls puncta in KapB-expressing cells.** HUVECs were transduced with KapB-expressing and empty vector lentivirus and selected with 5 μg/mL blasticidin. Cells were then transduced with shRNAs targeting ACTN1 and ACTN4 (shACTN1-1, shACTN1-2, shACTN4-1, shACTN4-2) or with a non-targeting (shNT) control and selected with 1 μg/mL puromycin. Cells were fixed for immunofluorescence. (A) Representative images of cells stained for PB-resident protein Hedls (green), KapB (blue), and F-actin (red, phalloidin). Boxes indicate images shown in Hedls (zoom) panel. Scale bar represents 20 μm. (B, C) Fixed cells were stained for CellProfiler analysis as detailed in the methods. (B) The number of Hedls puncta per cell was quantified and normalized to the vector NT control. (C) CellProfiler data was used to calculate the ratio of Hedls puncta count in KapB-expressing cells versus the vector control for each treatment condition. Error bars represent 95% confidence interval. Statistics were determined using a negative binomial regression, $p < 0.05$. N=1.

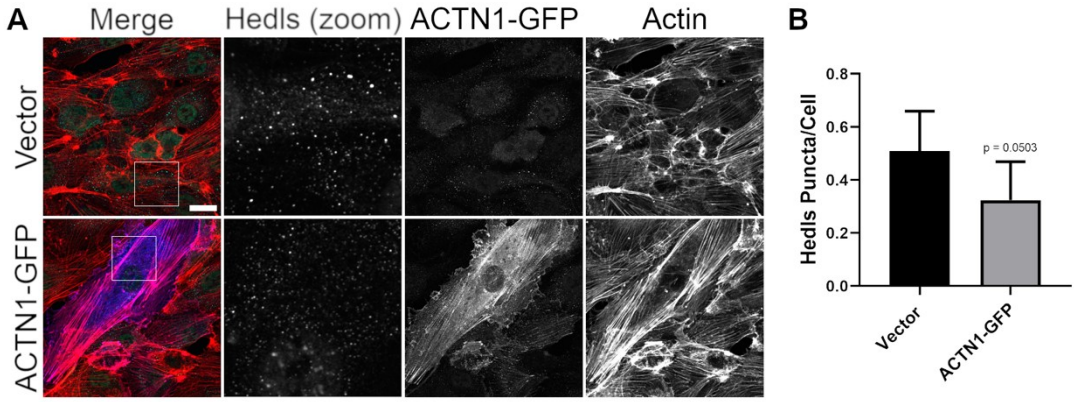


**Figure 3.12: Overexpression of α-actinin-1-GFP disassembles Hedls puncta in HUVECS.** HUVECs were transduced with α-actinin-1-GFP-expressing and empty vector lentivirus and selected with 1 μg/mL puromycin. Cells were fixed for immunofluorescence. (A) Representative images of cells stained for PB-resident protein Hedls (false-coloured green), α-actinin-1-GFP (false-coloured blue), and F-actin (red, phalloidin). Boxes indicate images shown in Hedls (zoom) panel. Scale bar represents 20 μm. (B) Fixed cells were stained for CellProfiler analysis as detailed in the methods. The number of Hedls puncta per cell was quantified and normalized to the vector control. CellProfiler quantification is representative of one independent experiment. Error bars represent 95% confidence interval. Statistics were determined using a negative binomial regression, $p < 0.05$. N=1.

### 3.4 Actin Contractility is Required for PB Disassembly

Since signalling controlling SF formation was required for PB disassembly, one of the functional consequences of SF formation was examined: actomyosin contractility. NMII is incorporated into SF bundles and, when phosphorylated, results in contraction of the fibres (Peterson et al. 2004). To determine if SF contractility is important for KapB-mediated PB disassembly, KapB-expressing cells were treated with blebbistatin, which inhibits NMII-mediated actomyosin contractility (Kovacs et al. 2004). Treatment of KapB-expressing cells with blebbistatin restored both Hedls puncta levels in KapB-expressing cells, as well as the KapB:vector ratio of Hedls puncta, indicating that contractility is required for KapB-induced PB disassembly (Figure 3.13 (A, B, C)). There were no significant changes in the actin cytoskeleton after blebbistatin treatment (Figure 3.13 (A)). In parallel, lysates from blebbistatin-treated cells were immunoblotted for DCP1a, a PB protein previously observed to decrease after expression of KapB (Robinson, unpublished). These data showed that blebbistatin treatment increased DCP1a steady-state protein levels relative to vehicle-treated KapB-expressing cells (Figure 3.13 (D)).

These data point to the downstream function of actin SFs, actomyosin contractility, as an essential signal that elicits PB disassembly. To determine if contraction would elicit the same phenotype in the absence of KapB, I treated cells with Calyculin A (CalA), an inhibitor of MLC phosphatase that induces NMII activity and actomyosin contraction (Asano and Mabuchi 2001). Inducing contraction with CalA decreased counts of Hedls puncta, supporting the hypothesis that actomyosin contractility controls PB disassembly (Figure 3.14 (A, B)). KapB may be dispersing PBs through induction of actin cytoskeleton contraction.

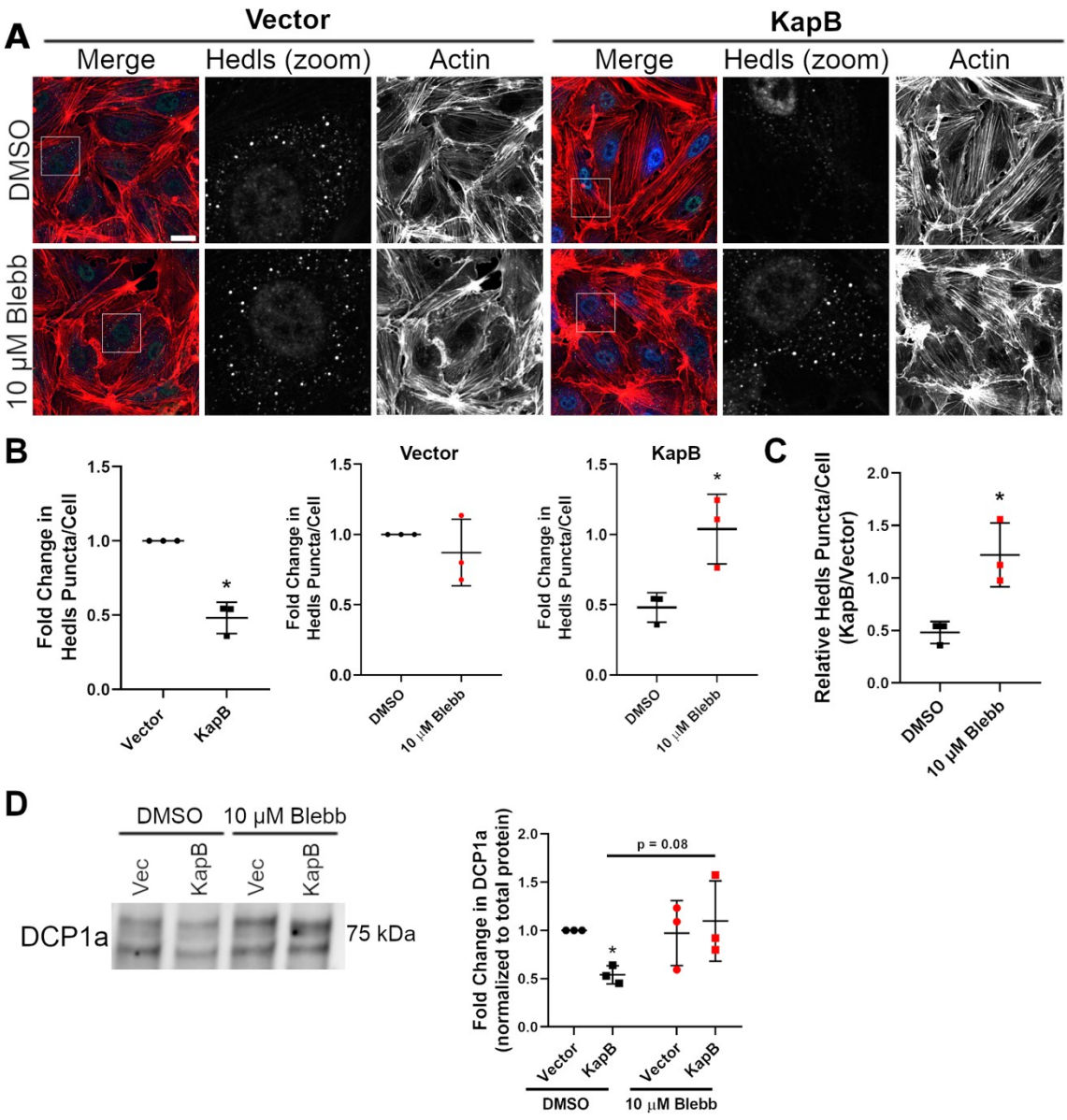
A
Vector
KapB
Merge
Hedls (zoom)
Actin
DMSO
10 μM Blebb
B
Fold Change in Hedls Puncta/Cell
Vector
KapB
DMSO
10 μM Blebb
C
Relative Hedls Puncta/Cell (KapB/Vector)
D
DMSO
10 μM Blebb
Vec
KapB
DCP1a
75 kDa
Fold Change in DCP1a (normalized to total protein)
p = 0.08

**Figure 3.13: Inhibition of actin contractility restores Hedls puncta in KapB-expressing cells.** HUVECs were transduced with KapB-expressing and empty vector lentivirus and selected with 5 $\mu$g/mL blasticidin. In parallel, cells were treated with 10 ∝M blebbistatin or DMSO for 30 min and fixed for immunofluorescence or lysed for immunoblotting. (A) Representative images of cells stained for PB-resident protein Hedls (green), KapB (blue), and F-actin (red, phalloidin). Boxes indicate images shown in Hedls (zoom) panel. Scale bar represents 20 $\mu$m. (B, C) Fixed cells were stained for CellProfiler analysis as detailed in the methods. (B) The number of Hedls puncta per cell was quantified and normalized to the vector NT control. (C) CellProfiler data was used to calculate the ratio of Hedls puncta count in KapB-expressing cells versus the vector control for each treatment condition. (D) Representative blot and quantification of lysates immunoblotted with antibodies specific to the PB-resident protein DCP1a. DCP1a protein levels in each condition were normalized to total protein (not shown). All treatments were normalized to vector DMSO control. Error bars represent standard deviation. Statistics were determined using a ratio paired t-test, n=3, $p < 0.05$.

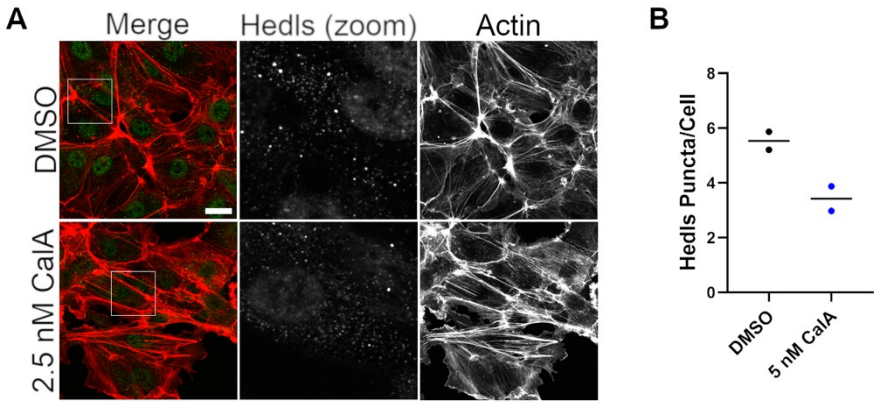


**Figure 3.14: Stimulation of actin contractility disassembles Hedls puncta.** HUVECs were treated with Calyculin A (CalA) or DMSO for 20 min and fixed for immunofluorescence. (A) Representative images of cells treated with 2.5 nM CalA and stained for PB-resident protein Hedls (green) and F-actin (red, phalloidin). Boxes indicate images shown in Hedls (zoom) panel. Scale bar represents 20 $\mu$m. (B) Cells treated with 5 nM CalA or DMSO were fixed and stained for CellProfiler analysis as detailed in the methods. Hedls puncta per cell were quantified. CellProfiler quantification is representative of two independent experiments.

### 3.5 Alteration to the Ratio of F:G-Actin Does Not Cause PB Disassembly

G-actin can act as a signalling molecule. This is illustrated by the observation that changes in the availability of G-actin monomers elicit activation of SRF response elements (Sotiropoulos et al. 1999). We wondered if KapB induced loss of monomeric G-actin and if this change controlled PB disassembly. To determine if KapB expression increased the F:G-actin ratio because it induced actin polymerization, KapB-expressing HUVECs were lysed in cold F-actin stabilization buffer, and the F- and G-actin fractions were separated using ultracentrifugation. As expected, there was an increase in the F-actin fraction in KapB-expressing cells (Figure 3.15 (A, C)). Jasplakinolide (Jasp), which increases the F-actin fraction in cells (Bubb et al. 1999), was used as a control to ensure proper separation of F- and G-actin fractions (Figure 3.15 (B, D)). To test whether PBs were controlled by the availability of G-actin, cells were treated with chemicals altering F:G-actin ratios in the absence of KapB, and Hedls puncta were quantified. Jasp treatment increases the F-actin fraction through facilitating actin nucleation resulting in aberrant polymerization of actin (Figure 3.16 (A), Bubb et al. 1999). If G-actin levels control PB disassembly, decreasing the availability of G-actin with Jasp would mimic effect of KapB, and should also result in PB disassembly. This was not observed, as treatment with Jasp increased Hedls puncta per cell (Figure 3.16 (B)), indicating that decreasing the availability of monomeric G-actin does not disassemble Hedls puncta. The actin polymerization inhibitor Latrunculin B (LatB) binds to G-actin monomers directly, preventing their incorporation into F-actin (Morton, Ayscough, and McLaughlin 2000; Wakatsuki et al. 2001). Similarly, the actin polymerization inhibitor Cytochalasin D (CytD) caps the barbed end of actin filaments, preventing further elongation of the actin filament (Wakatsuki et al. 2001). Treatment of cells with either LatB or CytD increases the availability of monomeric G-actin in the cell (Figure 3.16 (A)). CytD, like Jasp, also increased Hedls puncta in the cell, suggesting that the availability of G-actin is not a critical regulator of PB levels (Figure 3.16 (B)). LatB did not change the level of Hedls puncta in the cell. However, this may be due to the low effective concentration used for treatment, as it was difficult to find a concentration of LatB that visibly altered actin without causing cell loss. Overall, since both Jasp and CytD increased Hedls puncta in the cell, G-actin is not acting as the signalling molecule that elicits PB disassembly.

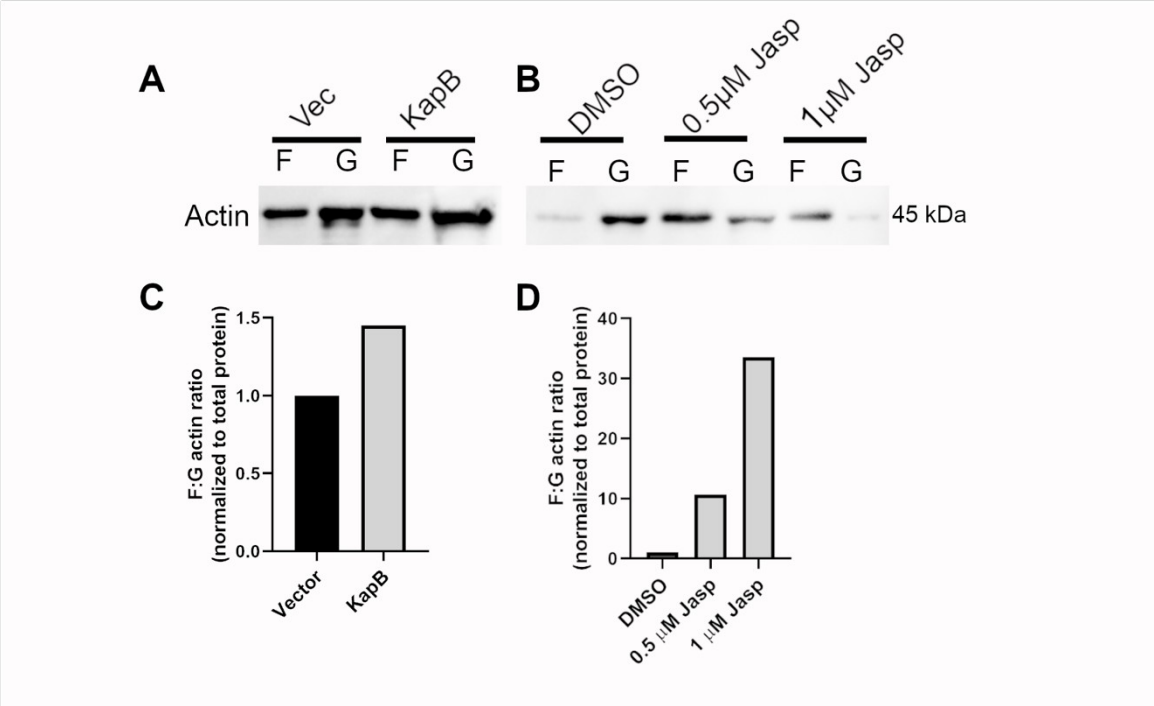


**Figure 3.15: KapB increases the F:G-actin ratio.** (A,C) HUVECs were transduced with KapB-expressing and empty vector lentivirus, selected with 5 $\mu$g/mL blasticidin and lysed for F-G actin fraction separation. (B,D) HUVECs were treated with 0.5 $\mu$M or 1 ∝M of the actin-polymerizing drug jasplakinolide (Jasp) or DMSO control for 30 min and lysed for F-actin fraction separation. (A,B) Representative immunoblot probed for β-actin. (C,D) Quantification of ratio of F:G actin from band intensity measurements normalized to Vector ratio. N=1.

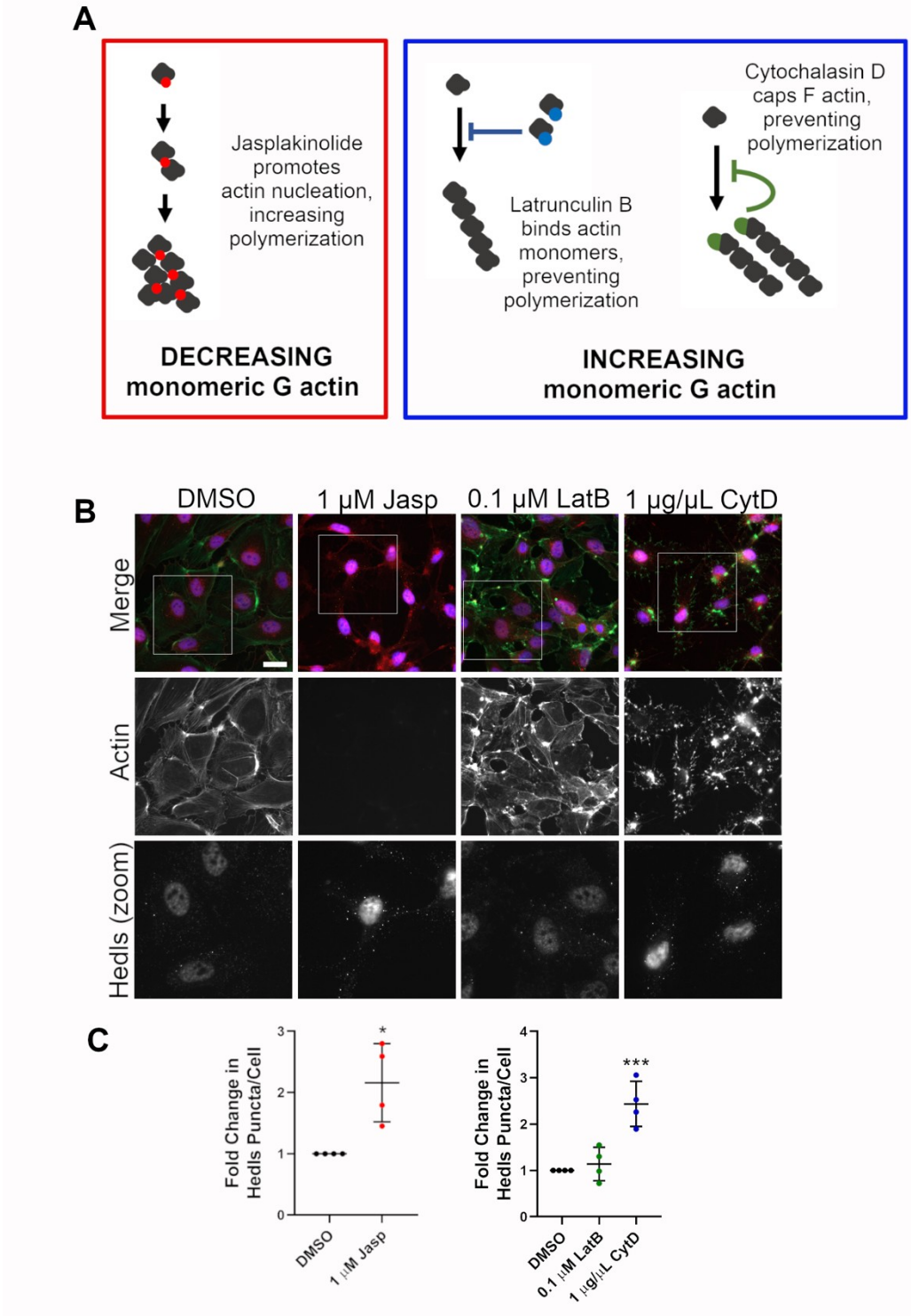
A
Jasplakinolide promotes actin nucleation, increasing polymerization
DECREASING monomeric G actin
Latrunculin B binds actin monomers, preventing polymerization
Cytochalasin D caps F actin, preventing polymerization
INCREASING monomeric G actin
B
DMSO
1 µM Jasp
0.1 µM LatB
1 µg/µL CytD
Merge
Actin
Hedls (zoom)
C
Fold Change in Hedls Puncta/Cell
DMSO
1 µM Jasp
0.1 µM LatB
1 µg/µL CytD

**Figure 3.16: Changes in the proportion of monomeric actin does not elicit PB disassembly.** (A) Diagram of mechanisms of action for jasplakinolide (Jasp), latrunculin B (LatB) and cytochalasin D (CytD). (B,C) HUVECs were treated with 1 ∝M Jasp to decrease monomeric G-actin, 0.1 $\mu$M LatB and 1 $\mu$g/$\mu$L CytD to increase monomeric G-actin or DMSO control for 30 min. (B) Representative CellProfiler images of cells stained for PB-resident protein Hedls (orange), actin (green), DAPI (blue), and wheat germ agglutinin (red). Boxes indicate images shown in Hedls (zoom) panel. Scale bar represents 30 $\mu$m. (C) Fixed cells were stained for CellProfiler analysis as detailed in the methods. The number of Hedls puncta per cell was quantified and normalized to the DMSO control. Error bars represent standard deviation. Statistics were determined using a ratio paired t-test, n=3, $p < 0.05$.

### 3.6 KapB Increases YAP Protein Levels

Following confirmation that SF and actomyosin contractility are required for PB disassembly, mechanoresponsive pathways that have been reported to respond to alterations in the actin cytoskeleton were investigated. A central regulator that responds to alterations in RhoA activity and cytoskeletal tension is the mechanoresponsive transcriptional regulator YAP (Dupont et al. 2011; Wada et al. 2011). To investigate if KapB altered YAP localization or phosphorylation status, KapB- and vector-transduced HUVECs were fixed for immunofluorescence and lysed for immunoblotting. KapB-expressing HUVECs showed increased levels of nuclear YAP, as well as increased total YAP intensity (Figure 3.17 (A, B, C)). This increase in both nuclear and total YAP was also seen in HeLa cells transfected with empty vector and KapB constructs (Figure 3.17 (D, E)). Phosphorylated YAP (P-YAP) is unable to enter the nucleus and is thus considered inactive (Zhao et al. 2007). In KapB-expressing cells, there was a decrease in the ratio of P-YAP to total YAP as measured by immunoblotting, suggesting a higher fraction of active YAP when KapB is expressed (Figure 3.17 (F, G)). There was also an increase in total cellular YAP levels, corroborating the increase in total YAP intensity seen by microscopy (Figure 3.17 (H)). Notably, despite the increase in total YAP protein levels, there was no change in YAP mRNA levels, suggesting that KapB may be preventing YAP degradation rather than driving its expression (Figure 3.17 (I)).

If YAP is dephosphorylated and nuclear, we would expect KapB expression to activate the transcription of endogenous genes known to respond to YAP. To investigate this, RNA was harvested from KapB- and vector-expressing HUVECs and RT-qPCR was performed for three YAP-responsive genes: connective tissue growth factor (CTGF), ankyrin repeat domain 1 (ANKRD1) and cysteine-rich angiogenic inducer 61 (CYR61) (Chen et al. 2013). These genes were chosen as they are conventionally-assayed to monitor YAP activation, including in the context of mechanical stressors (Chien et al. 2016; Dupont et al. 2011; Nakajima et al. 2017). Small increases (1.1- to 1.4-fold) of each gene were detected in KapB-expressing cells (Figure 3.18 (A, B, C)). Only increases in CTGF were significant. The positive control, a construct expressing constitutively active YAP (CA-YAP, serine to alanine mutations in the five YAP phosphorylation sites [Zhao et al. 2007]), increased all canonical YAP genes substantially (average 5- to 7-fold

increase). To confirm this result, HeLa cells were transduced with a high dose of KapB-expressing and vector lentivirus and the expression levels of these genes were measured again. Again, KapB-mediated increases of these canonical YAP activated genes was small, 1.1- to 1.4-fold (Figure 3.18 (D, E, F)).

### 3.7 YAP Is Required For PB Disassembly

After observing an upregulation of YAP expression in KapB-expressing cells, shRNAs targeting YAP genes were used to examine the role of YAP in PB disassembly (Figure 3.19 (A)). Genetic knockdown of YAP increased Hedls puncta in KapB-expressing cells and restored the ratio of KapB:vector Hedls puncta (Figure 3.19 (B, C, D)). Cells with YAP knockdown had primarily cortical actin, although several cells were elongated and had few, but prominent SFs (Figure 3.19 (B)). These results confirm that YAP is required for PB disassembly in KapB-expressing cells. To understand if YAP controls PB disassembly, constitutively-active YAP (CA-YAP) was expressed in HUVECs in the absence of KapB. Cells expressing CA-YAP grew very quickly and showed a notable loss of contact inhibition (not shown). These cells had few prominent F-actin fibres and distinctly diffuse cytoplasmic staining with phalloidin relative to control cells (Figure 3.20 (A)). Quantification of Hedls puncta in these cells showed that CA-YAP expression decreased the number of Hedls puncta per cell, showing that active YAP alone can elicit disassembly of PBs in the absence of KapB expression (Figure 3.20 (A, B)).

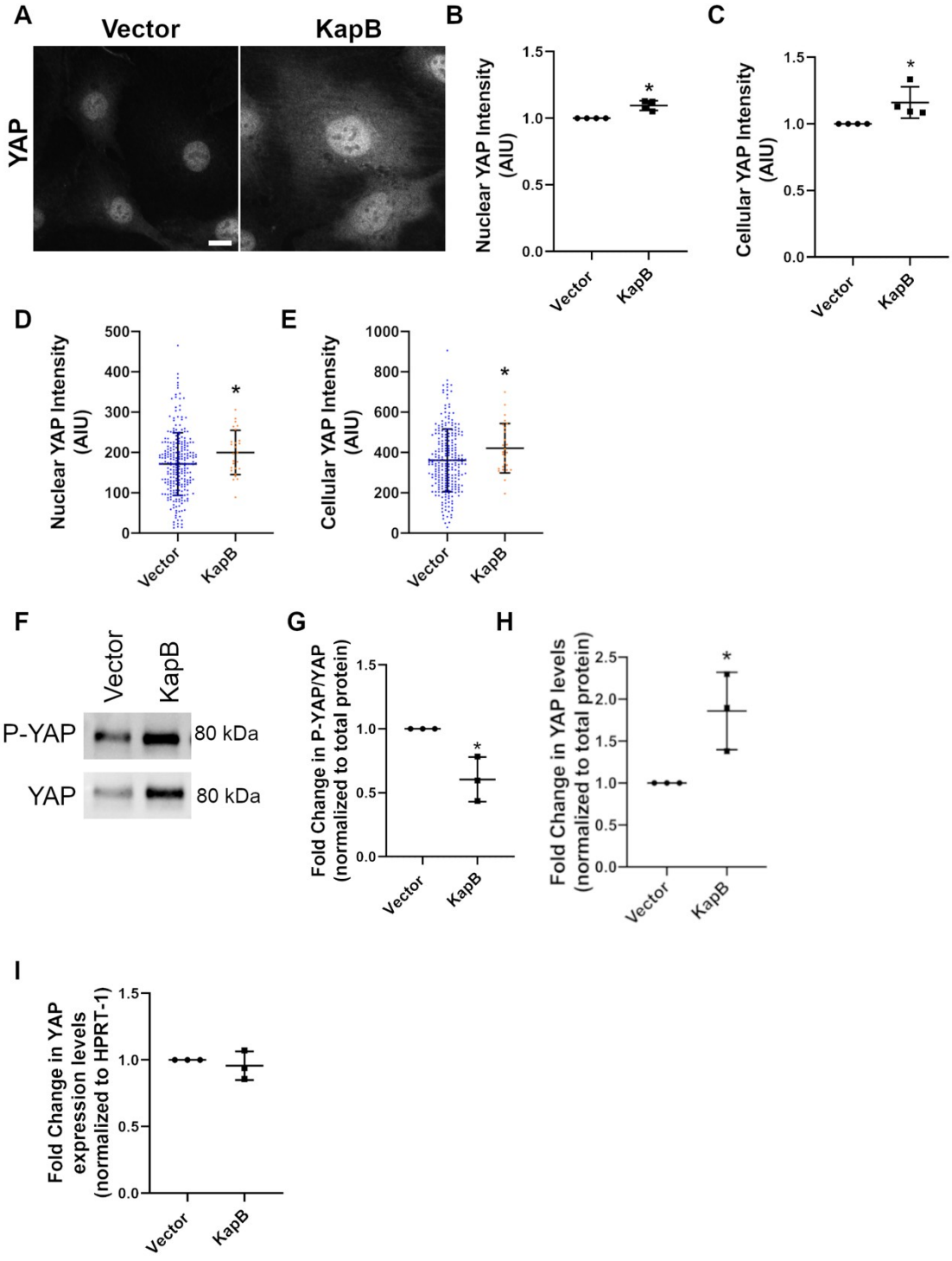
A
Vector
KapB
YAP
B
Nuclear YAP Intensity (AIU)
1.5
1.0
0.5
0.0
*
Vector
KapB
C
Cellular YAP Intensity (AIU)
1.5
1.0
0.5
0.0
*
Vector
KapB
D
Nuclear YAP Intensity (AIU)
500
400
300
200
100
0
*
Vector
KapB
E
Cellular YAP Intensity (AIU)
1000
800
600
400
200
0
*
Vector
KapB
F
Vector
KapB
P-YAP
80 kDa
YAP
80 kDa
G
Fold Change in P-YAP/YAP (normalized to total protein)
1.5
1.0
0.5
0.0
*
Vector
KapB
H
Fold Change in YAP levels (normalized to total protein)
2.5
2.0
1.5
1.0
0.5
0.0
*
Vector
KapB
I
Fold Change in YAP expression levels (normalized to HPRT-1)
1.5
1.0
0.5
0.0
Vector
KapB

**Figure 3.17: YAP protein levels are increased in KapB-expressing cells.** (A-C, F-I) HUVECs were transduced with KapB-expressing and empty vector lentivirus and selected with 5 $\mu$g/mL blasticidin. Cells were fixed for immunofluorescence, lysed for immunoblotting or harvested for RNA. (A) Representative CellProfiler images of cells stained for YAP. Scale bar represents 30 $\mu$M. Images were inputted into a modified CellProfiler and (B) nuclear YAP intensity and (C) cellular YAP intensity were quantified in each treatment. Error bars represent standard deviation. Statistics were determined using a ratio paired t-test, n=3, $p < 0.05$. (D,E) HeLa cells were transfected with using PEI and an expression plasmid for KapB or an empty vector control. After 72 h, cells were fixed for immunofluorescence. Images were input into CellProfiler and (D) nuclear YAP intensity and (E) cellular YAP intensity were quantified in each treatment. YAP levels in KapB-expressing cells were only measured in cells thresholded for KapB immunofluorescence staining above the average background intensity. CellProfiler quantification is representative of one independent experiment. Error bars represent standard deviation. Statistics were determined using a unpaired t-test with Welch's correction, $p < 0.05$. (F, G, H) Representative blot and quantification of HUVEC lysates immunoblotted with antibodies specific to phosphorylated YAP and YAP. Protein levels of phosphorylated YAP and total YAP in each condition were normalized to total protein (not shown). All treatments were normalized to vector control. (I) RNA was harvested from selected HUVECs and used for qRT-PCR analysis of steady state YAP mRNA levels, normalized to steady state HPRT-1 mRNA levels. Error bars represent standard deviation. Statistics were determined using a ratio paired t-test, n=3, $p < 0.05$.

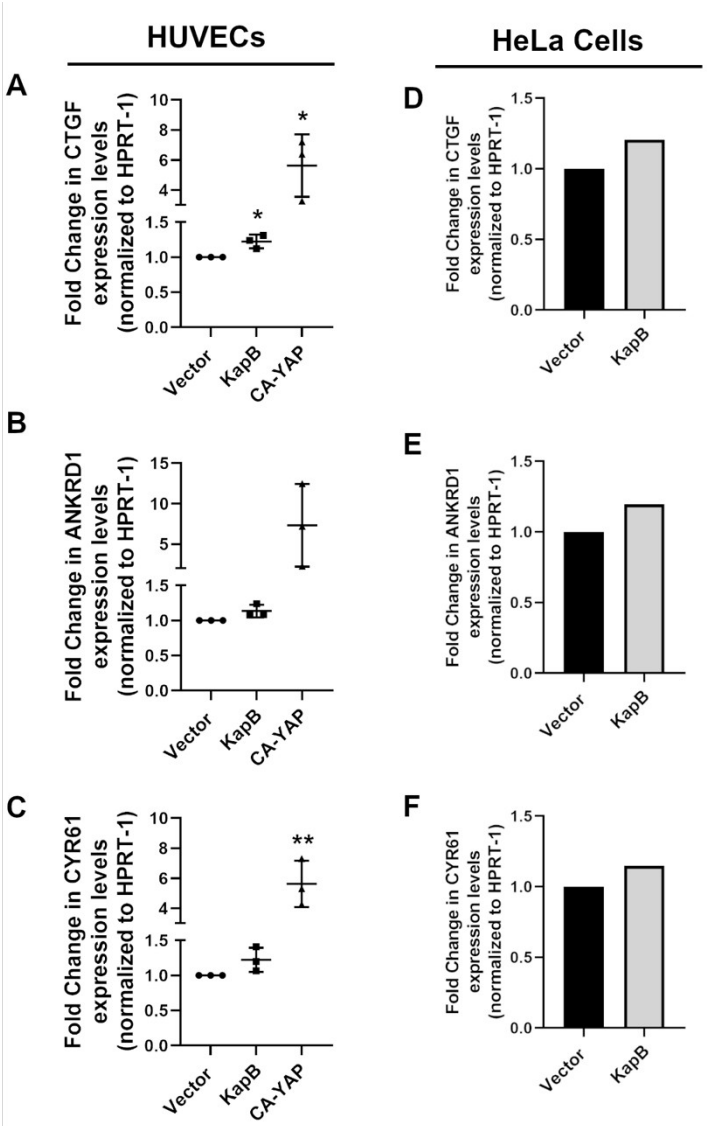


**Figure 3.18: Canonical YAP target genes demonstrate small changes in KapB-expressing cells.** (A-C) HUVECs were transduced with KapB-expressing, constitutively-active YAP (CA-YAP)-expressing and empty vector lentivirus and selected with 5 $\mu$g/mL blasticidin. RNA was harvested and used for qRT-PCR analysis of steady state YAP target mRNA levels, normalized to steady state HPRT-1 mRNA levels. CTGF (A), ANKRD1 (B) and CYR61 (C) levels are shown in vector and KapB-expressing cells, as well as vector and CA-YAP-expressing cells. Error bars represent standard deviation. Statistics were determined using a ratio paired t-test, n=3, $p < 0.05$. (D-F) HeLa cells were transduced with KapB-expressing and empty vector lentivirus. RNA was harvested from cells and used for qRT-PCR analysis of steady state YAP target mRNA levels, normalized to steady state HPRT-1 mRNA levels. CTGF (D), ANKRD1 (E) and CYR61 (F) levels are shown in vector and KapB-expressing cells. Quantification is representative of one independent experiment.

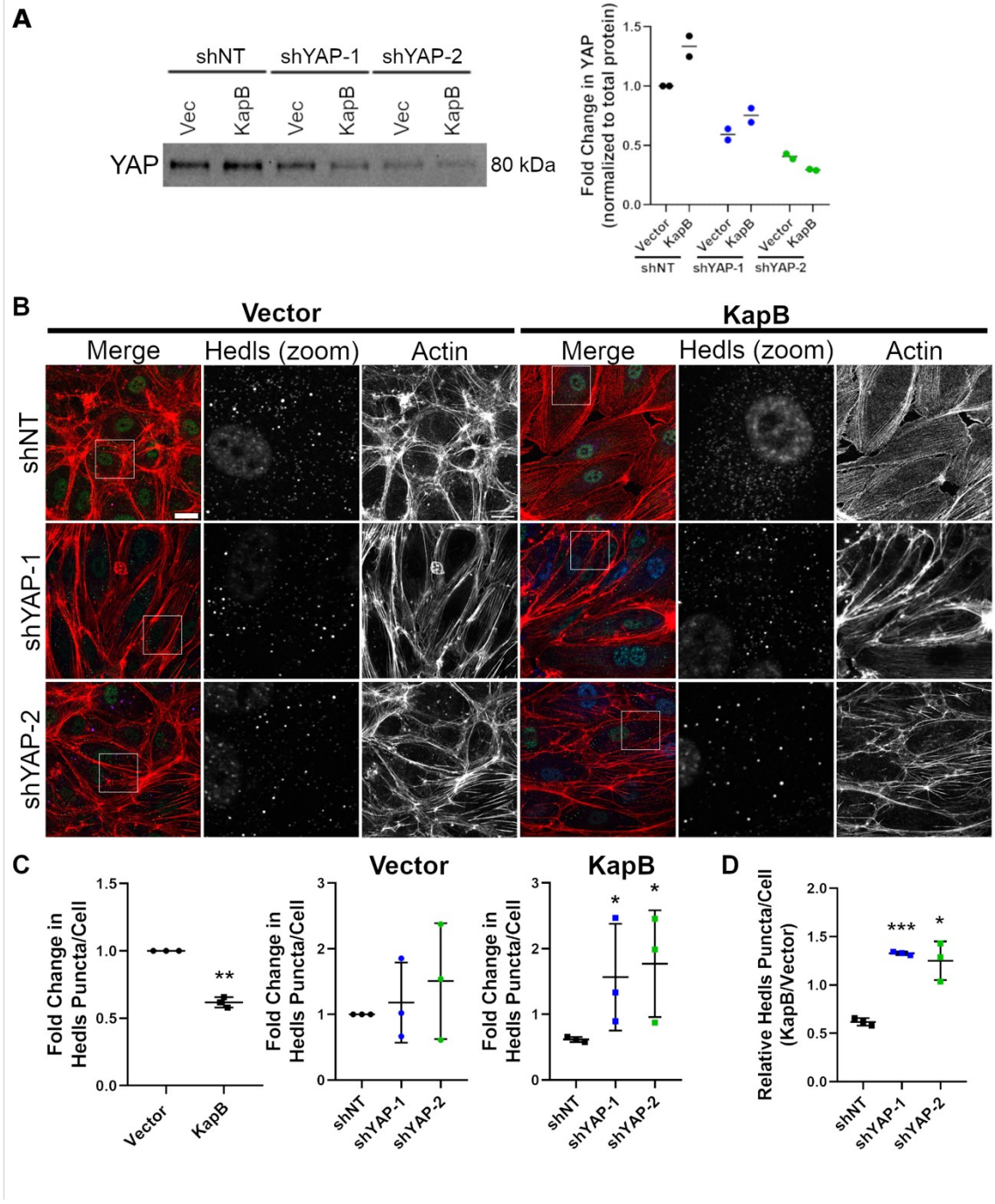
A
shNT
shYAP-1
shYAP-2
Vec
KapB
YAP
80 kDa
Fold Change in YAP (normalized to total protein)
Vector
KapB
shNT
shYAP-1
shYAP-2
B
Vector
KapB
Merge
Hedls (zoom)
Actin
shNT
shYAP-1
shYAP-2
C
Fold Change in Hedls Puncta/Cell
Vector
KapB
Vector
KapB
shNT
shYAP-1
shYAP-2
D
Relative Hedls Puncta/Cell (KapB/Vector)

**Figure 3.19: Knockdown of YAP restores Hedls puncta in KapB-expressing cells.** HUVECs were transduced with KapB-expressing and empty vector lentivirus and selected with 5 $\mu$g/mL blasticidin. Cells were then transduced with shRNAs YAP (shYAP-1, shYAP-2) or with a non-targeting (shNT) control and selected with 1 $\mu$g/mL puromycin. In parallel, cells were fixed for immunofluorescence or lysed for immunoblotting. (A) Representative blot and quantification of lysates immunoblotted using an antibody to YAP. YAP protein levels in each condition were normalized to total protein (not shown). All treatments were normalized to vector NT control. (B) Representative images of cells stained for PB-resident protein Hedls (green), KapB (blue), and F-actin (red, phalloidin). Boxes indicate images shown in Hedls (zoom) panel. Scale bar represents 20 $\mu$m. (C, D) Fixed cells were stained for CellProfiler analysis as detailed in the methods. (C) The number of Hedls puncta per cell was quantified and normalized to the vector NT control. (D) CellProfiler data was used to calculate the ratio of Hedls puncta count in KapB-expressing cells versus the vector control for each treatment condition. Error bars represent standard deviation. Statistics were determined using a ratio paired t-test, n=3, $p < 0.05$.

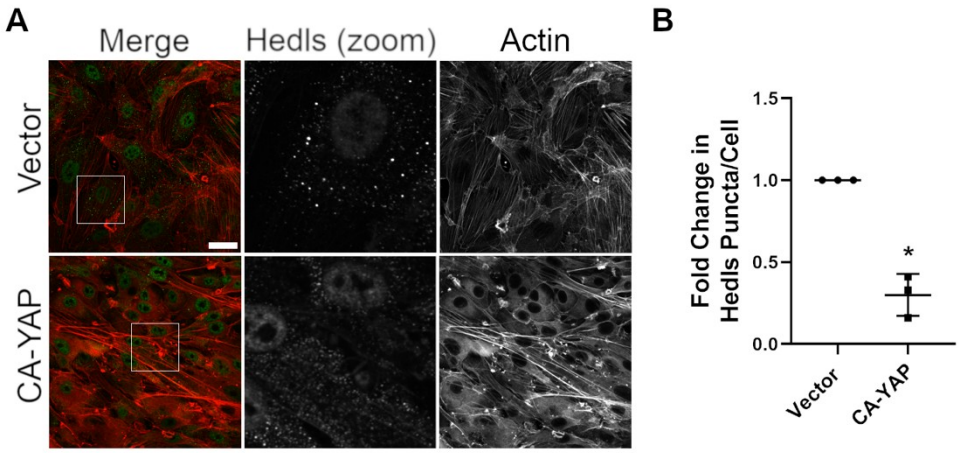


**Figure 3.20: Overexpression of constitutively-active YAP (CA-YAP) disassembles Hedls puncta in HUVECs.** HUVECs were transduced with CA-YAP-expressing and empty vector lentivirus and selected with 5 $\mu$g/mL blasticidin. Cells were fixed for immunofluorescence. (A) Representative images of cells stained for PB-resident protein Hedls (green) and F-actin (red, phalloidin). Boxes indicate images shown in Hedls (zoom) panel. Scale bar represents 20 $\mu$m. (B) Fixed cells were stained for CellProfiler analysis as detailed in the methods. The number of Hedls puncta per cell was quantified and normalized to the vector control. Error bars represent standard deviation. Statistics were determined using a ratio paired t-test, n=3, $p < 0.05$.

### 3.8 Certain Mechanical YAP Inputs Control PB Disassembly

Cell confluence and ECM stiffness are two well-described regulators of YAP nuclear translocation and activation (Boggiano and Fehon 2012). Cells at low density contain active YAP while high cell density promotes inactive YAP (Zhao et al. 2007). To determine if cell confluence influences PB disassembly, HUVECs were seeded at low, medium and high densities. As expected, YAP nuclear staining was increased at low density (Figure 3.21 (A)). The low density monolayer displayed more Hedls puncta per cell then those at medium and high densities (Figure 3.21 (A, B)). This suggests that PB dynamics are not regulated by changes in cell-to-cell contact, despite YAP activation in this context. Increasing ECM stiffness also correlates with increased YAP nuclear translocation and activation (Dupont et al. 2011). To test how ECM stiffness impacted PB disassembly, HUVECs were plated on coverslips coated with increasing densities of collagen (0 to 64 $\mu$g/mL). These data demonstrated that as collagen density increased, Hedls puncta decreased (Figure 3.22 (A, B)). However, immunofluorescence analysis of HUVECs at different collagen densities showed no visible changes in the levels of nuclear YAP or in the morphology of the actin cytoskeleton (Figure 3.22 (A)). Because cellular density modulates YAP primarily through cell to cell junctional signalling (Boggiano and Fehon 2012), while ECM stiffness activates YAP via enhanced cytoskeletal tension, these data support a model which suggests that only mechanical activators of YAP that increase cytoskeletal tension promote PB disassembly in HUVECs.

### 3.9 YAP Activation During Shear Stress Elicits PB Disassembly in HUVECs

To determine if other mechanical forces that induce SF formation and YAP activation can also disassemble PBs, HUVECs were subjected to shear stress by fluid flow and PBs were examined via immunofluorescence. Both 2 and 10 dyn/cm$^2$ of shear stress resulted in robust PB disassembly, confirming that mechanical inducers of SF formation also elicit PB disassembly (Figure 3.23 (A, B)). Cellular lysates of HUVECs that were subjected to fluid flow showed decreases in levels of PB protein DCP1a (Figure 3.23 (C)). Protein levels of another PB-resident protein, DDX6 remained unchanged in shear stress conditions. This is consistent with data seen in KapB-expressing cells, where

DCP1a protein levels are decreased, while DDX6 protein levels are unchanged (Robinson, unpublished).

To confirm if YAP was activated by shear stress in our system, HUVECs that had been subjected to 2 and 10 dyn/cm$^2$ of shear stress were lysed and used for immunoblotting of P-YAP and total YAP. Shear stress induced large decreases in P-YAP/YAP ratio levels in both conditions, suggesting increases in activated YAP (Figure 3.24 (A)). To assess if YAP was directly regulating PB disassembly in response to shear stress, YAP knockdown HUVECs were subjected to 10 dyn/cm$^2$ shear stress. Knockdown of YAP severely inhibited the ability of the cells to respond to shear stress. A much greater cell loss was observed in YAP knockdown cells, as indicated by the nucleus count per field of view (Figure 3.24 (B)). There was an increase in the average Hedls puncta per cell in YAP knockdown cells subjected to shear stress; however, two distinct phenotypes were observed depending on location of the cells the flow chamber (Figure 3.24 (B)). The cells near the inlet, where the force of fluid flow is greater, did not maintain SFs and had few but very intense PBs. Cells near the outlet, which are subjected to lower degrees of force, maintained SFs and displayed Hedls puncta staining in their cytoplasm that was more typical of the static NT control. Though confirmation of this phenotype with more experiments is necessary, the increase in Hedls puncta in both cases suggests that YAP activation regulates PB disassembly in response to mechanical forces, such as shear stress.

The data presented suggest that KapB is driving RhoA signalling to increase cytoskeletal tension and induce YAP in a manner that mimics its activation by external forces. This YAP signalling is required for KapB-mediated PB disassembly.

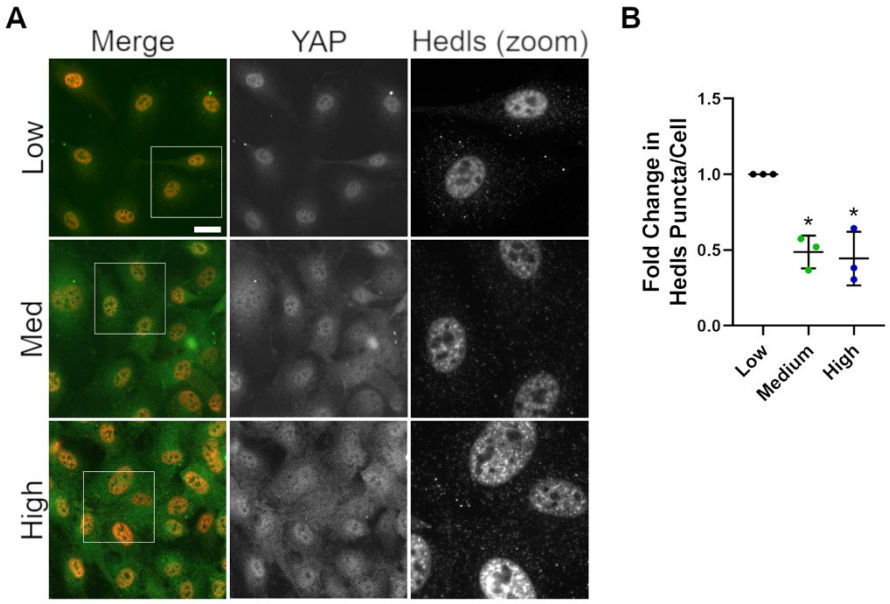


**Figure 3.21: Confluence-mediated activation of YAP does not disassemble Hedls puncta.** HUVECs were split at a low, medium and high-density confluence and fixed for immunofluorescence. (A) Representative CellProfiler images of cells stained for PB-resident protein Hedls (red) and YAP (green). Boxes indicate images shown in Hedls (zoom) panel. Scale bar represents 30 $\mu$m. (B) Fixed cells were stained for CellProfiler analysis as detailed in the methods. The number of Hedls puncta per cell was quantified and normalized to the low confluence condition. Error bars represent standard deviation. Statistics were determined using a ratio paired t-test, n=3, $p < 0.05$.

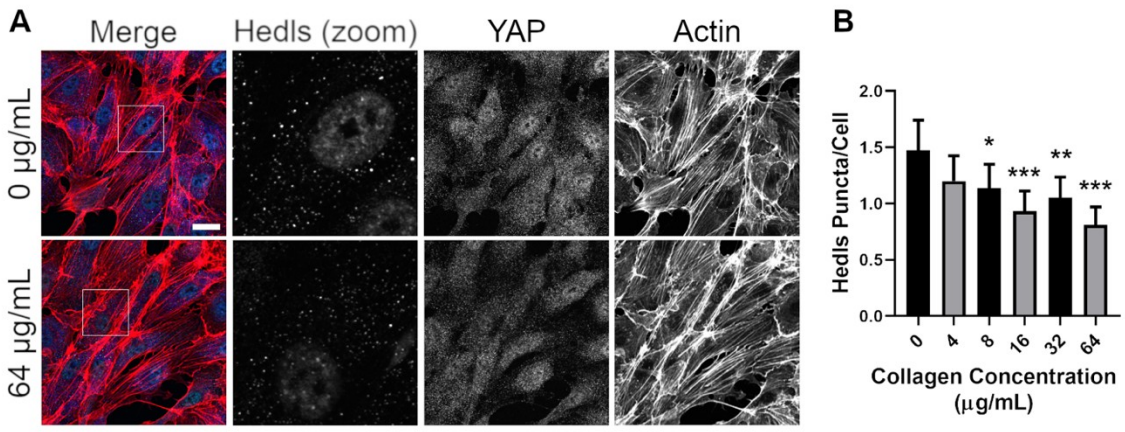


**Figure 3.22: Increasing matrix stiffness disassembles Hedls puncta.** Coverslips were coated for 1 h with 0 to 64 $\mu$g/mL of collagen in 0.02 mM acetic acid. HUVECs were grown for 72 h on coated coverslips and fixed for immunofluorescence. (A) Representative images of cells stained for PB-resident protein Hedls (green), YAP (blue) and F-actin (red, phalloidin). Boxes indicate images shown in Hedls (zoom) panel. Scale bar represents 20 $\mu$m. (B) Fixed cells were stained for CellProfiler analysis as detailed in the methods. The number of Hedls puncta per cell was quantified and normalized to the 0 $\mu$g/mL collagen-coating condition. Error bars represent 95% confidence interval. Statistics were determined using a negative binomial regression, $p < 0.05$. N=1.

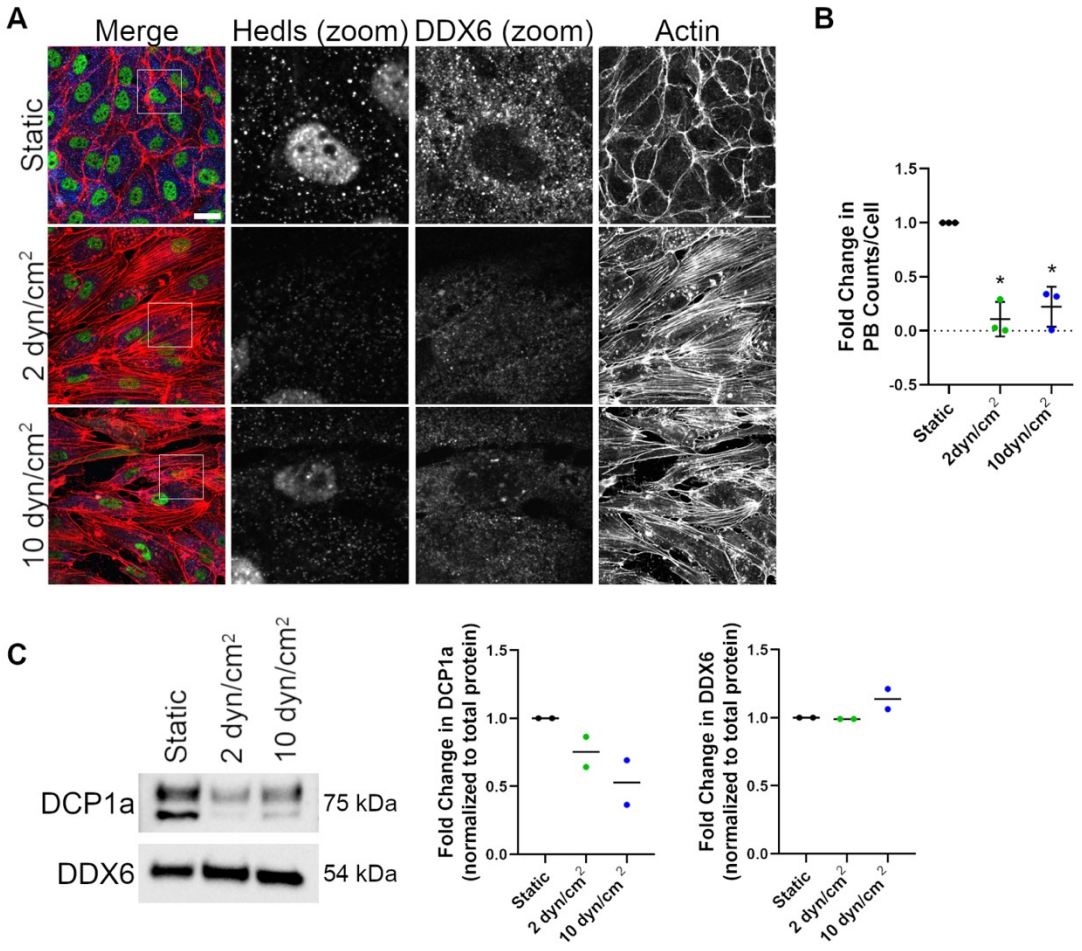


**Figure 3.23: Shear stress disassembles PBs in HUVECs.** HUVECs were seeded onto collagen-coated microscope slides and exposed to shear stresses of 2 dyn/cm$^2$, 10 dyn/cm$^2$ or a static control for 22h. Cells were fixed and stained for immunofluorescence or lysed for immunoblotting. (A) Representative images of cells stained for PB-resident proteins Hedls (green) and DDX6 (blue), as well as F-actin (red, phalloidin). Boxes indicate images shown in Hedls (zoom) and DDX6 (zoom) panels. Scale bar represents 20 $\mu$m. (B) CellProfiler was used to count nuclei, Hedls puncta and DDX6 puncta. In RStudio analysis, puncta with more than 70% correlation between Hedls and DDX6 (PBs) were counted in each condition and normalized to number of nuclei per condition. Statistics were determined using a ratio paired t-test, n=3, $p < 0.05$. (C) Representative blot and quantification of lysates immunoblotted with antibodies specific to the PB-resident proteins DCP1a and DDX6. DCP1a and DDX6 protein levels in each condition were normalized to total protein (not shown). All treatments were normalized to vector static control. Immunoblot quantification is representative of two independent experiments.

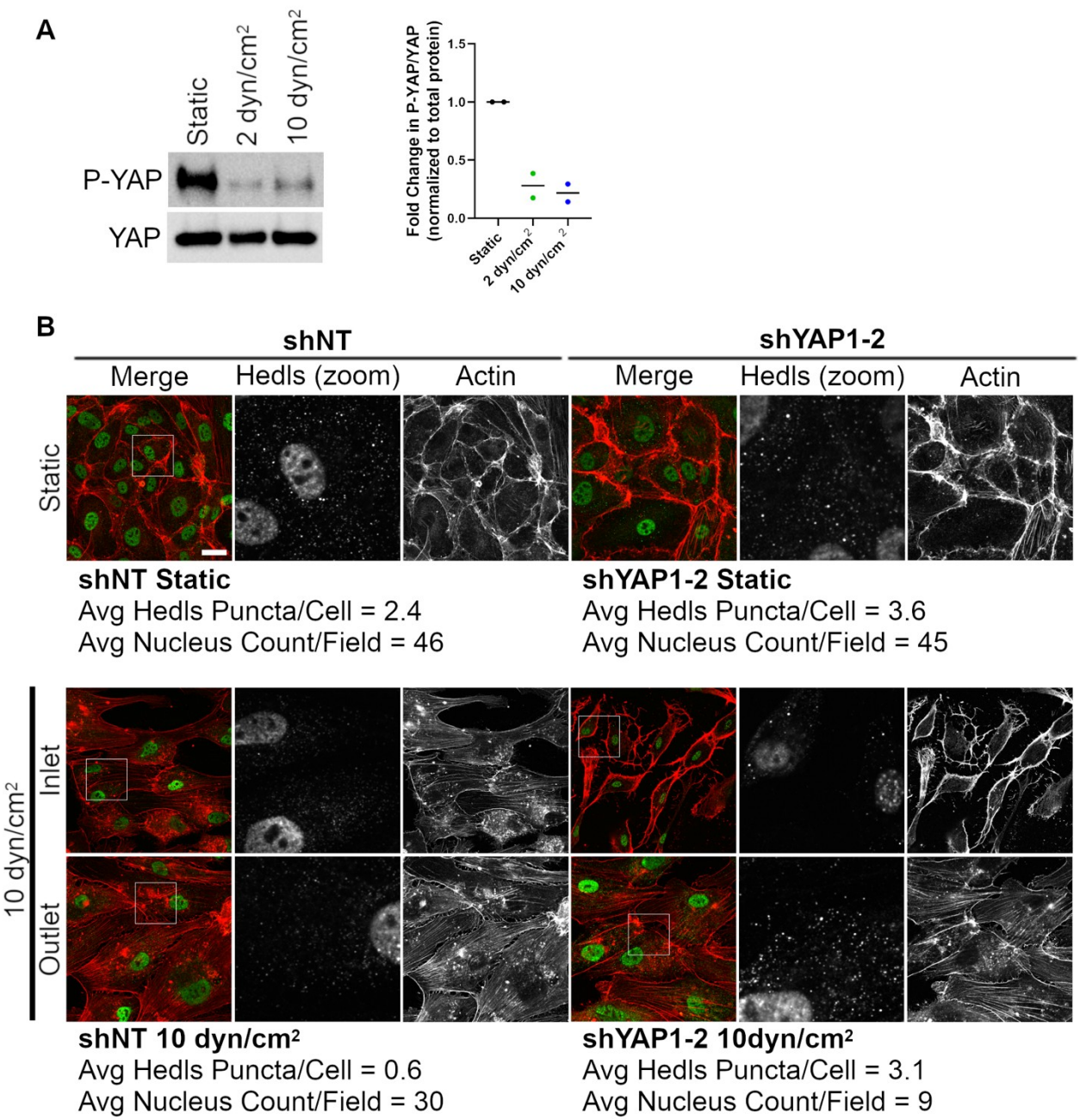
A
Static
2 dyn/cm2
10 dyn/cm2
P-YAP
YAP
Fold Change in P-YAP/YAP (normalized to total protein)
1.5
1.0
0.5
0.0
Static
2 dyn/cm2
10 dyn/cm2
B
shNT
shYAP1-2
Merge
Hedls (zoom)
Actin
Merge
Hedls (zoom)
Actin
Static
shNT Static
Avg Hedls Puncta/Cell = 2.4
Avg Nucleus Count/Field = 46
shYAP1-2 Static
Avg Hedls Puncta/Cell = 3.6
Avg Nucleus Count/Field = 45
10 dyn/cm2
Inlet
Outlet
shNT 10 dyn/cm2
Avg Hedls Puncta/Cell = 0.6
Avg Nucleus Count/Field = 30
shYAP1-2 10dyn/cm2
Avg Hedls Puncta/Cell = 3.1
Avg Nucleus Count/Field = 9

**Figure 3.24: YAP is likely required for Hedls puncta disassembly in HUVECs subjected to shear stress.** (A) Representative blot and quantification of lysates from cells exposed to shear stresses of 2 dyn/cm$^2$, 10 dyn/cm$^2$ or a static control for 22h. Lysates were immunoblotted with antibodies specific to phosphorylated YAP and YAP . Protein levels of phosphorylated YAP and total YAP in each condition were normalized to total protein (not shown). All treatments were normalized to vector static control and the ratio of phosphorylated YAP/YAP was calculated. Immunoblot quantification is representative of two independent experiments. (B) HUVECs were transduced with shRNAs targeting YAP (shYAP1-2) or with a non-targeting (shNT) control and selected with 1 $\mu$g/mL. Cells were seeded onto collagen-coated microscope slides and exposed to shear stresses of 10 dyn/cm$^2$ or a static control for 22h. Cells were fixed and stained for immunofluorescence. Representative images of cells stained for PB-resident protein Hedls (green) and F-actin (red, phalloidin are shown for two locations in the flow chamber. Boxes indicate images shown in Hedls (zoom) panels. Scale bar represents 20 $\mu$m. CellProfiler was used to count nuclei (nucleus count) and Hedls puncta. In RStudio analysis, Hedls puncta were normalized to number of nuclei per condition. Quantification is representative of one independent experiment.

# CHAPTER 4: DISCUSSION

## 4.1 Overview

Prior to this work, KapB was known to activate a non-canonical MK2-RhoA axis that mediated both SF formation and PB disassembly (Corcoran, Johnston, and McCormick 2015). RhoA has been well-characterized as a cytoskeletal regulatory protein, known to mediate SF formation (Ridley and Hall 1992). However, the demonstration that activation of RhoA altered PB dynamics after starvation, as well as after activation of the MK2-RhoA axis by KapB, was unexpected (Takahashi et al. 2011; Corcoran et al. 2012; Corcoran, Johnston, and McCormick 2015). More unexpected was the inability to uncouple the signalling controlling SF formation from that controlling PB disassembly, leading to my hypothesis that RhoA-activation of SF formation may precede PB disassembly. To test this hypothesis, I asked three different questions about SFs: (1) Does the signalling that controls SF formation also control PBs? (2) Is the structure of SFs required for PB disassembly? and (3) Does functional result of SF formation, for example, contractility and mechanotransduction, control PBs? I now show that PB disassembly is controlled by the same RhoA-effectors that control SF formation, mDia1 and ROCK. I also show that actomyosin contractility, a key characteristic of SFs, is required for KapB-mediated PB disassembly; furthermore, my model suggests that eliciting changes in cytoskeletal tension in the absence of KapB can regulate PB dynamics. SFs mediate changes in cytoskeletal tension that activate mechanoresponsive signalling, in particular, the mechanoresponsive transcriptional coactivator, YAP. I demonstrate that the mechanism of PB disassembly, induced both by KapB and external force, is accompanied by the nuclear translocation of YAP and relies on its presence in the cell.

Previous work from our lab and others showed that PBs regulate the stability of many transcripts that encode for inflammatory and angiogenic proteins (Corcoran, Johnston, and McCormick 2015; Vindry et al. 2017; Blanco et al. 2014). This knowledge, taken in combination with my results, leads to the following model. I propose that KapB activates a novel mechanoresponsive pathway, thereby controlling the stability of mRNA transcripts that may promote inflammation in the context of KSHV infection and KS tumorigenesis, and in other pathologies with dysregulated inflammation. In the discussion

that follows, I will highlight the main findings of this work that have led to the development of this model, including a new PB quantification platform, my evidence for a novel mechanoresponsive axis that regulates PBs, and how I believe that this signalling axis contributes to the current knowledge of the disease KS.

### 4.2 Quantitating Changes to PB Dynamics and their Functional Consequences

I developed the CellProfiler pipeline as a tool for large-scale, reliable PB quantification. The robust measurements provided by this pipeline can be combined with functional data to understand how post-transcriptional gene expression is regulated by PBs. CellProfiler accurately identified distinct puncta that were stained with an antibody for Hedls, a PB-resident protein, within the cytoplasm of a given cell. The program measured puncta intensity and evaluated nucleus-to-puncta distance (Figure 3.1). In KapB-expressing cells, CellProfiler evaluation of PB levels recapitulated previous data that were obtained using manual counting, confirming with an unbiased method, that KapB elicits PB disassembly (Corcoran, Johnston, and McCormick 2015). The accurate replication of these previously published results demonstrates that CellProfiler is able to robustly quantify these visible puncta within a cell.

Importantly, the follow-up of CellProfiler analysis requires linking the PB quantification phenotypes with PB functional output. This question highlights an important debate ongoing in the PB field: whether microscopically-visible PBs actually act as sites of decay. Initially, it was thought that because decay enzymes are localized to PBs, and RNA decay intermediates of artificial constructs have been detected at PBs, these cellular structures were sites of mRNA decay (Sheth and Parker 2003). However, mRNA decay visualized by single-molecule imaging indicated that decay events can occur diffusely in the cytosol (Horvathova et al. 2017). Furthermore, subsequent studies have shown that no mRNA decay intermediates were detected in fluorescently-sorted PBs (Hubstenberger et al. 2017). One study employing mathematical models of the movement of mRNA molecules suggested that mRNA decay is most efficient at the periphery of the PB while translationally-repressed mRNAs are stably localized within the PB (Pitchiaya et al. 2019). These studies indicate that, although the decay may not always be occurring directly within the PB, the presence of PBs are indicative of localized and concentrated

RNA translational suppression and/or decay. Thus, even if visible PBs are not exclusive sites of decay, their ability to concentration decay factors into visible cytoplasmic foci is important for mRNA translational suppression and decay.

Many different types of RNA decay are attributed to PBs, and whether the visible structure of the PB is important for function depends on which PB-related function is being examined. Though the enzymes for both nonsense-mediated decay and miRNA interference can be found in PBs, it has been shown that loss of PBs does not inhibit either process (Eulalio et al. 2007; Stalder and Mühlemann 2009). Therefore, visible PB foci are not required for nonsense-mediated decay or RNA interference, but rather, form as a result of high levels of either process. An important caveat to these studies is that they did not directly examine levels of mRNAs that are subject to rapid turnover, including ARE-containing mRNAs, a class of mRNAs that constitutively shuttle to PBs. ARE-mRNAs localize to PBs and to accumulate at PBs when mRNA decay is inhibited (Franks and Lykke-Andersen 2007). Studies that directly investigate ARE-mRNA decay consistently observe that the presence of visible PBs directly correlates with ARE-mRNA turnover. Blanco et al. (2014) showed that induction of PBs with TGFβ resulted in a decrease of ARE-mRNA expression. The converse is also true, as PB loss correlates with enhanced ARE-mRNA stability. Studies employing RNA transcriptomic analysis have shown striking upregulation of mRNAs containing AREs upon PB disassembly (Vindry et al. 2017). In the Corcoran Lab, we observe that decreased PB abundance correlates with increased stability of ARE-mRNAs and increased ARE-mRNA abundance (Corcoran et al. 2012; Corcoran and McCormick 2015; Singh 2019). Singh (2019) has shown that CellProfiler quantification correlated with increased steady-state levels of selected endogenous ARE-mRNAs as well as enhanced ARE-mRNA stability as measured by a luciferase reporter assay. These data indicate that CellProfiler quantification of PBs imparts an accurate representation of ARE-mRNA status. Thus, in studies examining PBs as potential mechanisms for the regulation of inflammatory ARE-mRNAs, PB presence or absence is a validated indicator of the ARE-mRNA suppression and decay occurring in a cell.

With the understanding that PB abundance reflects the stability of inflammatory mRNAs (Corcoran, Johnston, and McCormick 2015; Vindry et al. 2017; Blanco et al.

2014, Singh 2019), CellProfiler quantification enables rapid, large-scale analysis of potential changes to the inflammatory status of cell populations. Furthermore, because this pipeline can analyze different PB properties such as size and localization (Figure 3.1), it may extend our understanding of PB functional changes, describing novel PB properties that may be important for a given functional output. Because PBs are such dynamic granules, this pipeline enables a more comprehensive view of their behaviour within the cell. However, there are some technical limitations to this pipeline, which are discussed below.

### 4.2.1 Limitations of CellProfiler: Wheat Germ Agglutinin Staining

WGA is a lectin that binds to N-acetyl-D-glucosamine and sialic acid on the surface of the cell (Chazotte 2011). A common issue with the staining is internalization of the lectin and staining of the golgi apparatus (Chazotte 2011). This is a well-known issue for use of WGA with living cells but also occurs in fixed cells, likely due to the slight permeabilization of the cell membrane that can occur during fixation. This enables WGA to enter the cell and stain internal membranes. To minimize permeabilization in our system, 4% PFA was always made immediately prior to fixation since older PFA increased membrane permeabilization. Additionally, there are glycoproteins with binding sites for the lectin in the media from the FBS, so washing prior to fixation is required to avoid non-specific binding (Wang et al. 2014). Even with the above precautions, if the WGA is internalized to an extent that CellProfiler is unable to identify the outer edge of the cell, the distance from the nuclei measurement must be discounted because the PB may be associated with the wrong nucleus. The puncta count per cell is a still valid in this case since it is normalized to the nuclei count in the DAPI image. Other stains were examined, including CellMask (ThermoFisher), but this was discounted as the signal is not maintained after permeabilization treatment, so cannot be used for immunofluorescence. Another reagent, CellTracker (ThermoFisher), stains the cytoplasm of cells through complexing with amine groups on proteins. However, the protocol requires live-cell staining of the cells, which results in large cell loss when attempted using the primary cell line used in the studies described above, HUVECs. WGA was the

most economical and effective of the above options, though this sometimes resulted in some data loss.

### 4.2.2 Limitations of CellProfiler: Microscope Resolution

Very few studies have attempted to report on the size of PBs; one study has stated these structures range from 150 to 340 nm, as measured by electron microscopy (Cougot et al. 2012). Since the practical limit of resolution of a conventional light microscope is ~200 nm (Cox and Sheppard 2004), smaller PBs are not being measured accurately through this method. While measurement of clusters of molecules by intensity is valid (Waters 2009), the resolution prevents distinguishing clusters of small, individual PBs within what appears to be a larger PB. To solve this, examining PBs on a microscope with higher resolution would enable distinguishing these potential clusters of PBs, though this is not economical on a large scale. Regardless of these limitations, the results show that PB counts from CellProfiler correlate to ARE-mRNA stability (Corcoran, Johnston, and McCormick 2015; Corcoran, Khaperskyy, and McCormick 2011, Singh 2019), which demonstrates that this pipeline is valid for the purposes of examining PB levels and the correlative function, ARE-mRNA stability.

## 4.3 A Novel Mechanoresponsive Axis Controls PB disassembly

To briefly summarize the results shown in Section 3.2 to 3.6, PB disassembly is controlled by the RhoA-effectors known to coordinate SF formation, actin contractility and activation of the mechanoresponsive transcriptional activator YAP. The evidence for each component of this axis is described below.

### 4.3.1 RhoA-Effectors Involved in SF Formation Contribute to KapB-Mediated PB Disassembly

RhoA mediates SF formation through activation of mDia1 and ROCK (Watanabe et al. 1999). Alongside SF formation, RhoA controls PB disassembly in the context of KapB expression (Corcoran, Johnston, and McCormick 2015). To investigate whether SF formation was required for PB disassembly, the RhoA-effectors that mediate SF formation were interrogated. mDia1 coordinates SF formation through increased

polymerization of actin fibres (Watanabe et al. 1999). Knockdown of mDia1 restored PBs in KapB-expressing cells (Figure 3.2). Similarly, the inhibition of ROCK by both chemical inhibition and isoform-specific knockdown (Figure 3.4-3.6) also restored PBs in KapB-expressing cells. ROCK coordinates SF contractility and stability (Watanabe et al. 1999). Furthermore, mDia3, which is involved in coordinating the cytoskeleton during cell division (Yasuda et al. 2004) did not restore PBs in KapB-expressing cells (Figure 3.3). Taken together, the results demonstrating that ROCK and mDia1, but not mDia3, are required for PB disassembly, suggest there is a specific cellular process, requiring both mDia1 and ROCK, which is controlling PB disassembly. Such a process could be SF formation or focal adhesion formation and maintenance: these two processes are discussed in section 4.3.4. At this time, it is unclear whether combinatorial inhibition of mDia1 and ROCK further restores PBs compared to mDia1 knockdown alone (Figure 3.7). If the effect of combined inhibition is significant in future studies, it will support the idea that a process requiring both mDia1 and ROCK, such as SF formation, is required for PB disassembly. An alternative possibility is that ROCK inhibition does not augment the phenotype further than mDia1 knockdown alone, suggesting that the first treatment has exhausted the cell's capability to reform PBs and further inhibition of actin dynamics does not increase PB restoration. However, in this case, more experiments are needed to determine statistical significance.

Attributing a specific role in the PB disassembly phenotype to each of these RhoA-effectors is complicated by the diversity of actin phenotypes observed after effector knockdown. Cells after knockdown of mDia1 and ROCK2 (shROCK2-2 only) retained robust actin fibres in the cytoplasm of the cells. It is unclear from phalloidin staining alone what subtype(s) of SFs are retained in these cells (Small et al. 1998). In contrast, knockdown of ROCK1 and ROCK2 (shROCK2-1) showed, similar to treatment with the non-specific ROCK inhibitor, sparse disorganized actin that was highly cortical. Similar actin phenotypes were reported by Yoneda et al. (2005) for ROCK knockdowns, with ROCK1 knockdown resulting in sparse cortical actin, robust actin fibres in ROCK2 knockdown and intermediate phenotypes when both isoforms were targeted. Thus, the actin phenotypes in ROCK knockdown are likely a result of the complex interplay between isoforms. Additionally, mDia1 actin phenotypes are similar to those seen in

various truncation mutants of mDia that inhibited function (Watanabe et al. 1999), though a mechanism for how these fibres are formed in the absence of mDia1 has not been described. Since SF subtypes are formed through different pathways and mDia1 primarily controls dorsal SF disassembly (Hotulainen and Lappalainen 2006), it is possible that the absence of mDia1 promotes transverse arc formation in the cell to compensate. Regardless, since there is PB restoration in all of the described knockdown conditions, the results indicate that microscopically-visible actin fibres do not need to be eliminated to see PB restoration, as concept discussed more in section 4.3.4. It also suggests that there may be differences in the role of different SF subtypes in PB disassembly.

Though both ROCK1 and ROCK2 are implicated in various aspects of SF formation (Julian and Olson 2014), ROCK2 is specifically regulated by mechanical activation of YAP (Sugimoto et al. 2018). Sugimoto et al. (2018) show that with increased substrate-rigidity, YAP interacts with the ROCK2 promoter to increase ROCK2 levels. Increases in ROCK2 then promote actomyosin contraction and increase cytoskeletal tension. Increased cytoskeletal tension then promotes YAP localization to the nucleus, creating a positive-feedback loop (Shi et al. 2013; Sugimoto et al. 2018). Notably, slight increases in ROCK2 steady-state protein levels have been observed in KapB-expressing cells (data not shown), supporting that this ROCK2-YAP feedback loop may occur. Since YAP is also required for PB disassembly, this interplay between ROCK2 and YAP regulation may explain why ROCK2 knockdown showed greater restoration of PBs in KapB-expressing cells in comparison to ROCK1 knockdown (Figure 3.6).

ROCK2 is also thought to be the primary isoform of ROCK to inactivate cofilin through LimK phosphorylation (Shi et al. 2013). Experimentally, cofilin knockdown induced PB disassembly in vector cells and seemed to augment PB disassembly in KapB expressing cells (Figure 3.8). It can be inferred from this data that a lack of cofilin activity, through inactivation or knockdown, promotes PB disassembly. However, to conclusively identify whether or not the inhibition of cofilin activity is required for PB disassembly, future experiments should investigate the PB status in the context of overexpression of LimK, which would inactivate cofilin, as well as in the context of overexpression of a dominant-negative LimK, which would promote cofilin activity. I

would predict that cofilin inhibition in this manner would further augment the KapB PB disassembly phenotype, while cofilin activation would restore PBs. Maintaining actin stability through inhibition of cofilin activity by ROCK is required for SF formation (Shi et al. 2013), which suggests that the stability of actin SFs may contribute to KapB-mediated PB disassembly.

Though the roles of each protein in PB disassembly are not fully elucidated, these data suggest that many of the proteins involved in regulating SF formation are also involved in PB disassembly. However, the visible presence of actin fibres does not always correlate with PB disassembly. To try to understand the various actin phenotypes seen in the knockdown conditions described above and whether or not the structure of SFs, and more specifically, the bundling of actin filaments into a fibre, was required for PB disassembly, the α−actinins were investigated. The following section discusses the experimental results obtained while exploring this process.

### 4.3.2 SF Bundling May Not Be Required for PB Disassembly

The α−actinins are primarily known for their role in bundling actin fibres, though in non-muscle cells, α−actinin-1 and 4 do not both mediate actin bundling to the same extent (Pellegrin and Mellor 2007). α−actinin-4 can, at times, localize to dorsal SFs, but it primarily mediates focal adhesion turnover and can act as a transcriptional regulator of genes associated with cell proliferation and differentiation (Honda et al. 1998; Kovac 2010; Honda 2015). Conversely, α−actinin-1 primarily mediates SF bundling and formation, as well as focal adhesion maturation (Honda et al. 1998; Kovac 2010). The localization of the two isoforms seen in HUVECs (Figure 3.9) is congruent with the reported localization and function, as α−actinin-1 is localized to actin fibres and α−actinin-4 is more diffusely cytoplasmic and nuclear, with some actin fibre localization (Honda et al. 1998; Kovac 2010). In KapB-expressing cells, knockdown of α−actinin-4 restored PBs, while knockdown of α−actinin-1 was inconclusive because the two shRNAs gave opposite results (Figure 3.11). While it is possible that the phenotype of one of the shRNAs targeting α−actinin-1 is induced by an off-target effect, Kovac (2010) reported that, in the context of α−actinin-1 knockdown, α−actinin-4 can compensate for

the other isoform in the bundling of ventral SFs and transverse arcs, and thus α–actinin-1 knockdown cells maintained robust fibres throughout the cytoplasm. In my work, shACTN1-1 shows similar robust fibres, thus it is possible that shACTN1-1 confers the valid phenotype, and thus knockdown of α–actinin-1 does not restore PBs. This possibility implies that SF bundling and focal adhesion maturation, both controlled by α–actinin-1 (Honda et al. 1998; Kovac, Mäkela, and Vallenius 2018), are not required for PB disassembly.

However, overexpression of α–actinin-1-GFP disassembles PBs, suggesting that the activity of α–actinin-1 can control PB disassembly (Figure 3.12). α–actinin-1 overexpression can induce actin bundling and promote formation and maturation of focal adhesions (Edlund, Lotano, and Otey 2001). Thus, PB disassembly may rely on actin bundling or focal adhesion maturation. If both α–actinin-1 and -4 regulate PB dynamics, it suggests that the mechanism by which α–actinin is disassembling PBs is shared. The only known shared function between these two isoforms is in maintaining dorsal SFs. If maintenance of only dorsal SFs is required for PB disassembly, bundling of ventral SFs and transverse arcs is likely not critical for PB disassembly. Supporting this, and similar to what had been observed in knockdown of mDia1 and ROCK2 (shROCK2-2), prominent actin fibres can be seen in the context of α–actinin-4 knockdown, which also shows PB restoration (Figure 3.11). It is possible that the SFs seen in these cells are ventral SFs and transverse arcs, and that these SF types are not critical in PB disassembly. Notably, both isoforms can also regulate different aspects of focal adhesions. α–actinin-1 promotes focal adhesion formation and maturation (Kovac 2010), while α–actinin-4 promotes focal adhesion turnover (Fukumoto et al. 2015). Thus, it cannot be discounted that the regulation of PBs by α–actinin-1 and α–actinin-4 are mediated by different pathways, perhaps through the complex regulation of focal adhesions. Further investigation of this will include verifying current results, designing and testing other shRNAs for α–actinin-1 and examining localization of the two isoforms in KapB-expressing cells.

### 4.3.3 Cytoskeletal Tension Controls KapB-Mediated PB Disassembly

SFs are indicative of increased actomyosin contractility and increased cytoskeletal tension (Katoh et al. 1998; Tan et al. 2003). Several of the results presented in this thesis suggest that KapB requires increased cytoskeletal tension to disassemble PBs. This includes the demonstration that actin contractility controls PB disassembly (Figure 3.13, 3.14) Furthermore, increasing structural tension on a cell by exposing it to the mechanical force of shear stress (Li et al. 2018) can disassemble PBs (Figure 3.23), suggesting that mechanical changes controlling cytoskeletal tension can also control PB disassembly. This evidence is discussed in detail below.

Phosphorylation of MLC controls contractility of actin fibres in cells through NMII. This function is required for sensing of the ECM, SF formation, formation of cell junctions and mechanoresponsive signalling (Zaidel-bar, Zhenhuan, and Luxenburg 2015). Contraction of actomyosin fibres results in increased cytoskeletal tension when a cell is adhered to ECM (Tan et al. 2003). Treatment of KapB-expressing cells with blebbistatin, an inhibitor of contractility, restored PBs, indicating that actomyosin contractility is tightly tied to KapB-mediated PB disassembly (Figure 3.13). Since KapB-expressing cells are adherent to the ECM, KapB-mediated contractility could be causing an increase in cytoskeletal tension, resulting in disassembly of PBs. Treatment of cells (lacking KapB) with CalA, a MLC-phosphatase inhibitor, prevents dephosphorylation of MLC and induces actin contraction (Asano and Mabuchi 2001). Treatment with CalA also increases cytoskeletal tension through actomyosin contraction (Acharya et al. 2018). The induction of cell contraction and cytoskeletal tension through treatment with CalA disassembled PBs in HUVECs (Figure 3.14). Conversely, reduction of cytoskeletal tension through treatment of cells with Jasp and CytD (Rotsch and Radmacher 2000), resulted in an increase of PBs in HUVECs (Figure 3.16). These data suggest that cytoskeletal tension is closely linked to PB numbers in HUVECs.

External forces elicit a cellular response to maintain isometric tension within a cell (Discher, Janmey, and Wang 2005). Shear stress mediates SF formation, likely to maintain equivalent forces inside and outside of the cell (Noria et al. 2004; Wojciak-Stothard and Ridley 2003). Shear stress and RhoA activation both increase cytoskeletal tension (Tan et al. 2003; Wang Li et al. 2018). To examine whether or not mechanical

induction of SF formation and cytoskeletal tension resulted in PB disassembly, HUVECs were exposed to various levels of shear stress forces. Consistent with the literature, under both low and high shear stress conditions, cells showed alignment in the direction of fluid flow and stress fibre formation (Noria et al. 2004). Strikingly, exposure of HUVECs to shear stress conditions dramatically disassembled PBs (Figure 3.23).

These data indicate that inputs known to increase SFs and cytoskeletal tension disassemble PBs and support a model in which KapB is stimulating a mechanoresponsive pathway that responds to increases in cytoskeletal tension. To investigate whether KapB is changing cytoskeletal tension indirectly, the levels of phosphorylated MLC on SFs will be examined by immunofluorescence as an estimation of SF contractility levels in the context of KapB. Additional experiments could be performed to directly determine whether cytoskeletal tension is changing: cells could be grown on a contractible substrate, such as a film or soft microneedles, and the force generated from various treatments could be measured through induced changes in the substrate (Discher, Janmey, and Wang 2005).

### 4.3.4 Distinguishing Between SFs and Cell Adhesions

Both actomyosin contractility and cell adhesion are required to generate increases in cytoskeletal tension (Discher, Janmey, and Wang 2005). If increased cytoskeletal tension is contributing to PB disassembly in KapB-expressing cells, there are likely changes in cell adhesion alongside the increases in contractility. When there is a disproportional increase in RhoA activity and actomyosin contractility in comparison to the ability of a cell to adhere, the cells round up and develop a blebbing phenotype (Ikenouchi and Aoki 2017). The KSHV thymidine kinase (TK) both increases actomyosin contractility and disassembles focal adhesions (Gill et al. 2015). The increase in contractility and decrease in adhesion result in cell blebbing at the periphery (Gill et al. 2015). Since we do not see that blebbing in KapB-expressing cells, we presume that KapB increases the cell adhesion to match the force of the increased cytoskeletal tension that is likely occurring in KapB-expressing cells (discussed above).

As reported above, many of the components required for SFs are also required for PB disassembly. However, all of the proteins that have been shown to effect changes in

PB levels, including mDia1, ROCK1 and 2, α–actinin 1 and 4 and NMII, also regulate various aspects of cellular adhesion molecules (Acharya et al. 2017; Yamana et al. 2006; Shi et al. 2013; Ye et al. 2014; Wolfenson et al. 2011). Treatment with the ROCK inhibitor, blebbistatin and CalA, all rapidly change focal adhesion composition (Wolfenson et al. 2011). Furthermore, the cellular response to shear stress requires both the formation of actin SFs and rearrangements of focal adhesions (Noria et al. 2004; Verma et al. 2015). Since the data presented in this thesis does not distinguish between the roles of these proteins in SF formation or focal adhesion regulation, at this time it is not clear whether certain types of SFs, focal adhesions or both are important in the mechanism of PB disassembly. However, dorsal SFs require focal adhesions to form and focal adhesions require SFs to form and mature (Hotulainen and Lappalainen 2006; Oakes et al. 2012). Furthermore, increased cytoskeletal tension in the cell increases the formation of both focal adhesions and SFs (Hotulainen and Lappalainen 2006; Oakes et al. 2012). Since the two phenotypes are intertwined, it supports that both SFs and focal adhesions are altered in the KapB phenotype. Future studies will examine focal adhesion components by immunofluorescence to see if there are visible differences in adhesion composition or size. For example, with increased cytoskeletal tension, vinculin levels increase at focal adhesions, while paxillin levels decrease (Wolfenson et al. 2011), so a comparison of the levels of these two proteins at focal adhesions would inform on focal adhesion status. Taken together, I observed that many treatments that restore PBs do not disrupt visible actin fibres/SFs, suggesting that it is not the actin structure alone but its function as a mediator of cell contractility that is required for KapB-induced PB disassembly.

### 4.3.5 Mechanoresponsive Signalling by YAP Controls PB Disassembly

Increases in cytoskeletal tension can mediate signalling events, through a process called mechanotransduction. The sections below will discuss how the mechanoresponsive transcription factor YAP, but not SRF, is required for PB disassembly in response to KapB or mechanical force.

#### 4.3.5.1 Serum-Response Factor (SRF) Does Not Control PB Disassembly

SRF is a major regulator of actin dynamics that is, in turn, activated by changes in the cytoskeleton (Miano, Long, and Fujiwara 2007). In this case, SRF is activated by a reduction in the concentration of free monomeric G-actin that accompanies F-actin polymerization, to modulate genes involved in the actin cytoskeleton and growth (Sotiropoulos et al. 1999; Miano, Long, and Fujiwara 2007). Since KapB decreases monomeric G-actin (Figure 3.15), I considered the possibility that changes in monomeric G-actin were an important signaling event that controlled PB disassembly. To test this hypothesis, cells were treated with Jasp, previously shown to induce aberrant actin polymerization and decrease the monomeric G-actin; importantly, also activating SRF (Sotiropoulos et al. 1999; Bubb et al. 1999). Treatment with Jasp resulted in an increase in PBs, indicating that depleting the monomeric G-actin (and by implication, activating SRF) is not responsible for PB disassembly (Figure 3.16). Furthermore, I increased the monomeric G-actin fraction with CytD, a drug that caps actin, preventing polymerization (Wakatsuki et al. 2001) and showed the same effect, an increase in PBs (Figure 3.16). This further supports my conclusion that the concentration of monomeric G-actin is not responsible for changes in PB levels.

#### 4.3.5.2 YAP Activation Via Increased Cytoskeletal Tension Controls PB Disassembly

The mechanoresponsive transcriptional activator, YAP, responds to RhoA-mediated signalling and cytoskeletal tension (Dupont et al. 2011; Das et al. 2016). Knockdown of YAP restored PBs in KapB-expressing cells, indicating that YAP was integral to the mechanism of PB disassembly (Figure 3.19). Furthermore, ectopic expression of constitutively-active YAP induced PB disassembly, indicating that this is not only a KapB-specific effect, but that active YAP can induce PB disassembly (Figure 3.20).

Various YAP inputs, including shear stress, ECM stiffness and changes in cell confluence, were investigated to see if they controlled PB disassembly. Shear stress stimulated PB disassembly (Figure 3.23). Additionally, increasing stiffness through increasing concentration of collagen incrementally decreased PBs, suggesting that ECM stiffness, may control disassembly of PBs (Figure 3.22). However, due to small observed

changes in actin structure and YAP localization, this experiment must be repeated. Ideally, further replicates of this experiment will utilize matrices of different stiffness rather than increases in collagen concentration to directly alter ECM stiffness, rather than increasing ECM component concentration, a factor that also functions to increase adhesion binding sites. Previous work has demonstrated that YAP is active at low cell density and inactive at high cell density (Zhao et al. 2007). Experimentally, PB counts were higher in low density cells than in high density cells, suggesting that control of PB disassembly does not depend on YAP during changes in confluency (Figure 3.21). Since changes in YAP signalling due to confluency are thought to be primarily mediated by intracellular junctions (Boggiano and Fehon 2012), my data suggests that decreases in intracellular junctions at low confluency does not control PB disassembly. Notably, both shear stress and increased ECM concentration activate RhoA to form SFs (Noria et al. 2004; Lee and Kumar 2016). Furthermore, RhoA activation due to ECM changes has been directly controls YAP nuclear localization (Dupont et al. 2011). With YAP activation and PB disassembly both being closely tied to RhoA signalling and cytoskeletal contractility, it suggests any activator of YAP that induces cytoskeletal contractility through RhoA mediate will PB disassembly. In support of this idea, signalling through GPCRs, $G_{11/12}$ and $G_{q/11}$ activate YAP in a RhoA-dependent manner (Yu et al. 2012). Accordingly, LPA treatment, a known ligand to activate $G_{11/12}$, induces PB disassembly in HUVECs (Corcoran et al. 2012). Furthermore, overexpression of KSHV vGPCR (a constitutively active signaling molecule) also induces PB disassembly in a RhoA-dependent manner (Corcoran et al. 2012). Therefore, other RhoA-mediated YAP activation through GPCRs may also be able to disassemble PBs in a manner dependent on RhoA and cytoskeletal tension.

Though the experiments described above suggest that YAP activation mediated by increases in mechanical tension can control PB disassembly, none of these experiments directly show that YAP is mediating this change. To investigate if, similar to KapB, YAP is controlling PB disassembly in the context of shear stress, YAP knockdown cells were subjected to fluid flow and PBs were examined. Substantial cell loss was observed when YAP knockdown cells were subjected to shear stress (Figure 3.24). Since shear stress requires changes in cell adhesion and YAP can control focal adhesion dynamics (Zhou,

Li, and Chien 2014; Nardone et al. 2017), it is likely that the cells were not able to appropriately respond to the external force. It is also important to note that there is uneven distribution of the force of fluid flow depending on the cell position within the flow chamber (Vogel et al. 2007). PB levels were increased in YAP KD cells exposed to shear stress near the inlet, however, these cells displayed aberrantly large PBs that were phenotypically-different than those seen in the static controls (Figure 3.24, shYAP1-2, inlet), perhaps indicating associations with stress granules, as PBs can be associated with these structures during certain stressors (Stoecklin and Kedersha 2013). Given that these PBs were phenotypically-different and may not be performing the same roles as those in the static NT condition, these data should not be considered restoration at this time. Conversely, the cells in the center of the flow chamber maintained SFs and had PBs that looked akin those in the static controls, suggesting PB restoration (Figure 3.24, shYAP1-2, outlet). Regardless of the undetermined role of YAP in controlling PB disassembly during shear stress, the combined data demonstrates that mechanical forces that activate YAP via RhoA can also disassemble PBs. Moreover, during KapB expression, PB loss is dependent on YAP, thereby suggesting a role for YAP in controlling the stability of ARE-mRNAs through PB regulation.

Though there are no previous reports linking YAP and PB dynamics, several YAP-target genes contain ARE elements in their 3'UTR, including CTGF and ANKRD1 (Shen and Stanger 2015; Bakheet, Hitti, and Khabar 2017). Correspondingly, shear stress upregulates many genes containing ARE-mRNAs (Vozzi et al. 2018; Bakheet, Hitti, and Khabar 2017). Vozzi et al. (2018) performed microarray analysis of the transcriptomic changes in HUVECs subjected to shear stress. There was a 20% enrichment in the proportion of genes that contained AREs in the significantly upregulated transcripts from HUVECs subjected to shear stress (Vozzi et al. 2018; Bakheet, Hitti, and Khabar 2017). Though this does not directly indicate increased stability of the transcripts, it supports the working model that YAP-responsive genes may, after their transcription, be further enhanced by the decreased ARE-mRNA turnover that results from PB disassembly. Precisely how YAP may be mediating PB disassembly to ensure efficient translation of its target genes, explored in the following section.

#### 4.3.5.3 Autophagy as a Potential Mechanism for YAP-mediated PB Disassembly

We know that YAP activation can control PB disassembly. Most relevant to my work, is data derived from other studies in the Corcoran Lab that suggests PB disassembly requires KapB-mediated upregulation of the cellular catabolic program of autophagy (Robinson, Singh and Corcoran, unpublished). KapB can upregulate autophagy, which mediates the selective degradation of a subset of PB components, including DCP1a but not DDX6 (Robinson, Singh and Corcoran, unpublished). YAP has recently been linked with the regulation of autophagy, though this role appears to be context-dependent. In breast and thyroid cancer cells, YAP expression increases autophagic flux (Song et al. 2015; Liu et al. 2017), whereas in endometrial stromal cells, increased expression of YAP is correlated with decreased autophagy (Pei et al. 2019). Pavel et al. (2018) provide a more mechanistic view of the connection between YAP and autophagy. They show that YAP activity at both low confluence as well as increased matrix stiffness increases autophagy (Pavel et al. 2018). Furthermore, unidirectional shear stress in endothelial cells, hepatocellular carcinoma cells and HeLa cells upregulates autophagy (Liu et al. 2015; Yao et al. 2015; Wang et al. 2018; Das et al. 2018). In my work, similar to observations in KapB-expressing cells, shear stress resulted in degradation of DCP1a but not DDX6 (Figure 3.23), indicating that PB disassembly in shear stress may also be mediated by autophagy. Taken together, this suggests the possibility that YAP activation is required to elicit autophagy, which in turn is required for PB disassembly and that this mechanism is active during both shear stress and after KapB-expression. Markers of autophagic flux will be investigated in the context of KapB and +/- YAP knockdown to determine the contribution of YAP to KapB-mediated alterations in autophagic flux.

#### 4.3.5.4 KapB Alters YAP Dynamics

Despite the implications of YAP in PB dynamics discussed above, the status of YAP activation in KapB-expressing cells is unclear. YAP activation, in the literature, is often reported as: i) an increase in YAP nuclear localization, ii) a decrease in the phosphorylation of YAP at Ser127, and iii) an upregulation in mRNA transcript

abundance of the canonical YAP genes, including CTGF, ANKRD1 and CYR61. These activation markers were examined in KapB-expressing cells: KapB-expression in HUVECs induced a small but consistent increase in nuclear YAP localization, a decrease in the proportion of phosphorylated YAP and a slight upregulation of CTGF (Figure 3.17, 3.18). Studies of YAP activation during shear stress also show small (1.5- to 2.5-fold), but consistent increases in conventionally-assayed YAP target genes (Chien et al. 2016; Nakajima et al. 2017), indicating that gene expression changes at a low level can be expected with certain mechanical activators of YAP. Despite the reproducibility, qPCR may not be sensitive enough to accurately detect these small changes, indicating that this data must be replicated in a more sensitive system, such as droplet digital PCR. A previous student showed that KapB expression activates TEAD promoters, promoters YAP is known to bind, in a TEAD-based luciferase assay (O'Brien and McCormick, unpublished). These data argue that YAP is being transcriptionally activated in KapB-expressing cells. However, unlike what is conventionally reported with YAP transcriptional activation, KapB expression also increases total YAP protein levels in cells (Figure 3.17). It is possible that the YAP activation seen in KapB-expressing HUVECs is not an activation of a given pathway, but instead a passive increase in nuclear YAP due to the increase in total YAP. Supporting this, the other genes that are commonly activated during YAP mechanical activation, ANKRD1 and CYR61 (Chien et al. 2016; Nakajima et al. 2017), are not significantly upregulated in KapB-expressing cells (Figure 3.18). To discern whether YAP is acting as a transcriptional activator in KapB-expressing cells, additional genes known to be regulated by YAP, namely those involved in inflammation and angiogenesis, will be measured in the presence and absence of YAP, to determine if different, more robust YAP-mediated gene expression changes are occurring.

The specificity of the genes that are upregulated during YAP activation is directed by its binding partners (Kim, Jang, and Bae 2018). Intriguingly, a yeast two-hybrid screen using KapC, a protein that contains the same direct repeats as KapB with the addition of a transmembrane domain, indicated a potential direct interaction with YAP (McCormick, unpublished). Since KapB does not robustly induce canonical YAP targets, perhaps KapB has coopted YAP for another purpose, via a direct binding event. Alternatively, YAP may be binding to other transcriptional regulators. For example, YAP can bind and activate

STAT3 to promote angiogenesis (He et al. 2018). KapB activates STAT3 (King 2013), thus it is possible that YAP is playing a role in STAT3 transcription in KapB-expressing cells.

In KapB-expressing cells, the increase in total YAP tends to be more substantial than the increase in nuclear YAP (Figure 3.17), indicating that, in addition to mediating transcriptional changes, YAP could (1) have a functional role in the cytoplasm or (2) be sequestered in the cytoplasm to prevent certain signalling pathways. YAP can carry out cytoplasmic functions. For example, cytoplasmic YAP can regulate vascular inflammation by promoting degradation of TRAF6, a co-activator of NFKB signalling (Lv et al. 2018). NFκB reduces the spontaneous lytic activation of KSHV, suggesting that it contributes to the maintenance of latency (Grossmann and Ganem 2008). If YAP is increased in the cytoplasm of KapB-expressing cells, it is possible that YAP is decreasing NFκB activation by sequestering TRAF6. If KapB were to sequester TRAF6 to inhibit NFκB expression, it would suggest that KapB is involved in promoting lytic reactivation. Alternatively, YAP may be sequestered to promote cell survival through inhibition of apoptotic signalling pathways. Nuclear YAP can control apoptosis through p73 and EGR-1 (Kim, Jang, and Bae 2018). Furthermore, nuclear YAP can promote detachment-mediated apoptosis, called anoikis (Zhao et al. 2012), and anoikis resistance is required for angiogenesis (Gao et al. 2019). This presents the possibility that YAP is being sequestered in the cytoplasm to prevent certain signalling events, such as anoikis, resulting in an increase in angiogenesis. Finally, unphosphorylated YAP can inhibit activation of the interferon response through sequestration of the interferon-response activator TBK-1 in the cytoplasm (Zhang et al. 2017). Another herpesvirus, human herpesvirus-1 promotes YAP binding of TBK-1 (Zhang et al. 2017) indicating that KSHV may also promote this cytoplasmic function of YAP.

Investigating which proteins are acting as YAP binding partners will provide insight to which processes are differentially regulated by YAP in KapB-expressing cells. A co-immunoprecipitation of YAP in KapB-expressing cells will be performed to see if YAP can bind STAT3, TRAF6 or KapB in this context. To further examine whether KapB is binding YAP and to elucidate some of the other potential roles of KapB, a BioID

experiment in which interacting partners of KapB will be biotinylated, isolated and identified will be performed.

### 4.4 Potential KapB-Mediated Contributions to the KS Lesion

While KapB overexpression models have shown that KapB-mediated signalling causes PB disassembly in a YAP-dependent manner, it is important to consider what is happening in the context of the KS lesion. Some examples of the roles KapB-mediated YAP activation and PB disassembly could be playing in the context of cell angiogenesis and inflammation, two of the main characteristics of the KS lesion, are discussed below.

#### 4.4.1 Angiogenesis

Previous studies have shown that KapB increases endothelial cell tubule formation in matrigel, which is an *in vitro* assay for angiogenesis (Corcoran, Johnston, and McCormick 2015). YAP-mediated signalling may be contributing to the increase in angiogenic potential of KapB-expressing cells. YAP has been implicated as a critical activator of VEGF-mediated angiogenesis, as knockdown of YAP resulted in reduced sprouting of vessels (Kim et al. 2017). Since there are high levels of VEGF in the KS lesion (Samaniego et al. 1998), it is likely that YAP is acting as an effector of VEGF in this context and KapB-mediated alterations in YAP signalling may direct or contribute to these changes. Additionally, YAP may be increasing angiogenesis by upregulating certain genes. For example, the proangiogenic factor, angiopoeitin-2 (Ang-2) was identified as a target gene of YAP and YAP is required for Ang-2 mediated vessel growth (Choi et al. 2015). Furthermore, YAP activation may promote angiogenesis indirectly. For angiogenesis to occur, degradation of the ECM is required (Neve et al. 2014). Matrix metalloproteinases (MMPs) are proteins that cleave components of the ECM to promote cell migration. KSHV infection requires the secretion of MMP-1,-2 and -9 to promote HUVEC invasion into the ECM, a function required for the aberrant angiogenesis seen in KSHV (Qian et al. 2007). YAP upregulates MMP-7 on stiff substrates, indicating that activation of YAP can regulate changes in the ECM (Nukuda et al. 2015). These studies suggest that KapB-mediated activation of YAP may be directing responses to angiogenic stimuli, and regulating the expression of different genes that promote angiogenesis.

Furthermore, VEGF, the VEGF receptor, Ang-2 and several MMPs contain ARE-elements in the 3' UTR (Bakheet, Hitti, and Khabar 2017). This indicates that the KapB-mediated activation of YAP could contribute to angiogenesis through a combination of direct transcription regulation but also through PB disassembly, which would result in the enhanced stability of key angiogenic transcripts like VEGF.

### 4.4.2 Inflammation

The association of YAP to the regulation of inflammation is complex, with reports of YAP being both pro- and anti-inflammatory (reviewed in Zhou et al. 2018). For example, YAP upregulates IL-6 in endometrial cancer and hepatocellular carcinoma cells, as well as COX-2 in colorectal cancer cells (Li et al. 2017; Zhou et al. 2018; Wang et al. 2019). Notably, both IL-6 and COX-2 are implicated in KS pathology (Miles et al. 1990; Sharma-Walia et al. 2010). However, other reports suggest that YAP suppresses COX-2 in a cell-confluence dependent manner (Qiong Zhang et al. 2018). This suggests a complex and context-dependent regulation of inflammatory molecules by YAP. YAP can also act as an effector of inflammatory cytokines. For example, stimulation of endothelial cells with TNF induces YAP nuclear localization through RhoA activity, which then modulates upregulation of leukocyte adhesion molecule VCAM-1 (Choi et al. 2018). Thus, YAP has the potential to directly contribute to the upregulation of inflammatory transcripts and cellular responses to inflammation, but such hypotheses need to be confirmed in the context of KapB.

As mentioned above, many of the inflammatory cytokines stimulated in KS infection, including IL-6 and COX-2, also contain ARE-elements, indicating that PB disassembly is likely required for efficient expression of these molecules (Franks and Lykke-Andersen 2007; Bakheet, Hitti, and Khabar 2017). Therefore, the regulation of PB disassembly by YAP would putatively control expression of inflammatory molecules in KS through transcript stability.

### 4.4.3 Parallels with Atherosclerosis

The pathway described in this work is active in KapB-expressing cells, and is likely also active during shear stress. To gain insight about the physiologically-relevant

effects of this pathway, diseases arising from pathogenic shear stress can be examined. Atherosclerosis is the formation of a plaque in the wall of an artery, and is partially mediated by endothelial dysfunction due to disturbed, or atherogenic, blood flow. Recently, YAP has been implicated as a mediator of the pathogenicity in atherosclerosis (Chien et al. 2016; Li et al. 2019). Atherogenic shear stress upregulates YAP, which in turn upregulates ICAM-1 and VCAM-1, markers of pathogenesis in atherosclerosis (Chien et al. 2016). Increases in ICAM-1 and VCAM-1 are known to increase leukocyte recruitment (Sans et al. 1999). Accordingly, YAP activation in shear stress also resulted in an increased number of monocytes adhering to the endothelium (Chien et al. 2016). Notably, ICAM-1, but not VCAM-1, is significantly upregulated in the KS lesion following cytokine stimulation (Kaaya et al. 1996; Yang et al. 1994; Sciacca et al. 1994). Since KSHV can infect monocytes, YAP-mediated ICAM-1 upregulation may be a mechanism for the virus to recruit other cells for further infection (Blasig et al. 1997). Additionally, the cytokines promoting pathogenic progression of atherosclerosis include IL-1β, IL-6, IL-8, TNF, and GM-CSF (Tousoulis et al. 2016), similar to those seen in the KS lesion (Lee et al. 2010). Notably, each of these cytokines contain AREs, indicating they are regulated at PBs (Bakheet, Hitti, and Khabar 2017), so PB disassembly seen in shear stress and in KapB-expression is likely required for their expression increases. The similarities between the inflammatory environment in KS and atherosclerosis support the idea that the RhoA-YAP-PB disassembly axis may be mediating pathogenic changes due to activation by KapB and shear stress.

### 4.4.4 From the Perspective of KSHV

The present discussion has predominately focused on how KapB-mediated changes promote the tumorigenic environment in the context of the KS lesion, but has largely omitted the rationale for why these changes may be of benefit to the virus. The likely answer to this question is that the KS lesion is not actually beneficial to KSHV, but rather, is a side-effect of viral immune evasion (Douglas et al. 2010). Increased tumorigenesis, mediated in part via enhanced inflammation and angiogenesis, presents no clear advantage to the virus. However, both these processes increase the recruitment of immune cells to the site of infection; for KSHV, this is believed to facilitate local and

wide dissemination of the virus (Cavallin, Goldschmidt-Clermont, and Mesri 2014). KSHV may also induce the promotion of cytokines, such as IL-6, that can promote both cell survival and proliferation in order to copy the viral episome during latency, thereby maintaining chronic infection (Moreno et al. 2001; Meng et al. 2006; Douglas et al. 2010). Furthermore, the cytokines promoted by KSHV skew the immune response to a Th2 response, rather than a more antiviral Th1 response, promoting viral survival (Douglas et al. 2010). During such an immune modulation, the signalling pathways that are utilized to promote these cytokines, and the cytokines themselves, also mediate migration, angiogenesis and inflammation (Douglas et al. 2010). Thus, though this may not be a directed response of the virus, the pathway reported in this thesis likely promotes the disease state seen in KS and other inflammatory diseases, such as atherosclerosis.

### 4.5 Model and Conclusions

In my thesis, I propose a novel mechanoresponsive pathway that links actin SFs, actomyosin contractility, and the transcription factor YAP to the disassembly of PBs, corresponding to increased stability of angiogenic and inflammatory mRNAs (Figure 4.1). In this model, mechanical stresses (shear stress, increasing ECM stiffness) that activate the GTPase RhoA mediate formation of SFs through mDia and ROCK, and increase actomyosin contractility. Increases in contractility and predicted increases in adhesion to the ECM result in an increase in cytoskeletal tension which mechanically activates the transcriptional regulator YAP. YAP activation coordinates PB disassembly, through an as yet undefined mechanism which may involve the upregulation of autophagy. Unlike mechanical activation of YAP originating from an external force, KapB hijacks this pathway and activates the same mechanoresponsive pathway from the inside. KapB directly binds and activates MK2 and via a non-canonical signaling axis, activates RhoA (McCormick and Ganem 2005; Corcoran, Johnston, and McCormick 2015) to elicit the same constellation of signaling events that are also induced by external forces like shear stress. At this time, it is unclear whether YAP is conventionally ‘active’ with KapB expression or if it functions through alternative mechanisms, such as cytoplasmic sequestration of certain proteins. Regardless, the change in YAP signalling induces disassembly of PBs, and corresponds to an increase in the stability of

inflammatory and angiogenic transcripts. Changes in YAP signalling may also mediate direct transcriptional upregulation of these transcripts. Through direct gene regulation and increased transcript stability, KapB-mediated activation of YAP can increase inflammation and angiogenesis, which are hallmarks of KS.

This RhoA-YAP-PB disassembly axis is not restricted to KSHV latency, but is likely activated by any mechanical process that alters cell shape and increases cytoskeletal tension. The effects of the mechanical environment surrounding a cell has implications in the lab setting, as it informs on how tissue culture conditions may impact gene expression. The pathway also imparts mechanistic detail about conserved cell responses - how a cell can sense abnormalities in its physical environment and drive an immune response to restore homeostasis. Finally, it helps us to understand some of the mechanisms that can lead to pathologies in the context of dysregulated blood flow and stiffening ECM, such as atherosclerosis and fibrosis respectively. At a broad level, this work connects cell morphology with post-transcriptional gene regulation that enables rapid immunological responses, a relevant consideration in a wide array of biological contexts.

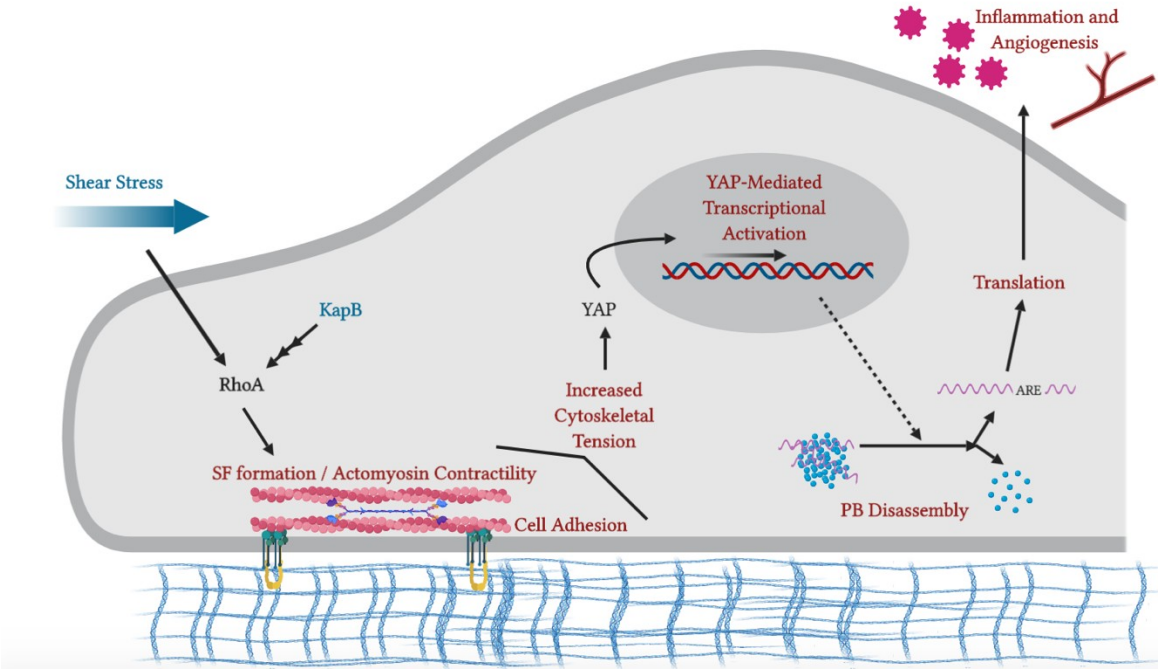


**Figure 4.1: Model of KapB-mediated activation of a mechanoresponsive pathway that mediates PB disassembly.** Mechanical forces such as shear stress activate RhoA to coordinate SF formation and increased actomyosin contractility. Increases in actomyosin contractility in combination with increases in cell adhesion result in increased cytoskeletal tension. This controls nuclear translocation of YAP and YAP-mediated transcriptional activity. Through an unknown mechanism, YAP activity controls PB disassembly. This increases the stability of transcripts with AU-rich elements, known to commonly encode inflammatory and angiogenic factors, promoting their expression. KapB activates this pathway from inside the cell, through activation of MK2, to control PB disassembly in the context of KSHV latent infection. Illustration made with: https://app.biorender.com/.

**BIBLIOGRAPHY**

Acharya, Bipul R., Alexander Nestor-Bergmann, Xuan Liang, Shafali Gupta, Kinga Duszyc, Estelle Gauquelin, Guillermo A. Gomez, et al. 2018. "A Mechanosensitive RhoA Pathway That Protects Epithelia against Acute Tensile Stress." *Developmental Cell* 47 (4): 439-452.e6. https://doi.org/10.1016/j.devcel.2018.09.016.

Acharya, Bipul R., Selwin K. Wu, Zi Zhao Lieu, Robert G. Parton, Stephan W. Grill, Alexander D. Bershadsky, Guillermo A. Gomez, and Alpha S. Yap. 2017. "Mammalian Diaphanous 1 Mediates a Pathway for E-Cadherin to Stabilize Epithelial Barriers through Junctional Contractility." *Cell Reports* 18 (12): 2854–67. https://doi.org/10.1016/j.celrep.2017.02.078.

Addgene. 2006. "PLKO.1 - TRC Cloning Vector." 2006. https://www.addgene.org/tools/protocols/plko/.

Aizer, Adva, Yehuda Brody, Lian Wee Ler, Nahum Sonenberg, Robert H. Singer, and Yaron Shav-Tal. 2008. "The Dynamics of Mammalian P Body Transport, Assembly, and Disassembly In Vivo." *Molecular Biology of the Cell* 19 (11): 4154–66. https://doi.org/10.1091/mbc.E08.

Amano, M, K Chihara, K Kimura, Y Fukata, N Nakamura, Y Matsuura, and K Kaibuchi. 1997. "Formation of Actin Stress Fibers and Focal Adhesions Enhanced by Rho-Kinase." *Science* 275 (5304): 1308–11. https://doi.org/10.1126/science.275.5304.1308.

Amano, Mutsuki, Masaaki Ito, Kazushi Kimura, Yuko Fukata, Kazuyasu Chihara, Takeshi Nakano, Yoshiharu Matsuura, and Kozo Kaibuchi. 1996. "Phosphorylation and Activation of Myosin by Rho-Associated Kinase (Rho-Kinase)." *The Journal of Biological Chemistry* 271 (34): 20246–49. https://doi.org/10.1074/jbc.271.34.20246.

Ambroziak, J., D. Blackbourn, B. Herndier, R. Glogau, J. Gullett, A. McDonald, E. Lennette, and J. Levy. 1995. "Herpes-like Sequences in HIV-Infected and Uninfected Kaposi's Sarcoma Patients." *Science* 268 (5210): 582–83. https://doi.org/10.1126/science.7725108.

Aneja, Kawalpreet K., and Yan Yuan. 2017. "Reactivation and Lytic Replication of Kaposi's Sarcoma-Associated Herpesvirus: An Update." *Frontiers in Microbiology* 8 (APR): 1–23. https://doi.org/10.3389/fmicb.2017.00613.

Antman, Karen, and Yuan Chang. 2000. “Kaposi’s Sarcoma.” *New England Journal of Medicine* 342 (14): 1027–38. https://doi.org/10.1056/NEJM200004063421407.

Araki, Nobukazu, Tenenori Hatae, Tesshi Yamada, and Setsu Hirohashi. 2000. “Actinin-4 Is Preferentially Involved in Circular Ruffling and Macropinocytosis in Mouse Macrophages: Analysis by Fluorescence Ratio Imaging.” *Journal of Cell Science* 113: 3329–40. http://jcs.biologists.org/content/113/18/3329.full.pdf.

Arias, Carolina, Ben Weisburd, Noam Stern-Ginossar, Alexandre Mercier, Alexis S. Madrid, Priya Bellare, Meghan Holdorf, Jonathan S. Weissman, and Don Ganem. 2014. “KSHV 2.0: A Comprehensive Annotation of the Kaposi’s Sarcoma-Associated Herpesvirus Genome Using Next-Generation Sequencing Reveals Novel Genomic and Functional Features.” *PLoS Pathogens* 10 (1). https://doi.org/10.1371/journal.ppat.1003847.

Asano, Yukako, and Issei Mabuchi. 2001. “Calyculin-A, an Inhibitor for Protein Phosphatases, Induces Cortical Contraction in Unfertilized Sea Urchin Eggs.” *Cell Motility and the Cytoskeleton* 48 (4): 245–61. https://doi.org/10.1002/cm.1013.

Bakheet, Tala, Edward Hitti, and Khalid S A Khabar. 2017. “ARED-Plus: An Updated and Expanded Database of AU-Rich Element-Containing MRNAs and Pre-MRNAs.” *Nucleic Acids Research* 46 (October 2017): 2017–19. https://doi.org/10.1093/nar/gkx975.

Bakheet, Tala, Bryan R G Williams, and Khalid S a Khabar. 2006. “ARED 3.0: The Large and Diverse AU-Rich Transcriptome.” *Nucleic Acids Research* 34 (Database issue): D111–14. https://doi.org/10.1093/nar/gkj052.

Bakin, Andrei V, Cammie Rinehart, Anne K Tomlinson, and Carlos L Arteaga. 2002. “P38 Mitogen-Activated Protein Kinase Is Required for TGFbeta-Mediated Fibroblastic Transdifferentiation and Cell Migration.” *Journal of Cell Science* 115 (Pt 15): 3193–3206.

Bakin, Andrei V, Alfiya Safina, Cammie Rinehart, Cecilia Daroqui, Huferesh Darbary, and David M Helfman. 2004. “A Critical Role of Tropomyosins in TGF- ᴺᴸ Regulation of the Actin Cytoskeleton and Cell Motility in Epithelial Cells” 15 (October): 4682–94. https://doi.org/10.1091/mbc.E04.

Bárány, K, M Bárány, J. M. Gillis, and M. J. Kushmerick. 1979. "Phosphorylation-Dephosphorylation of the 18,000-Dalton Light Chain of Myosin during the Contraction-Relaxation Cycle of Frog Muscle." *The Journal of Biological Chemistry* 254 (9): 3617–23.

Bashkirov, Vladimir I., Harry Scherthan, Jachen A. Solinger, Jean Marie Buerstedde, and Wolf Dietrich Heyer. 1997. "A Mouse Cytoplasmic Exoribonuclease (MXRN1p) with Preference for G4 Tetraplex Substrates." *Journal of Cell Biology* 136 (4): 761–73. https://doi.org/10.1083/jcb.136.4.761.

Blanco, Fernando F, Sandhya Sanduja, Natasha G Deane, Perry J Blackshear, and Dan a Dixon. 2014. "Transforming Growth Factor β Regulates P-Body Formation through Induction of the MRNA Decay Factor Tristetraprolin." *Molecular and Cellular Biology* 34 (2): 180–95. https://doi.org/10.1128/MCB.01020-13.

Blasig, Cornelia, Christian Zietz, Beate Haar, Frank Neipel, Stefan Esser, Norbert H Brockmeyer, Erwin Tschachler, Sandra Colombini, Barbara Ensoli, and Abteilung Virusforschung. 1997. "Monocytes in Kaposi ' s Sarcoma Lesions Are Productively Infected by Human Herpesvirus 8" 71 (10): 7963–68.

Blumenthal, J., and I. Ginzburg. 2008. "Zinc as a Translation Regulator in Neurons: Implications for P-Body Aggregation." *Journal of Cell Science* 121 (19): 3253–60. https://doi.org/10.1242/jcs.033266.

Boggiano, Julian C., and Richard G. Fehon. 2012. "Growth Control by Committee: Intercellular Junctions, Cell Polarity, and the Cytoskeleton Regulate Hippo Signaling." *Developmental Cell* 22 (4): 695–702. https://doi.org/10.1016/j.devcel.2012.03.013.

Boldogh, I., P. Szaniszlo, W. A. Bresnahan, C. M. Flaitz, M. C. Nichols, and T. Albrecht. 1996. "Kaposi's Sarcoma Herpesvirus-Like DNA Sequences in the Saliva of Individuals Infected with Human Immunodeficiency Virus." *Clinical Infectious Diseases* 23 (2): 406–7. https://doi.org/10.1093/clinids/23.2.406.

Boshoff, C, T F Schulz, M M Kennedy, a K Graham, C Fisher, a Thomas, J O McGee, R a Weiss, and J J O'Leary. 1995. "Kaposi's Sarcoma-Associated Herpesvirus Infects Endothelial and Spindle Cells." *Nature Medicine* 1 (12): 1274–78. https://doi.org/10.1038/nm1295-1274.

Braun, M. 1982. “Classics in Oncology. Idiopathic Multiple Pigmented Sarcoma of the Skin by Kaposi.” *CA: A Cancer Journal for Clinicians* 32 (6): 340–47.

Bubb, Michael R, Iain Spector, Bret B Beyer, and Katrina M Fatina. 1999. “Effect of Jasplakinolide on the Kinetics of Actin Polymerization.” *Biological Chemistry* 275 (7): 5163–70.

Burnette, Dylan T., Lin Shao, Carolyn Ott, Ana M. Pasapera, Robert S. Fischer, Michelle A. Baird, Christelle Der Loughian, et al. 2014. “A Contractile and Counterbalancing Adhesion System Controls the 3D Shape of Crawling Cells.” *Journal of Cell Biology* 205 (1): 83–96. https://doi.org/10.1083/jcb.201311104.

Burridge, Keith, and Krister Wennerberg. 2004. “Rho and Rac Take Center Stage.” *Cell* 116 (2): 167–79. https://doi.org/10.1016/S0092-8674(04)00003-0.

Burridge, Keith, and Erika S. Wittchen. 2013a. “The Tension Mounts: Stress Fibers as Force-Generating Mechanotransducers.” *Journal of Cell Biology* 200 (1): 9–19. https://doi.org/10.1083/jcb.201210090.

Cai, Jing, Xuewen Song, Wei Wang, Terry Watnick, York Pei, Feng Qian, and Duojia Pan. 2018. “A RhoA–YAP–c-Myc Signaling Axis Promotes the Development of Polycystic Kidney Disease.” *Genes and Development* 32 (11–12): 781–93. https://doi.org/10.1101/gad.315127.118.

Caput, D, B Beutler, K Hartog, R Thayer, S Brown-Shimer, and A Cerami. 1986. “Identification of a Common Nucleotide Sequence in the 3’-Untranslated Region of MRNA Molecules Specifying Inflammatory Mediators.” *Proceedings of the National Academy of Sciences of the United States of America* 83 (6): 1670–74.

Cavallin, Lucas E., Pascal Goldschmidt-Clermont, and Enrique A. Mesri. 2014. “Molecular and Cellular Mechanisms of KSHV Oncogenesis of Kaposi’s Sarcoma Associated with HIV/AIDS.” *PLoS Pathogens* 10 (7): 5–8. https://doi.org/10.1371/journal.ppat.1004154.

Cesarman, Ethel, Yuan Chang, Patrick S. Moore, Jonathan W. Said, and Daniel M. Knowles. 1995. “Kaposi’s Sarcoma–Associated Herpesvirus-Like DNA Sequences in AIDS-Related Body-Cavity–Based Lymphomas.” *New England Journal of Medicine* 332 (18): 1186–91. https://doi.org/10.1056/NEJM199505043321802.

Chai, J., and Andrzej S. Tarnawski. 2002. "Serum Response Factor: Discovery, Biochemistry, Biological Roles and Implications for Tissue Injury Healing." *Journal of Physiology and Pharmacology* 53 (2): 147–57. https://doi.org/10.1007/s12630-011-9636-x.

Chang, Y, E Cesarman, M S Pessin, F Lee, J Culpepper, D M Knowles, and P S Moore. 1994. "Identification of Herpes-like DNA Sequences in AIDS-Associated Kaposi's Sarcoma." *Science* 266: 1865–69. https://doi.org/10.1126/science.7997879.

Chazotte, B. 2011. "Labeling Membrane Glycoproteins or Glycolipids with Fluorescent Wheat Germ Agglutinin." *Cold Spring Harbor Protocols* 2011 (5): pdb.prot5623-pdb.prot5623. https://doi.org/10.1101/pdb.prot5623.

Chen, Gan, Lian Zhao, Jiantao Feng, Guoxing You, Quanmei Sun, Penglong Li, Dong Han, and Hong Zhou. 2013. "Validation of Reliable Reference Genes for Real-Time PCR in Human Umbilical Vein Endothelial Cells on Substrates with Different Stiffness." *PLoS ONE* 8 (6): 1–9. https://doi.org/10.1371/journal.pone.0067360.

Cheng, Lina, Jiayin Zhang, Sana Ahmad, Lorene Rozier, Haiqian Yu, Haiteng Deng, and Yinghui Mao. 2011. "Aurora B Regulates Formin MDia3 in Achieving Metaphase Chromosome Alignment." *Developmental Cell* 20 (3): 342–52. https://doi.org/10.1016/j.devcel.2011.01.008.

Chesarone, Melissa A., Amy Grace Dupage, and Bruce L. Goode. 2010. "Unleashing Formins to Remodel the Actin and Microtubule Cytoskeletons." *Nature Reviews Molecular Cell Biology* 11 (1): 62–74. https://doi.org/10.1038/nrm2816.

Chien, Shu, Phu Nguyen, Jocelyn Lopez, Satenick Thorossian, Kuei-Chun Wang, Yi-Ting Yeh, Yi-Shuan J. Li, Elaine Limqueco, and Kun-Liang Guan. 2016. "Flow-Dependent YAP/TAZ Activities Regulate Endothelial Phenotypes and Atherosclerosis." *Proceedings of the National Academy of Sciences* 113 (41): 11525–30. https://doi.org/10.1073/pnas.1613121113.

Choi, Colin K., Miguel Vicente-Manzanares, Jessica Zareno, Leanna A. Whitmore, Alex Mogilner, and Alan Rick Horwitz. 2008. "Actin and α-Actinin Orchestrate the Assembly and Maturation of Nascent Adhesions in a Myosin II Motor-Independent Manner." *Nature Cell Biology* 10 (9): 1039–50. https://doi.org/10.1038/ncb1763.

Choi, Hyun-Jung, Na-Eun Kim, Byeong Kim, Miran Seo, and Ji Heo. 2018. "TNF-α-Induced YAP/TAZ Activity Mediates Leukocyte-Endothelial Adhesion by Regulating VCAM1 Expression in Endothelial Cells." *International Journal of Molecular Sciences* 19 (11): 3428. https://doi.org/10.3390/ijms19113428.

Choi, Hyun Jung, Haiying Zhang, Hongryeol Park, Kyu Sung Choi, Heon Woo Lee, Vijayendra Agrawal, Young Myeong Kim, and Young Guen Kwon. 2015. "Yes-Associated Protein Regulates Endothelial Cell Contact-Mediated Expression of Angiopoietin-2." *Nature Communications* 6 (May): 1–14. https://doi.org/10.1038/ncomms7943.

Chrzanowska-Wodnicka, M. 2004. "Rho-Stimulated Contractility Drives the Formation of Stress Fibers and Focal Adhesions." *The Journal of Cell Biology* 133 (6): 1403–15. https://doi.org/10.1083/jcb.133.6.1403.

Chu, Chia Ying, and Tariq M. Rana. 2006. "Translation Repression in Human Cells by MicroRNA-Induced Gene Silencing Requires RCK/P54." *PLoS Biology* 4 (7): 1122–36. https://doi.org/10.1371/journal.pbio.0040210.

Coller, Jeff, and Roy Parker. 2005. "General Translational Repression by Activators of MRNA Decapping." *Cell* 122 (6): 875–86. https://doi.org/10.1016/j.cell.2005.07.012.

Conti, Mary Anne, and Robert S Adelstein. 2008. "Nonmuscle Myosin II Moves in New Directions." *Journal of Cell Science* 121 (Pt 1): 11–18. https://doi.org/10.1242/jcs.007112.

Cook-Mozaffari, P, R Newton, V Beral, and DP Burkitt. 1998. "The Geographical Distribution of Kaposi's Sarcoma and of Lymphomas in Africa before the AIDS Epidemic." *British Journal of Cancer* 78 (11): 1521–28. https://doi.org/10.1038/bjc.1998.717.

Corcoran, J., D. Khaperskyy, B. Johnston, C. King, D. Cyr, A. Olsthoorn, and C. McCormick. 2012. "Kaposi's Sarcoma-Associated Herpesvirus G-Protein-Coupled Receptor Prevents AU-Rich-Element-Mediated MRNA Decay." *Journal of Virology* 86 (16): 8859–71. https://doi.org/10.1128/JVI.00597-12.

Corcoran, J A, and C McCormick. 2015. "Viral Activation of Stress-Regulated Rho-GTPase Signaling Pathway Disrupts Sites of MRNA Degradation to Influence Cellular Gene Expression." *Small GTPases* 1248 (May 2016): 1–8. https://doi.org/10.1080/21541248.2015.1093068.

Corcoran, Jennifer A., Denys A. Khaperskyy, and Craig McCormick. 2011. "Assays for Monitoring Viral Manipulation of Host ARE-MRNA Turnover." *Methods* 55 (2): 172–81. https://doi.org/10.1016/j.ymeth.2011.08.005.

Corcoran, Jennifer, Benjamin Johnston, and Craig McCormick. 2015. "Viral Activation of MK2-Hsp27-P115RhoGEF-RhoA Signaling Axis Causes Cytoskeletal Rearrangements, P-Body Disruption and ARE-MRNA Stabilization." *PLoS Pathogens* 11 (1): e1004597. https://doi.org/10.1371/journal.ppat.1004597.

Cougot, Nicolas, Sylvie Babajko, and Bertrand Séraphin. 2004. "Cytoplasmic Foci Are Sites of MRNA Decay in Human Cells." *Journal of Cell Biology* 165 (1): 31–40. https://doi.org/10.1083/jcb.200309008.

Cougot, Nicolas, Annie Cavalier, Daniel Thomas, and Reynald Gillet. 2012. "The Dual Organization of P-Bodies Revealed by Immunoelectron Microscopy and Electron Tomography." *Journal of Molecular Biology* 420 (1–2): 17–28. https://doi.org/10.1016/j.jmb.2012.03.027.

Cox, Guy, and Colin J.R. Sheppard. 2004. "Practical Limits of Resolution in Confocal and Non-Linear Microscopy." *Microscopy Research and Technique* 63 (1): 18–22. https://doi.org/10.1002/jemt.10423.

Cramer, Louise P., Margaret Siebert, and Timothy J. Mitchison. 1997. "Identification of Novel Graded Polarity Actin Filament Bundles in Locomoting Heart Fibroblasts: Implications for the Generation of Motile Force." *Journal of Cell Biology* 136 (6): 1287–1305. https://doi.org/10.1083/jcb.136.6.1287.

Das, Arupratan, Robert S. Fischer, Duojia Pan, and Clare M. Waterman. 2016. "YAP Nuclear Localization in the Absence of Cell-Cell Contact Is Mediated by a Filamentous Actin-Dependent, Myosin IIand Phospho-YAP-Independent Pathway during Extracellular Matrix Mechanosensing." *Journal of Biological Chemistry* 291 (12): 6096–6110. https://doi.org/10.1074/jbc.M115.708313.

Das, Joyjyoti, Somnath Maji, Tarun Agarwal, Suman Chakraborty, and Tapas K. Maiti. 2018. "Hemodynamic Shear Stress Induces Protective Autophagy in HeLa Cells through Lipid Raft-Mediated Mechanotransduction." *Clinical and Experimental Metastasis* 35 (3): 135–48. https://doi.org/10.1007/s10585-018-9887-9.

Davies, Peter F. 1995. "Flow-Mediated Endothelial Mechanotransduction." *Physiological Reviews* 75 (3): 519–60. https://doi.org/10.1152/physrev.1995.75.3.519.

Dijk, Erwin Van, Nicolas Cougot, Sylke Meyer, Sylvie Babajko, Elmar Wahle, and Bertrand Séraphin. 2002. "Human Dcp2: A Catalytically Active MRNA Decapping Enzyme Located in Specific Cytoplasmic Structures." *EMBO Journal* 21 (24): 6915–24. https://doi.org/10.1093/emboj/cdf678.

Discher, Dennis E, Paul Janmey, and Yu-li Wang. 2005. "Tissue Cells Feel and Respond to the Stiffness of Their Substrate." *Science (New York, N.Y.)* 310 (5751): 1139–43. https://doi.org/10.1126/science.1116995.

Douglas, Janet L, Jean K Gustin, Ashlee V Moses, Bruce J Dezube, and Liron Pantanowitz. 2010. "Kaposi Sarcoma Pathogenesis: A Triad of Viral Infection, Oncogenesis and Chronic Inflammation." Edited by Halvard Bönig. *Translational Biomedicine* 1 (2): e0178059. https://doi.org/10.1371/journal.pone.0178059.

Downward, Julian, Marius Sudol, Nicholas F Totty, Subham Basu, and Meredith S Irwin. 2004. "Akt Phosphorylates the Yes-Associated Protein, YAP, to Induce Interaction with 14-3-3 and Attenuation of P73-Mediated Apoptosis." *Molecular Cell* 11 (1): 11–23. https://doi.org/10.1016/s1097-2765(02)00776-1.

Dross, Rukiyah Van, Shan Yao, Shaheena Asad, Grant Westlake, Deborah J. Mays, Laura Barquero, Stephanie Duell, Jennifer A. Pietenpol, and Philip J. Browning. 2005. "Constitutively Active K-Cyclin/Cdk6 Kinase in Kaposi Sarcoma-Associated Herpesvirus-Infected Cells." *Journal of the National Cancer Institute* 97 (9): 656–66. https://doi.org/10.1093/jnci/dji113.

Dupin, N., C. Fisher, P. Kellam, S. Ariad, M. Tulliez, N. Franck, E. van Marck, et al. 2002. "Distribution of Human Herpesvirus-8 Latently Infected Cells in Kaposi's Sarcoma, Multicentric Castleman's Disease, and Primary Effusion Lymphoma." *Proceedings of the National Academy of Sciences* 96 (8): 4546–51. https://doi.org/10.1073/pnas.96.8.4546.

Dupont, Sirio, Leonardo Morsut, Mariaceleste Aragona, Elena Enzo, Stefano Giulitti, Michelangelo Cordenonsi, Francesca Zanconato, et al. 2011. "Role of YAP/TAZ in Mechanotransduction." *Nature* 474 (7350): 179–84. https://doi.org/10.1038/nature10137.

Edlund, Magnus, Marc A. Lotano, and Carol A. Otey. 2001. "Dynamics of Alpha-Actinin in Focal Adhesions and Stress Fibers Visualized with Alpha-Actinin-Green Fluorescent Protein." *Cell Motility and the Cytoskeleton* 48 (3): 190–200. https://doi.org/10.1002/1097-0169.

Efimova, Nadia, and Tatyana M. Svitkina. 2018. "Branched Actin Networks Push against Each Other at Adherens Junctions to Maintain Cell-Cell Adhesion." *Journal of Cell Biology* 217 (5): 1827–45. https://doi.org/10.1083/jcb.201708103.

Eulalio, A., I. Behm-Ansmant, D. Schweizer, and E. Izaurralde. 2007. "P-Body Formation Is a Consequence, Not the Cause, of RNA-Mediated Gene Silencing." *Molecular and Cellular Biology* 27 (11): 3970–81. https://doi.org/10.1128/mcb.00128-07.

Eulalio, Ana, Isabelle Behm-Ansmant, and Elisa Izaurralde. 2007a. "P Bodies: At the Crossroads of Post-Transcriptional Pathways." *Nature Reviews. Molecular Cell Biology* 8 (1): 9–22. https://doi.org/10.1038/nrm2080.

Finch-Edmondson, Megan, and Marius Sudol. 2016. "Framework to Function: Mechanosensitive Regulators of Gene Transcription." *Cellular & Molecular Biology Letters* 21 (1): 28. https://doi.org/10.1186/s11658-016-0028-7.

Foley, Kate S., and Paul W. Young. 2014. "The Non-Muscle Functions of Actinins: An Update." *Biochemical Journal* 459 (1): 1–13. https://doi.org/10.1042/bj20131511.

Franks, Tobias M., and Jens Lykke-Andersen. 2007. "TTP and BRF Proteins Nucleate Processing Body Formation to Silence MRNAs with AU-Rich Elements." *Genes and Development* 21 (6): 719–35. https://doi.org/10.1101/gad.1494707.

Friedland, Julie C, Mark H Lee, and David Boettiger. 2009. "Mechanically Activated Integrin Switch Controls Alpha5 Beta1 Function." *Science* 323 (January): 642–44.

Friedman-Kien, Alvin E. 1981. "Disseminated Kaposi's Sarcoma Syndrome in Young Homosexual Men." *Journal of the American Academy of Dermatology* 5 (4): 468–71. https://doi.org/10.1016/S0190-9622(81)80010-2.

Fukumoto, Miki, Shusaku Kurisu, Tesshi Yamada, and Tadaomi Takenawa. 2015. "α-Actinin-4 Enhances Colorectal Cancer Cell Invasion by Suppressing Focal Adhesion Maturation." *PLoS ONE* 10 (4): 1–19. https://doi.org/10.1371/journal.pone.0120616.

"G-Actin / F-Actin In Vivo Assay Kit." n.d. *Cytoskeleton Inc*.

Gao, Ziran, Guo Sheng Zhao, Yangfan Lv, Dongbin Peng, Xuefeng Tang, Hanxiang Song, and Qiao Nan Guo. 2019. "Anoikis-Resistant Human Osteosarcoma Cells Display Significant Angiogenesis by Activating the Src Kinase-Mediated MAPK Pathway." *Oncology Reports* 41 (1): 235–45. https://doi.org/10.3892/or.2018.6827.

Garcia, Melissa C., Denise M. Ray, Brad Lackford, Mark Rubino, Kenneth Olden, and John D. Roberts. 2009. "Arachidonic Acid Stimulates Cell Adhesion through a Novel P38 MAPK-RhoA Signaling Pathway That Involves Heat Shock Protein 27." *Journal of Biological Chemistry* 284 (31): 20936–45. https://doi.org/10.1074/jbc.M109.020271.

Gill, M. B., R. Turner, P. G. Stevenson, and M. Way. 2015. "KSHV-TK Is a Tyrosine Kinase That Disrupts Focal Adhesions and Induces Rho-Mediated Cell Contraction." *The EMBO Journal* 34 (4): 448–65. https://doi.org/10.15252/embj.201490358.

Goffart, Steffi, Andras Franko, Christoph S. Clemen, and Rudolf J. Wiesner. 2006. "α-Actinin 4 and BAT1 Interaction with the Cytochrome c Promoter upon Skeletal Muscle Differentiation." *Current Genetics* 49 (2): 125–35. https://doi.org/10.1007/s00294-005-0043-0.

Goh, Wah Ing, Kim Buay Lim, Thankiah Sudhaharan, Kai Ping Sem, Wenyu Bu, Ai Mei Chou, and Sohail Ahmed. 2012. "MDia1 and WAVE2 Proteins Interact Directly with IRSp53 in Filopodia and Are Involved in Filopodium Formation." *Journal of Biological Chemistry* 287 (7): 4702–14. https://doi.org/10.1074/jbc.M111.305102.

Grashoff, Carsten, Brenton D. Hoffman, Michael D. Brenner, Ruobo Zhou, Maddy Parsons, Michael T. Yang, Mark A. McLean, et al. 2010. "Measuring Mechanical Tension across Vinculin Reveals Regulation of Focal Adhesion Dynamics." *Nature* 466 (7303): 263–66. https://doi.org/10.1038/nature09198.

Grossmann, Claudia, and Don Ganem. 2008. "Effects of NFκB Activation on KSHV Latency and Lytic Reactivation Are Complex and Context-Dependent." *Virology* 375 (1): 94–102. https://doi.org/10.1016/j.virol.2007.12.044.

Gupton, S. L., K. Eisenmann, A. S. Alberts, and C. M. Waterman-Storer. 2007. "MDia2 Regulates Actin and Focal Adhesion Dynamics and Organization in the Lamella for Efficient Epithelial Cell Migration." *Journal of Cell Science* 120 (19): 3475–87. https://doi.org/10.1242/jcs.006049.

Gurkar, Aditi U., Kiki Chu, Lakshmi Raj, Richard Bouley, Seung Hwan Lee, Young Bum Kim, Sandra E. Dunn, Anna Mandinova, and Sam W. Lee. 2013. "Identification of ROCK1 Kinase as a Critical Regulator of Beclin1-Mediated Autophagy during Metabolic Stress." *Nature Communications* 4: 1–13. https://doi.org/10.1038/ncomms3189.

Halder, Georg, Sirio Dupont, and Stefano Piccolo. 2012. "Transduction of Mechanical and Cytoskeletal Cues by YAP and TAZ." *Nature Publishing Group* 13 (9): 591–600. https://doi.org/10.1038/nrm3416.

Hamada, Takahiro, Motoki Tominaga, Takashi Fukaya, Masayoshi Nakamura, Akihiko Nakano, Yuichiro Watanabe, Takashi Hashimoto, and Tobias I Baskin. 2012. "RNA Processing Bodies, Peroxisomes, Golgi Bodies, Mitochondria, and Endoplasmic Reticulum Tubule Junctions Frequently Pause at Cortical Microtubules." *Plant & Cell Physiology* 53 (4): 699–708. https://doi.org/10.1093/pcp/pcs025.

Hanna, A. N., L. G. Berthiaume, Y. Kikuchi, D. Begg, S. Bourgoin, and D. N. Brindley. 2001. "Tumor Necrosis Factor-Alpha Induces Stress Fiber Formation through Ceramide Production: Role of Sphingosine Kinase." *Molecular Biology of the Cell* 12 (11): 3618–30. https://doi.org/10.1091/mbc.12.11.3618.

Hansen, Carsten Gram, Toshiro Moroishi, and Kun Liang Guan. 2015. "YAP and TAZ: A Nexus for Hippo Signaling and Beyond." *Trends in Cell Biology* 25 (9): 499–513. https://doi.org/10.1016/j.tcb.2015.05.002.

Haskins, Jonathan W., Don X. Nguyen, and David F. Stern. 2014. "Neuregulin 1-Activated ERBB4 Interacts with YAP to Induce Hippo Pathway Target Genes and Promote Cell Migration." *Science Signaling* 7 (355). https://doi.org/10.1126/scisignal.2005770.

He, Jinlong, Qiankun Bao, Yan Zhang, Mingming Liu, Huizhen Lv, Yajin Liu, Liu Yao, et al. 2018. "Yes-Associated Protein Promotes Angiogenesis via Signal Transducer and Activator of Transcription 3 in Endothelial Cells." *Circulation Research* 122 (4): 591–605. https://doi.org/10.1161/CIRCRESAHA.117.311950.

Heath, J P. 1983. "Behaviour and Structure of the Leading Lamella in Moving Fibroblasts. I. Occurrence and Centripetal Movement of Arc-Shaped Microfilament Bundles beneath the Dorsal Cell Surface." *Journal of Cell Science* 60: 331–54.

Heath, J P, and G A Dunn. 1978. "Cell to Substratum Contacts of Chick Fibroblasts and Their Relation to the Microfilament System. A Correlated Interference-Reflexion and High-Voltage Electron-Microscope Study." *Journal of Cell Science* 29: 197–212.

Hladik, Wolfgang, Sheila C. Dollard, Jonathan Mermin, Ashley L. Fowlkes, Robert Downing, Minal M. Amin, Flora Banage, et al. 2006. "Transmission of Human Herpesvirus 8 by Blood Transfusion." *New England Journal of Medicine* 355 (13): 1331–38. https://doi.org/10.1056/NEJMoa055009.

Holmes, Kenneth C. 2008. "Myosin Structure." In *Myosins*, 35–54. Dordrecht: Springer Netherlands. https://doi.org/10.1007/978-1-4020-6519-4_2.

Honda, K, T Yamada, R Endo, Y Ino, M Gotoh, H Tsuda, Y Yamada, H Chiba, and S Hirohashi. 1998. "Actinin-4, a Novel Actin-Bundling Protein Associated with Cell Motility and Cancer Invasion.[Erratum Appears in J Cell Biol 1998 Oct 5;143(1):Following 276]." *Journal of Cell Biology* 140 (6): 1383–93. https://doi.org/10.1083/jcb.140.6.1383.

Honda, Kazufumi. 2015. "The Biological Role of Actinin-4 (ACTN4) in Malignant Phenotypes of Cancer." *Cell and Bioscience* 5 (1): 1–9. https://doi.org/10.1186/s13578-015-0031-0.

Hong, Young Kwon, Natasha Harvey, Yun Hee Noh, Vivien Schacht, Satoshi Hirakawa, Michael Detmar, and Guillermo Oliver. 2002. "Prox1 Is a Master Control Gene in the Program Specifying Lymphatic Endothelial Cell Fate." *Developmental Dynamics* 225 (3): 351–57. https://doi.org/10.1002/dvdy.10163.

Horvathova, Ivana, Franka Voigt, Anna V. Kotrys, Yinxiu Zhan, Caroline G. Artus-Revel, Jan Eglinger, Michael B. Stadler, Luca Giorgetti, and Jeffrey A. Chao. 2017. "The Dynamics of MRNA Turnover Revealed by Single-Molecule Imaging in Single Cells." *Molecular Cell* 68 (3): 615-625.e9. https://doi.org/10.1016/j.molcel.2017.09.030.

Hotulainen, Pirta, and Pekka Lappalainen. 2006. "Stress Fibers Are Generated by Two Distinct Actin Assembly Mechanisms in Motile Cells." *Journal of Cell Biology* 173 (3): 383–94. https://doi.org/10.1083/jcb.200511093.

Hubstenberger, Arnaud, Maïté Courel, Marianne Bénard, Sylvie Souquere, Michèle Ernoult-Lange, Racha Chouaib, Zhou Yi, et al. 2017. "P-Body Purification Reveals the Condensation of Repressed MRNA Regulons." *Molecular Cell* 68 (1): 144-157.e5. https://doi.org/10.1016/j.molcel.2017.09.003.

Iglesias-Bexiga, Manuel, Francisco Castillo, Eva S. Cobos, Tsutomu Oka, Marius Sudol, and Irene Luque. 2015. "WW Domains of the Yes-Kinase-Associated-Protein (YAP) Transcriptional Regulator Behave as Independent Units with Different Binding Preferences for PPxY Motif-Containing Ligands." *PLoS ONE* 10 (1): 1–22. https://doi.org/10.1371/journal.pone.0113828.

Ikenouchi, Junichi, and Kana Aoki. 2017. "Membrane Bleb: A Seesaw Game of Two Small GTPases." *Small GTPases* 8 (2): 85–89. https://doi.org/10.1080/21541248.2016.1199266.

Ingelfinger, Dierk, Donna J Arndt-Jovin, Reinhard Lührmann, and Tilmann Achsel. 2002. "The Human LSm1-7 Proteins Colocalize with the MRNA-Degrading Enzymes Dcp1/2 and Xrnl in Distinct Cytoplasmic Foci." *RNA (New York, N.Y.)* 8 (12): 1489–1501.

Ishizaki, T, Y Morishima, M Okamoto, T Furuyashiki, T Kato, and S Narumiya. 2001. "Coordination of Microtubules and the Actin Cytoskeleton by the Rho Effector MDia1." *Nature Cell Biology* 3 (1): 8–14. https://doi.org/10.1038/35050598.

Ishizaki, T, M Uehata, I Tamechika, J Keel, K Nonomura, M Maekawa, and S Narumiya. 2000. "Pharmacological Properties of Y-27632, a Specific Inhibitor of Rho-Associated Kinases." *Molecular Pharmacology* 57 (5): 976–83. http://www.ncbi.nlm.nih.gov/pubmed/10779382.

Isogai, T., R. van der Kammen, D. Leyton-Puig, K. M. Kedziora, K. Jalink, and M. Innocenti. 2015. "Initiation of Lamellipodia and Ruffles Involves Cooperation between MDia1 and the Arp2/3 Complex." *Journal of Cell Science* 128 (20): 3796–3810. https://doi.org/10.1242/jcs.176768.

Jakob, Lena, Gisela Metzler, Ko Ming Chen, and Claus Garbe. 2011. "Non-Aids Associated Kaposi's Sarcoma: Clinical Features and Treatment Outcome." *PLoS ONE* 6 (4): 1–7. https://doi.org/10.1371/journal.pone.0018397.

Jang, J. W., M. K. Kim, Y. S. Lee, J. W. Lee, D. M. Kim, S. H. Song, J. Y. Lee, et al. 2017. "RAC-LATS1/2 Signaling Regulates YAP Activity by Switching between the YAP-Binding Partners TEAD4 and RUNX3." *Oncogene* 36 (7): 999–1011. https://doi.org/10.1038/onc.2016.266.

Julian, Linda, and Michael F Olson. 2014. "Rho-Associated Coiled-Coil Containing Kinases (ROCK)." *Small GTPases* 5 (2): e29846. https://doi.org/10.4161/sgtp.29846.

KAAYA, E.E., E. CASTAÑOS-VELEZ, H. AMIR, L. LEMA, J. LUANDE, J. KITINYA, M. PATARROYO, and P. BIBERFELD. 1996. "Expression of Adhesion Molecules in Endemic and Epidemic Kaposi's Sarcoma." *Histopathology* 29 (4): 337–46. https://doi.org/10.1111/j.1365-2559.1996.tb01417.x.

Kamentsky, Lee, Thouis R Jones, Adam Fraser, Mark-Anthony Bray, David J Logan, Katherine L Madden, Vebjorn Ljosa, Curtis Rueden, Kevin W Eliceiri, and Anne E Carpenter. 2011. "Improved Structure, Function and Compatibility for CellProfiler: Modular High-Throughput Image Analysis Software." *Bioinformatics (Oxford, England)* 27 (8): 1179–80. https://doi.org/10.1093/bioinformatics/btr095.

Katoh, K., Y. Kano, M. Masuda, H. Onishi, and K. Fujiwara. 1998. "Isolation and Contraction of the Stress Fiber." *Molecular Biology of the Cell* 9 (7): 1919–38. https://doi.org/10.1091/mbc.9.7.1919.

Kedersha, Nancy, Sarah Tisdale, Tyler Hickman, and Paul Anderson. 2008. *Chapter 26 Real-Time and Quantitative Imaging of Mammalian Stress Granules and Processing Bodies*. *Methods in Enzymology*. 1st ed. Vol. 448. Elsevier Inc. https://doi.org/10.1016/S0076-6879(08)02626-8.

Khurana, Simran, Sharmistha Chakraborty, Xiwen Cheng, Yu Ting Su, and Hung Ying Kao. 2011. "The Actin-Binding Protein, Actinin Alpha 4 (ACTN4), Is a Nuclear Receptor Coactivator That Promotes Proliferation of MCF-7 Breast Cancer Cells." *Journal of Biological Chemistry* 286 (3): 1850–59. https://doi.org/10.1074/jbc.M110.162107.

Kim, Jongshin, Yoo Hyung Kim, Jaeryung Kim, Do Young Park, Hosung Bae, Da-hye Lee, Kyun Hoo Kim, et al. 2017. "YAP/TAZ Regulates Sprouting Angiogenesis and Vascular Barrier Maturation." *Journal of Clinical Investigation* 127 (9): 3441–61. https://doi.org/10.1172/JCI93825.

Kim, Min Kyu, Ju Won Jang, and Suk Chul Bae. 2018. "DNA Binding Partners of YAP/TAZ." *BMB Reports* 51 (3): 126–33. https://doi.org/10.5483/BMBRep.2018.51.3.015.

Kimura, K, M Ito, M Amano, K Chihara, Y Fukata, M Nakafuku, B Yamamori, et al. 1996. "Regulation of Myosin Phosphatase by Rho and Rho-Associated Kinase (Rho-Kinase)." *Science (New York, N.Y.)* 273 (5272): 245–48. https://doi.org/10.1126/science.273.5272.245.

King, C. A. 2013. "Kaposi's Sarcoma-Associated Herpesvirus Kaposin B Induces Unique Monophosphorylation of STAT3 at Serine 727 and MK2-Mediated Inactivation of the STAT3 Transcriptional Repressor TRIM28." *Journal of Virology* 87 (15): 8779–91. https://doi.org/10.1128/JVI.02976-12.

King, Christine a. 2013. "Kaposi's Sarcoma-Associated Herpesvirus Kaposin B Induces Unique Monophosphorylation of STAT3 at Serine 727 and MK2-Mediated Inactivation of the STAT3 Transcriptional Repressor TRIM28." *Journal of Virology* 87 (15): 8779–91. https://doi.org/10.1128/JVI.02976-12.

Kliche, Stefanie, Wolfgang Nagel, Elisabeth Kremmer, Christine Atzler, Alexander Ege, Thomas Knorr, Ulrich Koszinowski, Waldemar Kolanus, and J??rgen Haas. 2001. "Signaling by Human Herpesvirus 8 Kaposin a through Direct Membrane Recruitment of Cytohesin-1." *Molecular Cell* 7 (4): 833–43. https://doi.org/10.1016/S1097-2765(01)00227-1.

Komuro, Akihiko, Makoto Nagai, Nicholas E. Navin, and Marius Sudol. 2003. "WW Domain-Containing Protein YAP Associates with ErbB-4 and Acts as a Co-Transcriptional Activator for the Carboxyl-Terminal Fragment of ErbB-4 That Translocates to the Nucleus." *Journal of Biological Chemistry* 278 (35): 33334–41. https://doi.org/10.1074/jbc.M305597200.

Kong, Fang, Andrés J. García, A. Paul Mould, Martin J. Humphries, and Cheng Zhu. 2009. "Demonstration of Catch Bonds between an Integrin and Its Ligand." *Journal of Cell Biology* 185 (7): 1275–84. https://doi.org/10.1083/jcb.200810002.

Kovac, Bianca. 2010. "Role and Function of Nonmuscle Alpha-Actinin-1 and -4 in Regulating Distinct Subcategories of Actin Stress Fibers in Mammalian Cells," no. March: 1–36.

Kovac, Bianca, Tomi P. Mäkela, and Tea Vallenius. 2018. "Increased α-Actinin-1 Destabilizes e-Cadherin-Based Adhesions and Associates with Poor Prognosis in Basal-like Breast Cancer." *PLoS ONE* 13 (5): 6–8. https://doi.org/10.1371/journal.pone.0196986.

Kovacs, M., J. Toth, C. Hetenyi, A. Malnasi-Csizmadia, and J. R. Sellers. 2004. "Mechanism of Blebbistatin Inhibition of Myosin II." *Journal of Biological Chemistry* 279 (34): 35557–63. https://doi.org/10.1074/jbc.M405319200.

Kumar, Binod, and Bala Chandran. 2016. "KSHV Entry and Trafficking in Target Cells—Hijacking of Cell Signal Pathways,Actin and Membrane Dynamics." *Viruses* 8 (11). https://doi.org/10.3390/v8110305.

Kümper, Sandra, Faraz K Mardakheh, Afshan McCarthy, Maggie Yeo, Gordon W Stamp, Angela Paul, Jonathan Worboys, et al. 2016. "Rho-Associated Kinase (ROCK) Function Is Essential for Cell Cycle Progression, Senescence and Tumorigenesis." *ELife* 5: e12203. https://doi.org/10.7554/eLife.12203.

Lamalice, Laurent, Fabrice Le Boeuf, and Jacques Huot. 2007. "Endothelial Cell Migration during Angiogenesis." *Circulation Research* 100 (6): 782–94. https://doi.org/10.1161/01.RES.0000259593.07661.1e.

Laukaitis, Christina M, Donna J Webb, Karen Donais, and Alan F Horwitz. 2001. "Differential Dynamics of A5 Integrin, Paxillin, and α-Actinin during Formation and Disassembly of Adhesions in Migrating Cells." *The Journal of Cell Biology* 153 (7): 1427–40. https://doi.org/10.1083/jcb.153.7.1427.

Lazarides, Elias, and Keith Burridge. 1975. "α-Actinin: Immunofluorescent Localization of a Muscle Structural Protein in Nonmuscle Cells." *Cell* 6 (3): 289–98. https://doi.org/10.1016/0092-8674(75)90180-4.

Lee, Hye-Ra, Stacy Lee, Preet M Chaudhary, Parkash Gill, and Jae U Jung. 2010. "Immune Evasion by Kaposi's Sarcoma-Associated Herpesvirus." Edited by Halvard Bönig. *Future Microbiology* 5 (9): 1349–65. https://doi.org/10.2217/fmb.10.105.

Lee, Hyun Jung, Miguel F. Diaz, Katherine M. Price, Joyce A. Ozuna, Songlin Zhang, Eva M. Sevick-Muraca, John P. Hagan, and Pamela L. Wenzel. 2017. "Fluid Shear Stress Activates YAP1 to Promote Cancer Cell Motility." *Nature Communications* 8. https://doi.org/10.1038/ncomms14122.

Lee, Stacey, and Sanjay Kumar. 2016. "Actomyosin Stress Fiber Mechanosensing in 2D and 3D." *F1000Research* 5 (0): 2261. https://doi.org/10.12688/f1000research.8800.1.

Li, Bochuan, Jinlong He, Huizhen Lv, Yajin Liu, Xue Lv, Chenghu Zhang, Yi Zhu, and Ding Ai. 2019. "C-Abl Regulates YAPY357 Phosphorylation to Activate Endothelial Atherogenic Responses to Disturbed Flow." *Journal of Clinical Investigation* 129 (3): 1167–79. https://doi.org/10.1172/JCI122440.

Li, Fang, and Henry N. Higgs. 2003. "The Mouse Formin MDia1 Is a Potent Actin Nucleation Factor Regulated by Autoinhibition." *Current Biology* 13 (15): 1335–40. https://doi.org/10.1016/S0960-9822(03)00540-2.

Li, Wang, Xinlei Yu, Fei Xie, Baohong Zhang, Shuai Shao, Chunyang Geng, Aziz ur Rehman Aziz, Xiaoling Liao, and Bo Liu. 2018. "A Membrane-Bound Biosensor Visualizes Shear Stress-Induced Inhomogeneous Alteration of Cell Membrane Tension." *IScience* 7 (September): 180–90. https://doi.org/10.1016/j.isci.2018.09.002.

Li, Wei, Yuanyuan Cao, Jinling Xu, Ying Wang, Weijie Li, Qian Wang, Ziwei Hu, et al. 2017. "YAP Transcriptionally Regulates COX-2 Expression and GCCSysm-4 (G-4), a Dual YAP/COX-2 Inhibitor, Overcomes Drug Resistance in Colorectal Cancer." *Journal of Experimental and Clinical Cancer Research* 36 (1): 1–20. https://doi.org/10.1186/s13046-017-0612-3.

Lindsay, Andrew J., and Mary W. McCaffrey. 2011. "Myosin Va Is Required for P Body but Not Stress Granule Formation." *Journal of Biological Chemistry* 286 (13): 11519–28. https://doi.org/10.1074/jbc.M110.182808.

Liu, J., X. Bi, T. Chen, Q. Zhang, S. X. Wang, J. J. Chiu, G. S. Liu, Y. Zhang, P. Bu, and F. Jiang. 2015. "Shear Stress Regulates Endothelial Cell Autophagy via Redox Regulation and Sirt1 Expression." *Cell Death and Disease* 6 (7). https://doi.org/10.1038/cddis.2015.193.

Liu, Ming, Zheng Zhang, Leesa Sampson, Xuan Zhou, Kodandaramireddy Nalapareddy, Yuxin Feng, Shailaja Akunuru, et al. 2017. "RHOA GTPase Controls YAP-Mediated EREG Signaling in Small Intestinal Stem Cell Maintenance." *Stem Cell Reports* 9 (6): 1961–75. https://doi.org/10.1016/j.stemcr.2017.10.004.

Liu, Zeming, Wen Zeng, Shi Wang, Xiangwang Zhao, Yawen Guo, Pan Yu, Xingjie Yin, Chunping Liu, and Tao Huang. 2017. "A Potential Role for the Hippo Pathway Protein, YAP, in Controlling Proliferation, Cell Cycle Progression, and Autophagy in BCPAP and KI Thyroid Papillary Carcinoma Cells." *American Journal of Translational Research* 9 (7): 3212–23.

Loschi, Mariela, Claudia C Leishman, Neda Berardone, and Graciela L Boccaccio. 2009. "Dynein and Kinesin Regulate Stress-Granule and P-Body Dynamics." *Journal of Cell Science* 122 (Pt 21): 3973–82. https://doi.org/10.1242/jcs.051383.

Luo, Yang, Zhenkun Na, and Sarah A. Slavoff. 2018. "P-Bodies: Composition, Properties, and Functions." *Biochemistry* 57 (17): 2424–31. https://doi.org/10.1021/acs.biochem.7b01162.

Lv, Yang, Kyungho Kim, Yue Sheng, Jaehyung Cho, Zhijian Qian, You-yang Zhao, Gang Hu, Duojia Pan, Asrar B Malik, and Guochang Hu. 2018. "YAP Controls Endothelial Activation and Vascular Inflammation Through TRAF6." *Circulation Research* 123 (1): 43–56. https://doi.org/10.1161/CIRCRESAHA.118.313143.

Maiti, Sankar, Alphee Michelot, Christopher Gould, Laurent Blanchoin, Olga Sokolova, and Bruce L. Goode. 2012. "Structure and Activity of Full-Length Formin MDia1." *Cytoskeleton* 69 (6): 393–405. https://doi.org/10.1002/cm.21033.

Mana-Capelli, S., M. Paramasivam, S. Dutta, and D. McCollum. 2014. "Angiomotins Link F-Actin Architecture to Hippo Pathway Signaling." *Molecular Biology of the Cell* 25 (10): 1676–85. https://doi.org/10.1091/mbc.e13-11-0701.

McCormick, Craig, and Don Ganem. 2005. "The Kaposin B Protein of KSHV Activates the P38/MK2 Pathway and Stabilizes Cytokine MRNAs." *Science* 307 (5710): 739–41. https://doi.org/10.1126/science.1105779.

Meng, Fanyin, Yoko Yamagiwa, Yoshiyuki Ueno, and Tushar Patel. 2006. "Over-Expression of Interleukin-6 Enhances Cell Survival and Transformed Cell Growth in Human Malignant Cholangiocytes." *Journal of Hepatology* 44 (6): 1055–65. https://doi.org/10.1016/j.jhep.2005.10.030.

Mesri, E A. 1999. "Inflammatory Reactivation and Angiogenicity of Kaposi's Sarcoma-Associated Herpesvirus/HHV8: A Missing Link in the Pathogenesis of Acquired Immunodeficiency Syndrome-Associated Kaposi's Sarcoma." *Blood* 93 (12): 4031–33. https://doi.org/10.1645/GE-2366.1.

Mesri, Enrique a, Ethel Cesarman, and Chris Boshoff. 2010. "Kaposi's Sarcoma and Its Associated Herpesvirus." *Nature Reviews. Cancer* 10 (10): 707–19. https://doi.org/10.1038/nrc2888.

Miano, Joseph M, Xiaochun Long, and Keigi Fujiwara. 2007. "Serum Response Factor: Master Regulator of the Actin Cytoskeleton and Contractile Apparatus." *American Journal of Physiology-Cell Physiology* 292 (1): C70–81. https://doi.org/10.1152/ajpcell.00386.2006.

Miles, Steven A, Ahmad R Rezai, Jesus F Salazar-gonzalez, Meta Vander Meydent, Ronald H Stevens, Diane M Logan, Ronald T Mitsuyasu, et al. 1990. "AIDS Kaposi Sarcoma-Derived Cells Produce and Respond to Interleukin 6" 87 (June): 4068–72.

Millán, Jaime, Robert J. Cain, Natalia Reglero-Real, Carolina Bigarella, Beatriz Marcos-Ramiro, Laura Fernández-Martín, Isabel Correas, and Anne J. Ridley. 2010. "Adherens Junctions Connect Stress Fibres between Adjacent Endothelial Cells." *BMC Biology* 8. https://doi.org/10.1186/1741-7007-8-11.

Minhas, Veenu, and Charles Wood. 2014. "Epidemiology and Transmission of Kaposi's Sarcoma-Associated Herpesvirus." *Viruses* 6 (11): 4178–94. https://doi.org/10.3390/v6114178.

Mo, Jung Soon, Zhipeng Meng, Young Chul Kim, Hyun Woo Park, Carsten Gram Hansen, Soohyun Kim, Dae Sik Lim, and Kun Liang Guan. 2015. "Cellular Energy Stress Induces AMPK-Mediated Regulation of YAP and the Hippo Pathway." *Nature Cell Biology* 17 (4): 500–510. https://doi.org/10.1038/ncb3111.

Moreno, Ana, María Luisa Villar, Carmen Cámara, Rosario Luque, Constantino Cespón, Pedro González-Porqué, Garbiñe Roy, Javier López-Jiménez, Alfredo Bootello, and Ernesto Roldán Santiago. 2001. "Interleukin-6 Dimers Produced by Endothelial Cells Inhibit Apoptosis of B-Chronic Lymphocytic Leukemia Cells." *Blood* 97 (1): 242–49. https://doi.org/10.1182/blood.V97.1.242.

Morgan, M, S Victor Perry, and June Ottaway. 1976. "Myosin Light-Chain Phosphatase." *Biochemical Journal* 157 (3): 687–97. https://doi.org/10.1042/bj1570687.

Moriyama, Kenji, Kazuko Iida, and Ichiro Yahara. 1996. "Phosphorylation of Ser-3 of Cofilin Regulates Its Essential Function on Actin." *Genes to Cells* 1 (1): 73–86. https://doi.org/10.1046/j.1365-2443.1996.05005.x.

Morton, W M, K R Ayscough, and P J McLaughlin. 2000. "Latrunculin Alters the Actin-Monomer Subunit Interface to Prevent Polymerization." *Nature Cell Biology* 2 (6): 376–78. https://doi.org/10.1038/35014075.

Mosam, A., J. Aboobaker, and F. Shaik. 2010. "Kaposi's Sarcoma in Sub-Saharan Africa: A Current Perspective." *Current Opinion in Infectious Diseases* 23 (2): 119–23. https://doi.org/10.1097/QCO.0b013e328335b01a.

Muralidhar, Sumitra, Anne Pumfery, Morad Hassani, M. Reza Sadaie, Norio Azumi, John N. Brady, Peter Medveczky, and Leonard J. Rosenthal. 1998. "Identification of Kaposin (ORF K12) as a Human Herpesvirus 8 (Kaposi's Sarcoma Associated Herpesvirus) Oncogene." *Journal of Acquired Immune Deficiency Syndromes and Human Retrovirology* 17 (4): A27. https://doi.org/10.1097/00042560-199804010-00077.

Nakajima, Hiroyuki, Kimiko Yamamoto, Sobhika Agarwala, Kenta Terai, Hajime Fukui, Shigetomo Fukuhara, Koji Ando, et al. 2017. "Flow-Dependent Endothelial YAP Regulation Contributes to Vessel Maintenance." *Developmental Cell* 40 (6): 523-536.e6. https://doi.org/10.1016/j.devcel.2017.02.019.

Nardone, Giorgia, Jorge Oliver-De La Cruz, Jan Vrbsky, Cecilia Martini, Jan Pribyl, Petr Skládal, Martin Pešl, et al. 2017. "YAP Regulates Cell Mechanics by Controlling Focal Adhesion Assembly." *Nature Communications* 8 (1): 15321. https://doi.org/10.1038/ncomms15321.

Neve, Anna, Francesco Paolo Cantatore, Nicola Maruotti, Addolorata Corrado, and Domenico Ribatti. 2014. "Extracellular Matrix Modulates Angiogenesis in Physiological and Pathological Conditions." *BioMed Research International* 2014. https://doi.org/10.1155/2014/756078.

Nikolopoulos, Sotiris N., Barbara A. Spengler, Kristin Kisselbach, Audrey E. Evans, June L. Biedler, and Robert A. Ross. 2000. "The Human Non-Muscle α-Actinin Protein Encoded by the ACTN4 Gene Suppresses Tumorigenicity of Human Neuroblastoma Cells." *Oncogene* 19 (3): 380–86. https://doi.org/10.1038/sj.onc.1203310.

Nishimura, Koutarou, Yoshikazu Johmura, Katashi Deguchi, Zixian Jiang, Kazuhiko S.K. Uchida, Narumi Suzuki, Midori Shimada, et al. 2019. "Cdk1-Mediated DIAPH1 Phosphorylation Maintains Metaphase Cortical Tension and Inactivates the Spindle Assembly Checkpoint at Anaphase." *Nature Communications* 10 (1). https://doi.org/10.1038/s41467-019-08957-w.

Noria, Sabrena, Feng Xu, Shannon McCue, Mara Jones, Avrum I Gotlieb, and B Lowell Langille. 2004. "Assembly and Reorientation of Stress Fibers Drives Morphological Changes to Endothelial Cells Exposed to Shear Stress." *The American Journal of Pathology* 164 (4): 1211–23. https://doi.org/10.1016/S0002-9440(10)63209-9.

Nukuda, A., C. Sasaki, S. Ishihara, T. Mizutani, K. Nakamura, T. Ayabe, K. Kawabata, and H. Haga. 2015. "Stiff Substrates Increase YAP-Signaling-Mediated Matrix Metalloproteinase-7 Expression." *Oncogenesis* 4 (June): 1–11. https://doi.org/10.1038/oncsis.2015.24.

Oakes, Patrick W, Yvonne Beckham, Jonathan Stricker, and Margaret L Gardel. 2012. "Tension Is Required but Not Sufficient for Focal Adhesion Maturation without a Stress Fiber Template" 196 (3): 363–74. https://doi.org/10.1083/jcb.201107042.

Ohashi, Kazumasa, Kyoko Nagata, Midori Maekawa, Toshimasa Ishizaki, Shuh Narumiya, and Kensaku Mizuno. 2000. "Rho-Associated Kinase ROCK Activates LIM-Kinase 1 by Phosphorylation at Threonine 508 within the Activation Loop." *Journal of Biological Chemistry* 275 (5): 3577–82. https://doi.org/10.1074/jbc.275.5.3577.

Oka, Tsutomu, Eline Remue, Kris Meerschaert, Berlinda Vanloo, Ciska Boucherie, David Gfeller, Gary D. Bader, et al. 2010. "Functional Complexes between YAP2 and ZO-2 Are PDZ Domain-Dependent, and Regulate YAP2 Nuclear Localization and Signalling." *Biochemical Journal* 432 (3): 461–78. https://doi.org/10.1042/BJ20100870.

Parker, Roy, and Ujwal Sheth. 2007. "P Bodies and the Control of MRNA Translation and Degradation." *Molecular Cell* 25 (5): 635–46. https://doi.org/10.1016/j.molcel.2007.02.011.

Pavel, Mariana, Maurizio Renna, So Jung Park, Fiona M. Menzies, Thomas Ricketts, Jens Füllgrabe, Avraham Ashkenazi, et al. 2018. "Contact Inhibition Controls Cell Survival and Proliferation via YAP/TAZ-Autophagy Axis." *Nature Communications* 9 (1). https://doi.org/10.1038/s41467-018-05388-x.

Pei, Tianjiao, Xin Huang, Ying Long, Changling Duan, Tingting Liu, Yujing Li, and Wei Huang. 2019. "Increased Expression of YAP Is Associated with Decreased Cell Autophagy in the Eutopic Endometrial Stromal Cells of Endometriosis." *Molecular and Cellular Endocrinology* 491 (April): 110432. https://doi.org/10.1016/j.mce.2019.04.012.

Pellegrin, S., and H. Mellor. 2007. "Actin Stress Fibres." *Journal of Cell Science* 120 (20): 3491–99. https://doi.org/10.1242/jcs.018473.

Peterson, Lynda J, Zenon Rajfur, Amy S Maddox, Christopher D Freel, Yun Chen, Magnus Edlund, Carol Otey, and Keith Burridge. 2004. "Simultaneous Stretching and Contraction of Stress Fibers in Vivo." *Molecular Biology of the Cell* 15 (7): 3497–3508. https://doi.org/10.1091/mbc.e03-09-0696.

Pitchiaya, Sethuramasundaram, Marcio D.A. Mourao, Ameya P. Jalihal, Lanbo Xiao, Xia Jiang, Arul M. Chinnaiyan, Santiago Schnell, and Nils G. Walter. 2019. "Dynamic Recruitment of Single RNAs to Processing Bodies Depends on RNA Functionality." *Molecular Cell* 74 (3): 521-533.e6. https://doi.org/10.1016/j.molcel.2019.03.001.

Plouffe, Steven W, Kimberly C Lin, Jerrell L. Moore, Frederick E Tan, Shenghong Ma, Zhen Ye, Yunjiang Qiu, Bing Ren, and Kun-Liang Guan. 2018. "The Hippo Pathway Effector Proteins YAP and TAZ Have Both Distinct and Overlapping Functions in the Cell." *Journal of Biological Chemistry* 293 (28): 11230–40. https://doi.org/10.1074/jbc.RA118.002715.

Pollard, Thomas D. 2016. "Actin and Actin-Binding Proteins." *Cold Spring Harbor Perspectives in Biology* 8 (8): a018226. https://doi.org/10.1101/cshperspect.a018226.

Purushothaman, Pravinkumar, Prerna Dabral, Namrata Gupta, Roni Sarkar, and Subhash C. Verma. 2016. "KSHV Genome Replication and Maintenance." *Frontiers in Microbiology* 7 (FEB). https://doi.org/10.3389/fmicb.2016.00054.

Qian, L.-W., Jianping Xie, Fengchun Ye, and S.-J. Gao. 2007. "Kaposi's Sarcoma-Associated Herpesvirus Infection Promotes Invasion of Primary Human Umbilical Vein Endothelial Cells by Inducing Matrix Metalloproteinases." *Journal of Virology* 81 (13): 7001–10. https://doi.org/10.1128/JVI.00016-07.

Qu, Xiaoyi, Feng Ning Yuan, Carlo Corona, Silvia Pasini, Maria Elena Pero, Gregg G. Gundersen, Michael L. Shelanski, and Francesca Bartolini. 2017. "Stabilization of Dynamic Microtubules by MDia1 Drives Tau-Dependent Aβ1-42 Synaptotoxicity." *Journal of Cell Biology* 216 (10): 3161–78. https://doi.org/10.1083/jcb.201701045.

Rasmussen, Izabela, Line H Pedersen, Luise Byg, Kazuhiro Suzuki, Hideki Sumimoto, and Frederik Vilhardt. 2010. "Effects of F/G-Actin Ratio and Actin Turn-over Rate on NADPH Oxidase Activity in Microglia." *BMC Immunology* 11: 44. https://doi.org/10.1186/1471-2172-11-44.

Ridley, Anne J., and Alan Hall. 1992. "The Small GTP-Binding Protein Rho Regulates the Assembly of Focal Adhesions and Actin Stress Fibers in Response to Growth Factors." *Cell* 70 (3): 389–99. https://doi.org/10.1016/0092-8674(92)90163-7.

Rio, Armando del, Raul Perez-jimenez, Ruchuan Liu, Pere Roca-cusachs, Julio M Fernandez, and Michael P Sheetz. 2009. "Stretching Single Talin Rod." *Science* 323 (5914): 638–41.

Rosenbluh, Joseph, Deepak Nijhawan, Andrew G. Cox, Xingnan Li, James T. Neal, Eric J. Schafer, Travis I. Zack, et al. 2012. "β-Catenin-Driven Cancers Require a YAP1 Transcriptional Complex for Survival and Tumorigenesis." *Cell* 151 (7): 1457–73. https://doi.org/10.1016/j.cell.2012.11.026.

Rotsch, Christian, and Manfred Radmacher. 2000. "Drug-Induced Changes of Cytoskeletal Structure and Mechanics in Fibroblasts: An Atomic Force Microscopy Study." *Biophysical Journal* 78 (1): 520–35. https://doi.org/10.1016/S0006-3495(00)76614-8.

Russo, James J, Roy A Bohenzky, Ming-cheng Chien, Jing Chen, Ming Yan, Dawn Maddalena, J Preston Parry, et al. 1996. "Nucleotide Sequence of the Kaposi Sarcoma-Associated Herpesvirus." *Proceedings of the National Academy of Sciences of the United States of America* 93 (25): 14862–67.

Sadler, R, L Wu, B Forghani, R Renne, W Zhong, B Herndier, and D Ganem. 1999. "A Complex Translational Program Generates Multiple Novel Proteins from the Latently Expressed Kaposin (K12) Locus of Kaposi's Sarcoma-Associated Herpesvirus." *Journal of Virology* 73 (7): 5722–30.

Samaniego, Felipe, Phillip D Markham, Rita Gendelman, Yoshiki Watanabe, Vivien Kao, Kimberly Kowalski, Joseph A Sonnabend, Aldo Pintus, Robert C Gallo, and Barbara Ensoli Ii. 1998. "Vascular Endothelial Growth Factor and Basic Fibroblast Growth Factor Present in Kaposi ' s Sarcoma ( KS ) Are Induced by Inflammatory Cytokines and Synergize to Promote Vascular Permeability and KS Lesion Development" 152 (6): 1433–43.

Sans, M., J. Panes, E. Ardite, J. I. Elizalde, Y. Arce, M. Elena, A. Palacin, et al. 1999. "VCAM-1 and ICAM-1 Mediate Leukocyte-Endothelial Cell Adhesion in Rat Experimental Colitis." *Gastroenterology* 116 (4): 874–83. https://doi.org/10.1016/S0016-5085(99)70070-3.

Sathish, Narayanan, Xin Wang, and Yan Yuan. 2012. "Tegument Proteins of Kaposi's Sarcoma-Associated Herpesvirus and Related Gamma-Herpesviruses." *Frontiers in Microbiology* 3 (MAR): 1–13. https://doi.org/10.3389/fmicb.2012.00098.

Schirenbeck, Antje, Till Bretschneider, Rajesh Arasada, Michael Schleicher, and Jan Faix. 2005. "The Diaphanous-Related Formin DDia2 Is Required for the Formation and Maintenance of Filopodia." *Nature Cell Biology* 7 (6): 619–25. https://doi.org/10.1038/ncb1266.

Schmitz, A, E E Govek, B Böttner, and L Van Aelst. 2000. "Rho GTPases: Signaling, Migration, and Invasion." *Experimental Cell Research* 261 (1): 1–12. https://doi.org/10.1006/excr.2000.5049.

Sciacca, F L, M Stürzl, F Bussolino, M Sironi, Heinz Brandstetter, Christian Zietz, Dan Zhou, Cristian Matteucci, G Peri, and S Sozzani. 1994. "Expression of Adhesion Molecules, Platelet-Activating Factor, and Chemokines by Kaposi's Sarcoma Cells." *Journal of Immunology (Baltimore, Md. : 1950)* 153 (10): 4816–25.

Semeere, Aggrey S., Naftali Busakhala, and Jeffrey N. Martin. 2012. "Impact of Antiretroviral Therapy on the Incidence of Kaposi's Sarcoma in Resource-Rich and Resource-Limited Settings." *Current Opinion in Oncology* 24 (5): 522–30. https://doi.org/10.1097/CCO.0b013e328355e14b.

Senger, Fabrice, Amandine Pitaval, Hajer Ennomani, Laetitia Kurzawa, Laurent Blanchoin, and Manuel Théry. 2019. "Spatial Integration of Mechanical Forces by Alpha-Actinin Establishes Actin Network Symmetry." *BioRxiv*, 578799. https://doi.org/10.1101/578799.

Sharma-Walia, Neelam, Arun George Paul, Virginie Bottero, Sathish Sadagopan, Mohanan Valiya Veettil, Nagaraj Kerur, and Bala Chandran. 2010. "Kaposi's Sarcoma Associated Herpes Virus (KSHV) Induced COX-2: A Key Factor in Latency, Inflammation, Angiogenesis, Cell Survival and Invasion." Edited by Jay A. Nelson. *PLoS Pathogens* 6 (2): e1000777. https://doi.org/10.1371/journal.ppat.1000777.

Sheth, Ujwal, and Roy Parker. 2003. "Decapping and Decay of Messenger RNA Occur in Cytoplasmic Processing Bodies." *Science* 300 (5620): 805–8. https://doi.org/10.1126/science.1082320.

Shi, Jianjian, Xiangbing Wu, Michelle Surma, Sasidhar Vemula, Lumin Zhang, Yu Yang, Reuben Kapur, and Lei Wei. 2013. "Distinct Roles for ROCK1 and ROCK2 in the Regulation of Cell Detachment." *Cell Death and Disease* 4 (2): e483. https://doi.org/10.1038/cddis.2013.10.

Shimomura, Tadanori, Norio Miyamura, Shoji Hata, Ryota Miura, Jun Hirayama, and Hiroshi Nishina. 2014. "The PDZ-Binding Motif of Yes-Associated Protein Is Required for Its Co-Activation of TEAD-Mediated CTGF Transcription and Oncogenic Cell Transforming Activity." *Biochemical and Biophysical Research Communications* 443 (3): 917–23. https://doi.org/10.1016/j.bbrc.2013.12.100.

Sjöblom, B., A. Salmazo, and K. Djinović-Carugo. 2008. "α-Actinin Structure and Regulation." *Cellular and Molecular Life Sciences* 65 (17): 2688–2701. https://doi.org/10.1007/s00018-008-8080-8.

Small, J. Victor, K. Rottner, I. Kaverina, and K. I. Anderson. 1998. "Assembling an Actin Cytoskeleton for Cell Attachment and Movement." *Biochimica et Biophysica Acta - Molecular Cell Research* 1404 (3): 271–81. https://doi.org/10.1016/S0167-4889(98)00080-9.

Song, Qinghe, Beibei Mao, Jinbo Cheng, Yuhao Gao, Ke Jiang, Jun Chen, Zengqiang Yuan, and Songshu Meng. 2015. "YAP Enhances Autophagic Flux to Promote Breast Cancer Cell Survival in Response to Nutrient Deprivation." *PLoS ONE* 10 (3). https://doi.org/10.1371/journal.pone.0120790.

Sotiropoulos, Athanassia, Dziugas Gineitis, John Copeland, and Richard Treisman. 1999. "Signal-Regulated Activation of Serum Response Factor Is Mediated by Changes in Actin Dynamics." *Cell* 98 (2): 159–69. https://doi.org/10.1016/S0092-8674(00)81011-9.

Soulier, J, L Grollet, E Oksenhendler, P Cacoub, D Cazals-Hatem, P Babinet, M F d'Agay, J P Clauvel, M Raphael, and L Degos. 1995. "Kaposi's Sarcoma-Associated Herpesvirus-like DNA Sequences in Multicentric Castleman's Disease." *Blood* 86 (4): 1276–80.

Stalder, Lukas, and Oliver Mühlemann. 2009. "Processing Bodies Are Not Required for Mammalian Nonsense-Mediated MRNA Decay." *Rna* 15 (7): 1265–73. https://doi.org/10.1261/rna.1672509.

Steffens, Alexandra, Benjamin Jaegle, Achim Tresch, Martin Hülskamp, and Marc Jakoby. 2014a. “Processing-Body Movement in Arabidopsis Depends on an Interaction between Myosins and DECAPPING PROTEIN1.” *Plant Physiology* 164 (4): 1879–92. https://doi.org/10.1104/pp.113.233031.

Stoecklin, Georg, and Nancy Kedersha. 2013. “Relationship of GW/P-Bodies with Stress Granules.” In , 768:197–211. https://doi.org/10.1007/978-1-4614-5107-5_12.

Strano, Sabrina, Olimpia Monti, Natalia Pediconi, Alessia Baccarini, Giulia Fontemaggi, Eleonora Lapi, Fiamma Mantovani, et al. 2005. “The Transcriptional Coactivator Yes-Associated Protein Drives P73 Gene-Target Specificity in Response to DNA Damage.” *Molecular Cell* 18 (4): 447–59. https://doi.org/10.1016/j.molcel.2005.04.008.

Sudol, M. 1994. “Yes-Associated Protein (YAP65) Is a Proline-Rich Phosphoprotein That Binds to the SH3 Domain of the Yes Proto-Oncogene Product.” *Oncogene* 9 (8): 2145–52.

Sudol, Marius, Peer Bork, Aaron Einbond, Kumar Kastury, Teresa Druck, Massimo Negrini, Kay Huebner, and David Lehman. 1995. “Characterization of the Mammalian YAP (Yes-Associated Protein) Gene and Its Role in Defining a Novel Protein Module, the WW Domain.” *Journal of Biological Chemistry* 270 (24): 14733–41. https://doi.org/10.1074/jbc.270.24.14733.

Sugimoto, Wataru, Katsuhiko Itoh, Yasumasa Mitsui, Takahiro Ebata, Hideaki Fujita, Hiroaki Hirata, and Keiko Kawauchi. 2018. “Substrate Rigidity-Dependent Positive Feedback Regulation between YAP and ROCK2.” *Cell Adhesion and Migration* 12 (2): 101–8. https://doi.org/10.1080/19336918.2017.1338233.

Takahashi, Shinya, Kyoko Sakurai, Arisa Ebihara, Hiroaki Kajiho, Kota Saito, Kenji Kontani, Hiroshi Nishina, and Toshiaki Katada. 2011. “RhoA Activation Participates in Rearrangement of Processing Bodies and Release of Nucleated AU-Rich MRNAs.” *Nucleic Acids Research* 39 (8): 3446–57. https://doi.org/10.1093/nar/gkq1302.

Tan, John L, Joe Tien, Dana M Pirone, Darren S Gray, Kiran Bhadriraju, and Christopher S Chen. 2003. "Cells Lying on a Bed of Microneedles: An Approach to Isolate Mechanical Force." *Proceedings of the National Academy of Sciences* 100 (4): 1484–89. https://doi.org/10.1073/pnas.0235407100.

Teixeira, Daniela, Ujwal Sheth, Marco a Valencia-Sanchez, Muriel Brengues, and Roy Parker. 2005. "Processing Bodies Require RNA for Assembly and Contain Nontranslating MRNAs." *RNA (New York, N.Y.)* 11 (4): 371–82. https://doi.org/10.1261/rna.7258505.

Tojkander, Sari, Gergana Gateva, and Pekka Lappalainen. 2012. "Actin Stress Fibers - Assembly, Dynamics and Biological Roles." *Journal of Cell Science* 125 (Pt 8): 1855–64. https://doi.org/10.1242/jcs.098087.

Torrino, Stéphanie, François-René Roustan, Lisa Kaminski, Thomas Bertero, Sabrina Pisano, Damien Ambrosetti, Maeva Dufies, et al. 2019. "UBTD1 Is a Mechano-regulator Controlling Cancer Aggressiveness." *EMBO Reports*, e46570. https://doi.org/10.15252/embr.201846570.

Tousoulis, Dimitris, Evangelos Oikonomou, Evangelos K Economou, Filippo Crea, and Juan Carlos Kaski. 2016. "Inflammatory Cytokines in Atherosclerosis : Current Therapeutic Approaches," 1723–35. https://doi.org/10.1093/eurheartj/ehv759.

Treeck, Briana Van, and Roy Parker. 2018. "Emerging Roles for Intermolecular RNA-RNA Interactions in RNP Assemblies." *Cell* 174 (4): 791–802. https://doi.org/10.1016/j.cell.2018.07.023.

Trus, B. L., J. B. Heymann, K. Nealon, N. Cheng, W. W. Newcomb, J. C. Brown, D. H. Kedes, and A. C. Steven. 2002. "Capsid Structure of Kaposi's Sarcoma-Associated Herpesvirus, a Gammaherpesvirus, Compared to Those of an Alphaherpesvirus, Herpes Simplex Virus Type 1, and a Betaherpesvirus, Cytomegalovirus." *Journal of Virology* 75 (6): 2879–90. https://doi.org/10.1128/jvi.75.6.2879-2890.2001.

Uppal, Timsy, Sagarika Banerjee, Zhiguo Sun, Subhash C. Verma, and Erle S. Robertson. 2014. "KSHV LANA—The Master Regulator of KSHV Latency." *Viruses* 6 (12): 4691–4998. https://doi.org/10.3390/v6124961.

Vallenius, Tea. 2013. "Actin Stress Fibre Subtypes in Mesenchymal-Migrating Cells." *Open Biology* 3 (6): 130001. https://doi.org/10.1098/rsob.130001.

Varelas, Xaralabos, Payman Samavarchi-Tehrani, Masahiro Narimatsu, Alexander Weiss, Katie Cockburn, Brett G. Larsen, Janet Rossant, and Jeffrey L. Wrana. 2010. "The Crumbs Complex Couples Cell Density Sensing to Hippo-Dependent Control of the TGF-β-SMAD Pathway." *Developmental Cell* 19 (6): 831–44. https://doi.org/10.1016/j.devcel.2010.11.012.

Vassilev, Alex, Kotaro J. Kaneko, Hongjun Shu, Yingming Zhao, and Melvin L. DePamphilis. 2001. "TEAD/TEF Transcription Factors Utilize the Activation Domain of YAP65, a Src/Yes-Associated Protein Localized in the Cytoplasm." *Genes and Development* 15 (10): 1229–41. https://doi.org/10.1101/gad.888601.

Verma, Deepika, Fanjie Meng, Frederick Sachs, and Susan Z. Hua. 2015. "Flow-Induced Focal Adhesion Remodeling Mediated by Local Cytoskeletal Stresses and Reorganization." *Cell Adhesion and Migration* 9 (6): 432–40. https://doi.org/10.1080/19336918.2015.1089379.

Vindry, Caroline, Aline Marnef, Helen Broomhead, Laure Twyffels, Sevim Ozgur, Georg Stoecklin, Miriam Llorian, et al. 2017. "Dual RNA Processing Roles of Pat1b via Cytoplasmic Lsm1-7 and Nuclear Lsm2-8 Complexes." *Cell Reports* 20 (5): 1187–1200. https://doi.org/10.1016/j.celrep.2017.06.091.

Vogel, Markus, Jörg Franke, Wolfram Frank, and Horst Schroten. 2007. "Flow in the Well: Computational Fluid Dynamics Is Essential in Flow Chamber Construction." *Cytotechnology* 55 (1): 41–54. https://doi.org/10.1007/s10616-007-9101-4.

Vozzi, Federico, Jonica Campolo, Lorena Cozzi, Gianfranco Politano, Stefano Di Carlo, Michela Rial, Claudio Domenici, and Oberdan Parodi. 2018. "Computing of Low Shear Stress-Driven Endothelial Gene Network Involved in Early Stages of Atherosclerotic Process" 2018.

Wada, K.-I., K. Itoga, T. Okano, S. Yonemura, and H. Sasaki. 2011. "Hippo Pathway Regulation by Cell Morphology and Stress Fibers." *Development* 138 (18): 3907–14. https://doi.org/10.1242/dev.070987.

Wakatsuki, T, B Schwab, N Thompson, and EL Elson. 2001. "Effects of Cytochalasin D and Latrunculin B on Mechanical Properties of Cells." *Journal of Cell Science* 114 (5): 1025–36.

Wang, Jing, Tiefang Song, Suiyang Zhou, and Xianchao Kong. 2019. "YAP Promotes the Malignancy of Endometrial Cancer Cells via Regulation of IL-6 and IL-11." *Molecular Medicine* 25 (1): 32. https://doi.org/10.1186/s10020-019-0103-4.

Wang, Libo, Dan Wang, Xiang Zhou, Lijun Wu, and Xue-Long Sun. 2014. "Systematic Investigation of Quinoxaline Derivatization of Sialic Acids and Their Quantitation Applicability Using High Performance Liquid Chromatography." *RSC Adv*. 4 (86): 45797–803. https://doi.org/10.1039/C4RA08930H.

Wang, Xiaohui, Liang Chang, Huanru Wang, Airong Su, and Zhiwei Wu. 2017. "Dcp1a and GW182 Induce Distinct Cellular Aggregates and Have Different Effects on MicroRNA Pathway." *DNA and Cell Biology* 36 (7): 565–70. https://doi.org/10.1089/dna.2017.3633.

Wang, Xiaoli, Yingying Zhang, Tang Feng, Guanyue Su, Jia He, Wenbo Gao, Yang Shen, and Xiaoheng Liu. 2018. "Fluid Shear Stress Promotes Autophagy in Hepatocellular Carcinoma Cells." *International Journal of Biological Sciences* 14 (10): 1277–90. https://doi.org/10.7150/ijbs.27055.

Watanabe, N, T Kato, A Fujita, T Ishizaki, and S Narumiya. 1999. "Cooperation between MDia1 and ROCK in Rho-Induced Actin Reorganization." *Nature Cell Biology* 1 (3): 136–43. https://doi.org/10.1038/11056.

Watanabe, Naoki, Pascal Madaule, Tim Reid, Toshimasa Ishizaki, Go Watanabe, Akira Kakizuka, Yuji Saito, Kazuwa Nakao, Brigitte M. Jockusch, and Shuh Narumiya. 1997. "P140mDia, a Mammalian Homolog of Drosophila Diaphanous, Is a Target Protein for Rho Small GTPase and Is a Ligand for Profilin." *EMBO Journal* 16 (11): 3044–56. https://doi.org/10.1093/emboj/16.11.3044.

Watanabe, Sadanori, Yoshikazu Ando, Shingo Yasuda, Hiroshi Hosoya, Naoki Watanabe, Toshimasa Ishizaki, and Shuh Narumiya. 2008. "MDia2 Induces the Actin Scaffold for the Contractile Ring and Stabilizes Its Position during Cytokinesis in NIH 3T3 Cells." Edited by Fred Chang. *Molecular Biology of the Cell* 19 (5): 2328–38. https://doi.org/10.1091/mbc.e07-10-1086.

Watanabe, Sadanori, Tihana DeZan, Toshimasa Ishizaki, Shingo Yasuda, Hiroshi Kamijo, Daisuke Yamada, Tomohiro Aoki, et al. 2013. "Loss of a Rho-Regulated Actin Nucleator, MDia2, Impairs Cytokinesis during Mouse Fetal Erythropoiesis." *Cell Reports* 5 (4): 926–32. https://doi.org/10.1016/j.celrep.2013.10.021.

Waters, Jennifer C. 2009. "Accuracy and Precision in Quantitative Fluorescence Microscopy." *Journal of Cell Biology* 185 (7): 1135–48. https://doi.org/10.1083/jcb.200903097.

Wilson, Ross C., and Jennifer A. Doudna. 2013. "Molecular Mechanisms of RNA Interference." *Annual Review of Biophysics* 42 (1): 217–39. https://doi.org/10.1146/annurev-biophys-083012-130404.

Wojciak-Stothard, Beata, and Anne J Ridley. 2003. "Shear Stress–Induced Endothelial Cell Polarization Is Mediated by Rho and Rac but Not Cdc42 or PI 3-Kinases." *The Journal of Cell Biology* 161 (2): 429–39. https://doi.org/10.1083/jcb.200210135.

Wolfenson, H., A. Bershadsky, Y. I. Henis, and B. Geiger. 2011. "Actomyosin-Generated Tension Controls the Molecular Kinetics of Focal Adhesions." *Journal of Cell Science* 124 (9): 1425–32. https://doi.org/10.1242/jcs.077388.

Wu, Y.-H., T.-F. Hu, Y.-C. Chen, Y.-N. Tsai, Y.-H. Tsai, C.-C. Cheng, and H.-W. Wang. 2011. "The Manipulation of MiRNA-Gene Regulatory Networks by KSHV Induces Endothelial Cell Motility." *Blood* 118 (10): 2896–2905. https://doi.org/10.1182/blood-2011-01-330589.

Yamana, N., Y. Arakawa, T. Nishino, K. Kurokawa, M. Tanji, R. E. Itoh, J. Monypenny, et al. 2006a. "The Rho-MDia1 Pathway Regulates Cell Polarity and Focal Adhesion Turnover in Migrating Cells through Mobilizing Apc and c-Src." *Molecular and Cellular Biology* 26 (18): 6844–58. https://doi.org/10.1128/mcb.00283-06.

Yan, Lijun, Vladimir Majerciak, Zhi Ming Zheng, and Ke Lan. 2019. "Towards Better Understanding of KSHV Life Cycle: From Transcription and Posttranscriptional Regulations to Pathogenesis." *Virologica Sinica* 34 (2): 135–61. https://doi.org/10.1007/s12250-019-00114-3.

Yang, Changsong, Lubov Czech, Silke Gerboth, Shin Ichiro Kojima, Giorgio Scita, and Tatyana Svitkina. 2007. "Novel Roles of Formin MDia2 in Lamellipodia and Filopodia Formation in Motile Cells." *PLoS Biology* 5 (11): 2624–45. https://doi.org/10.1371/journal.pbio.0050317.

Yang, J, Y Xu, C Zhu, M K Hagan, T Lawley, and M K Offermann. 1994. "Regulation of Adhesion Molecule Expression in Kaposi's Sarcoma Cells." *Journal of Immunology (Baltimore, Md. : 1950)* 152 (1): 361–73. https://doi.org/7504714.

Yang, Zheng, Andrew Jakymiw, Malcolm R Wood, Theophany Eystathioy, Robert L Rubin, Marvin J Fritzler, and Edward K L Chan. 2004. "GW182 Is Critical for the Stability of GW Bodies Expressed during the Cell Cycle and Cell Proliferation." *Journal of Cell Science* 117 (23): 5567–78. https://doi.org/10.1242/jcs.01477.

Yao, Pingbo, Hong Zhao, Wenjuan Mo, and Pingping He. 2015. "Laminar Shear Stress Promotes Vascular Endothelial Cell Autophagy Through Upregulation with Rab4." *DNA and Cell Biology* 35 (3): 118–23. https://doi.org/10.1089/dna.2015.3041.

Yasuda, Shingo, Fabian Oceguera-Yanez, Takayuki Kato, Muneo Okamoto, Shigenobu Yonemura, Yasuhiko Terada, Toshimasa Ishizaki, and Shuh Narumiya. 2004. "Cdc42 and MDia3 Regulate Microtubule Attachment to Kinetochores." *Nature* 428 (6984): 767–71. https://doi.org/10.1038/nature02452.

Ye, Nannan, Deepika Verma, Fanjie Meng, Michael W. Davidson, Kevin Suffoletto, and Susan Z. Hua. 2014. "Direct Observation of α-Actinin Tension and Recruitment at Focal Adhesions during Contact Growth." *Experimental Cell Research* 327 (1): 57–67. https://doi.org/10.1016/j.yexcr.2014.07.026.

Ylänne, Jari, Klaus Scheffzek, Paul Young, and Matti Saraste. 2001. "Crystal Structure of the α-Actinin Rod Reveals an Extensive Torsional Twist." *Structure* 9 (7): 597–604. https://doi.org/10.1016/S0969-2126(01)00619-0.

Yoneda, A., D. Ushakov, H. A.B. Multhaupt, and J. R. Couchman. 2007. "Fibronectin Matrix Assembly Requires Distinct Contributions from Rho Kinases I and -II." *Molecular Biology of the Cell* 18 (1): 66–75. https://doi.org/10.1091/mbc.E06-08-0684.

Yoneda, Atsuko, Hinke a B Multhaupt, and John R. Couchman. 2005. "The Rho Kinases I and II Regulate Different Aspects of Myosin II Activity." *Journal of Cell Biology* 170 (3): 443–53. https://doi.org/10.1083/jcb.200412043.

Yoo, Jaehyuk, Jinjoo Kang, Ha Neul Lee, Berenice Aguilar, Darren Kafka, Sunju Lee, Inho Choi, et al. 2010. "Kaposin-B Enhances the PROX1 MRNA Stability during Lymphatic Reprogramming of Vascular Endothelial Cells by Kaposi's Sarcoma Herpes Virus." *PLoS Pathogens* 6 (8): 37–38. https://doi.org/10.1371/journal.ppat.1001046.

Yu, Fa Xing, Bin Zhao, Nattapon Panupinthu, Jenna L. Jewell, Ian Lian, Lloyd H. Wang, Jiagang Zhao, et al. 2012. "Regulation of the Hippo-YAP Pathway by G-Protein-Coupled Receptor Signaling." *Cell* 150 (4): 780–91. https://doi.org/10.1016/j.cell.2012.06.037.

Yu, Hua, Drew Pardoll, and Richard Jove. 2009. "STATs in Cancer Inflammation and Immunity: A Leading Role for STAT3." *Nature Reviews. Cancer* 9 (11): 798–809. https://doi.org/10.1038/nrc2734.

Yu, Jiang Hong, Wei-Hong Yang, Tod Gulick, Kenneth D Bloch, and Donald B Bloch. 2005. "Ge-1 Is a Central Component of the Mammalian Cytoplasmic MRNA Processing Body." *RNA* 11 (12): 1795–1802. https://doi.org/10.1261/rna.2142405.

Zagurovskaya, M., M. M. Shareef, A. Das, A. Reeves, S. Gupta, M. Sudol, M. T. Bedford, J. Prichard, M. Mohiuddin, and M. M. Ahmed. 2009. "EGR-1 Forms a Complex with YAP-1 and Upregulates Bax Expression in Irradiated Prostate Carcinoma Cells." *Oncogene* 28 (8): 1121–31. https://doi.org/10.1038/onc.2008.461.

Zaidel-bar, Ronen, Guo Zhenhuan, and Chen Luxenburg. 2015. "The Contractome – a Systems View of Actomyosin Contractility in Non-Muscle Cells," 2209–17. https://doi.org/10.1242/jcs.170068.

Zhang, Qian, Fansen Meng, Shasha Chen, Steven W Plouffe, Shiying Wu, Shengduo Liu, Xinran Li, et al. 2017. "Hippo Signalling Governs Cytosolic Nucleic Acid Sensing through YAP / TAZ-Mediated TBK1 Blockade." *Nature Cell Biology* 19 (4): 362–74. https://doi.org/10.1038/ncb3496.

Zhang, Qiong, Xu Han, Jinfeng Chen, Xiaomei Xie, Jiafeng Xu, Yang Zhao, Jie Shen, et al. 2018. "Yes-Associated Protein ( YAP ) and Transcriptional Coactivator with PDZ-Binding Motif ( TAZ ) Mediate Cell Density – Dependent Proinflammatory Responses." *Journal of Biological Chemistry* 293 (47): 18071–85. https://doi.org/10.1074/jbc.RA118.004251.

Zhao, B., L. Li, Q. Lu, L. H. Wang, C.-Y. Liu, Q. Lei, and K.-L. Guan. 2011. "Angiomotin Is a Novel Hippo Pathway Component That Inhibits YAP Oncoprotein." *Genes & Development* 25 (1): 51–63. https://doi.org/10.1101/gad.2000111.

Zhao, Bin, Li Li, Lloyd Wang, Cun Yu Wang, Jindan Yu, and Kun Liang Guan. 2012. "Cell Detachment Activates the Hippo Pathway via Cytoskeleton Reorganization to Induce Anoikis." *Genes and Development* 26 (1): 54–68. https://doi.org/10.1101/gad.173435.111.

Zhao, Bin, Xin Ye, Jindan Yu, Li Li, Weiquan Li, Siming Li, Jianjun Yu, et al. 2008. "TEAD Mediates YAP-Dependent Gene Induction and Growth Control." *Genes and Development* 22 (14): 1962–71. https://doi.org/10.1101/gad.1664408.

Zhao, Bin, Bin Zhao, Xiaomu Wei, Xiaomu Wei, Weiquan Li, Weiquan Li, Ryan S Udan, et al. 2007. "Inactivation of YAP Oncoprotein by the Hippo Pathway Is Involved in Cell Contact Inhibition and Tissue Growth Control." *Genes and Development* 21: 2747–61. https://doi.org/10.1101/gad.1602907.Hpo/Sav.

Zhou, Jing, Yi-Shuan Li, and Shu Chien. 2014. "Shear Stress–Initiated Signaling and Its Regulation of Endothelial Function." *Arteriosclerosis, Thrombosis, and Vascular Biology* 34 (10): 2191–98. https://doi.org/10.1161/ATVBAHA.114.303422.

Zhou, Tian yi, Yu lu Zhou, Mei jia Qian, Yi zheng Fang, Song Ye, Wen xiu Xin, Xiao chun Yang, and Hong hai Wu. 2018. "Interleukin-6 Induced by YAP in Hepatocellular Carcinoma Cells Recruits Tumor-Associated Macrophages." *Journal of Pharmacological Sciences* 138 (2): 89–95. https://doi.org/10.1016/j.jphs.2018.07.013.

Zhou, Yuhang, Tingting Huang, Jinglin Zhang, Alfred S.L. Cheng, Jun Yu, Wei Kang, and Ka Fai To. 2018. “Emerging Roles of Hippo Signaling in Inflammation and YAP-Driven Tumor Immunity.” *Cancer Letters* 426 (July): 73–79. https://doi.org/10.1016/j.canlet.2018.04.004.

## APPENDIX A: Template R Code for CellProfiler Output Analysis

```
#set up packages that are needed
library("tidyverse")
library("pracma")
library("plyr")
library("reshape")
library("MASS")
library("ggplot2")
#set the working directory
setwd(...)
#import files to read
dfcytoplasm = read.csv("FileName_Cytoplasm.csv", header = T)
dfnuclei = read.csv("FileName_Nuclei.csv", header = T)
dfnames = read.csv("FileName_Image.csv", header = T)
dfPBs = read.csv("FileName_P_Bodies.csv", header = T)
dfcells = read.csv("FileName_Cells.csv", header = T)
#set up dataframes needed for analysis
subsetdfcytoplasm = subset(dfcytoplasm, select= c("ImageNumber"
                                                  , "ObjectNumber"
                                                  ,
"Children_P_Bodies_Count"
                                                  , "Parent_Nuclei"))
subsetdfcells = subset(dfcells, select = c("ImageNumber",
                                           "ObjectNumber",
"Children_Cytoplasm_Count"))
subsetdfnuclei = subset(dfnuclei, select = c("ImageNumber",
                                             "ObjectNumber",
                                             "Children_Cytoplasm_Count"))
subsetdfnames = subset(dfnames, select = c("ImageNumber",
                                           "Count_Cells",
                                           "FileName_Dapi",
                                           "Count_P_Bodies"))
subsetdfPBsize = subset(dfPBs, select= c("ImageNumber"
                                         , "ObjectNumber"
                                         , "Parent_Nuclei"
                                         , "AreaShape_Area"
                                         , "AreaShape_MeanRadius"
                                         ,
"Intensity_IntegratedIntensity_CytoplasmicFoci"))
subsetdfNloc = subset(dfnuclei, select = c("ImageNumber",
                                           "ObjectNumber",
                                           "Children_Cytoplasm_Count",
                                           "Location_Center_X",
                                           "Location_Center_Y"))
subsetdfPBloc = subset(dfPBs, select = c("ImageNumber",
                                         "ObjectNumber",
                                         "Location_Center_X",
                                         "Location_Center_Y"
                                         , "Parent_Cytoplasm"))
#rename certain columns so dataframes can join and stay distinguished in
one data set
subsetdfNloc = plyr::rename(subsetdfNloc, c("ObjectNumber" =
"Parent_Cytoplasm"
"Nuclei_Center_X"
"Nuclei_Center_Y"))
, "Location_Center_X" =
```

```
, "Location_Center_Y" =
subsetdfPBloc = plyr::rename(subsetdfPBloc, c("ObjectNumber" =
"PBnumber"
                                    , "Location_Center_X" = "PB_Center_X"
                                   , "Location_Center_Y" = "PB_Center_Y"))
#count number of cells in each treatment
##note: the X,Y is the coordinates of the characters that distinguish
the treatments in the filename
subsetdfnames$filefactor = substr(subsetdfnames$FileName_Dapi, X, Y)
sumTX_1 = sum(subsetdfnames$Count_Cells[subsetdfnames$filefactor ==
"TX_1"])
sumTX_2 = sum(subsetdfnames$Count_Cells[subsetdfnames$filefactor ==
"TX_2"])
sumTX_3 = sum(subsetdfnames$Count_Cells[subsetdfnames$filefactor ==
"TX_3"])
sumTX_4 = sum(subsetdfnames$Count_Cells[subsetdfnames$filefactor ==
"TX_4"])
sumTX_5 = sum(subsetdfnames$Count_Cells[subsetdfnames$filefactor ==
"TX_5"])
sumTX_6 = sum(subsetdfnames$Count_Cells[subsetdfnames$filefactor ==
"TX_6"])
#add treatment labels to the dataframes
subsetdfcytoplasm$Treatment <- rep(c("TX_1","TX_2","TX_3",
                                     "TX_4","TX_5",  "TX_6"),
                                   times = c(sumTX_1,
                                             sumTX_2,
                                             sumTX_3,
                                             sumTX_4,
                                             sumTX_5,
                                             sumTX_6))

subsetdfnuclei$Treatment <- rep(c("TX_1","TX_2","TX_3",
                                  "TX_4","TX_5",  "TX_6"),
                                times = c(sumTX_1,
                                          sumTX_2,
                                          sumTX_3,
                                          sumTX_4,
                                          sumTX_5,
                                          sumTX_6))

subsetdfNloc$Treatment <- rep(c("TX_1","TX_2","TX_3",
                                "TX_4","TX_5",  "TX_6"),
                              times = c(sumTX_1,
                                        sumTX_2,
                                        sumTX_3,
                                        sumTX_4,
                                        sumTX_5,


sumTX_6))

#count number of processing bodies in each treatment
sumTX_1PBs = sum(subsetdfnames$Count_P_Bodies[subsetdfnames$filefactor
== "TX_1"])
sumTX_2PBs = sum(subsetdfnames$Count_P_Bodies[subsetdfnames$filefactor
== "TX_2"])
sumTX_3PBs = sum(subsetdfnames$Count_P_Bodies[subsetdfnames$filefactor
== "TX_3"])
sumTX_4PBs = sum(subsetdfnames$Count_P_Bodies[subsetdfnames$filefactor
```

```
== "TX_4"])
sumTX_5PBs = sum(subsetdfnames$Count_P_Bodies[subsetdfnames$filefactor
== "TX_5"])
sumTX_6PBs = sum(subsetdfnames$Count_P_Bodies[subsetdfnames$filefactor
== "TX_6"])
#add treatment labels to the processing body dataframes
subsetdfPBsize$Treatment <-rep(c("TX_1","TX_2", "TX_3",
###calculate PB count per cell
dfmeanPBcount <-
  aggregate(
  formula = Children_P_Bodies_Count ~ Treatment
  , data = subsetdfcytoplasm
  , FUN = mean

)

  "TX_4","TX_5", "TX_6"),
times = c(sumTX_1PBs,
          sumTX_2PBs,
          sumTX_3PBs,
          sumTX_4PBs,
          sumTX_5PBs,
          sumTX_6PBs))
write.csv(dfmeanPBcount, file = "FileName_dfmeanPBcount.csv")
###calculate PB count per cell without cells with counts = 0
subsetdfcytoplasm %>%
  dplyr::filter(Children_P_Bodies_Count > 0) %>%
  group_by(Treatment) %>%
  dplyr::summarise(x = mean(Children_P_Bodies_Count)) ->
dfmeanPBcountwithout0
write.csv(dfmeanPBcountwithout0, file =
"FileName_dfmeanPBcountwithout0.csv")
##calculate the percent of cells with PBs
detach(package:plyr)
percentcellswithPBs = subsetdfcytoplasm %>%
  group_by(Treatment) %>%
    summarise (mean(Children_P_Bodies_Count > 0))
library(plyr)
write.csv(percentcellswithPBs, file =
"FileName_percentcellswithPBs.csv")
###calculate the PB distance from the nucleus
#join the nuclear localization dataframe with the PB localization
dataframe
subsetNPBdist <- join(subsetdfNloc, subsetdfPBloc)
#calculate the distance in the X and Y positions from the parent nucleus
subsetNPBdistcalc = subset (transform(subsetNPBdist
                                      , "diff_x" =
abs(subsetNPBdist$Nuclei_Center_X - subsetNPBdist$PB_Center_X)
                                      , "diff_y" =
abs(subsetNPBdist$Nuclei_Center_Y - subsetNPBdist$PB_Center_Y))
                            , select = c(diff_x, diff_y))
#add the treatment labels to the NPB distance dataframe
sumTX_1 = sum(subsetNPBdist$Treatment == "TX_1")
sumTX_2 = sum(subsetNPBdist$Treatment == "TX_2")
sumTX_3 = sum(subsetNPBdist$Treatment == "TX_3")
sumTX_4 = sum(subsetNPBdist$Treatment == "TX_4")
sumTX_5 = sum(subsetNPBdist$Treatment == "TX_5")
sumTX_6 = sum(subsetNPBdist$Treatment == "TX_6")
```

```
subsetNPBdistcalc$Treatment <-rep(c("TX_1","TX_2", "TX_3","TX_4","TX_5",
"TX_6"),
                                  times = c(sumTX_1nuc,
                                            sumTX_2nuc,
                                            sumTX_3nuc,
                                            sumTX_4nuc,
                                            sumTX_5nuc,
                                            sumTX_6nuc))
#get rid of the cells without PBs by getting rid of the NAs
subsetNPBdistcalc = na.omit(subsetNPBdistcalc)
#calculate the hypotenuse distance from the X and Y distances
subsetNPBdistcalc$dist_tot = hypot(subsetNPBdistcalc$diff_x,
subsetNPBdistcalc$diff_y)
#multiply the calculated pixel distance by the distance value per pixel
subsetNPBdistcalc$dist_totum = subsetNPBdistcalc$dist_tot*0.21
#get the average distance from the nucleus per treatment
dfmeanNPBdist <-
  aggregate(
    formula = dist_totum ~ Treatment
    , data = subsetNPBdistcalc
    , FUN = mean
  )
write.csv(dfmeanNPBdist, file = "FileName_dfmeanNPBdist.csv")
##calculate the average PB intensity as a measure of size
dfmeanPBintensity =
  aggregate(
    formula = Intensity_IntegratedIntensity_CytoplasmicFoci ~ Treatment
    , data = subsetdfPBsize
    , FUN = mean
  )
write.csv(dfmeanPBintensity, file = "FileName_dfmeanPBintensity.csv")
##statistics on the PB counts per cell
#negative binomial model
summary(NB <-
          glm.nb(Children_P_Bodies_Count ~ Treatment
                 , data = subsetdfcytoplasm
                 , init.theta = 0.95))
pred = predict(NB, se.fit = T)
fits = unique(pred$fit)
ses = unique(pred$se.fit)
to_plot1 = data.frame(fits = fits, ses = ses)
to_plot1$upper = to_plot1$fits + to_plot1$ses*1.96
to_plot1$lower = to_plot1$fits - to_plot1$ses *1.96
#neg binom is in log space - exponenciate
to_plot1$expU = exp(to_plot1$upper)
to_plot1$expL = exp(to_plot1$lower)
to_plot1$expF = exp(to_plot1$fits)
#add labels to the statistics file
to_plot1$Treatment = c("TX_1","TX_2","TX_3",
                       "TX_4","TX_5", "TX_6")
write.csv(to_plot1, file = "FileName_to_plot1.csv")
#base graphing code to check
ggplot()+
  geom_bar(aes(Treatment, expF),
           data = to_plot1,
           stat = "identity"
  )+
  geom_errorbar(data = to_plot1
```

```
              , aes(x=Treatment, ymin = expL, ymax = expU)
              , width = .5
)+
xlab("")+
ylab("Hedls Puncta per Cell")+
scale_color_grey()+
theme_classic()+
theme(text=element_text(size=25),
      legend.position = "none",
      axis.text.x = element_text(angle = 90, hjust = 1),
      panel.grid.major.y = element_line(color = "grey", size=0.2),
      panel.grid.minor = element_line(color = "grey", size=0.2))
```

**APPENDIX B: The role of MyoVa in PB disassembly is inconclusive**

**Introduction**: Myosin Va (MyoVa) is an actin cargo transport protein that is associated with PBs (Lindsay and McCaffrey 2011). Lindsay and McCaffrey (2011) showed that MyoVa colocalized with several PB components and actin, and could interact with PB-resident protein eIF4E. Further, knockdown of MyoVa disassembled PBs (Lindsay and McCaffrey 2011). Thus, MyoVa likely acts as the linker between actin and PBs.

**Results**: Since the relationship between PBs and actin was being examined, I investigated whether there were any changes in MyoVa in KapB-expressing cells. Lysates from HUVECs transduced with KapB-expressing lentivirus or vector were immunoblotted for MyoVa. MyoVa levels decreased in KapB-expressing cells (Figure A1). To examine if MyoVa contributed KapB-mediated PB disassembly in HUVECs, shRNAs were designed to MyoVa and a reduction in MyoVa protein levels was verified by immunoblot (Figure A2 (A)). Despite similar knockdown efficacies, the impact of each shRNA on PB disassembly was inconsistent. One shRNA (shMYOVA-1) had no effect on PB levels in vector and KapB-expressing cells (Figure A2 (B, C)). The other shRNA increased PB levels in both vector and KapB conditions (Figure A2, (B, C)).

**Discussion:** The KapB-specific decrease in MyoVa levels suggests that MyoVa is being degraded in KapB-expressing cells. Since data from the lab indicates that autophagy is mediating PB degradation (Robinson, Singh, and Corcoran, unpublished), it may be that autophagy is mediating the degradation of MyoVa. Notably, the *Aradopsis* homologue of MyoVa, Myo2P interacts with DCP1, the homologue for DCP1a (Steffens et al. 2014b). DCP1a is one of the PB proteins that is degraded in KapB-expressing cells (Robinson, Singh, and Corcoran, unpublished), suggesting the association between the proteins may promote degradation of both components. It is unclear whether degradation of MyoVa is happening passively with components of the PB, or MyoVa is being selectively targeted.

The role of MyoVa in PB disassembly was inconclusive because of inconsistencies between the behavior of the two shRNAs I used. Neither shRNA decreased Hedls puncta levels, which is inconsistent with a previous study that clearly showed that MyoVa

knockdown decreased PBs (Lindsay and McCaffrey 2011). This may be due to inconsistencies between cell type, as they used HeLa cells. In my project, HeLas do not always display PB phenotypes that are congruent with HUVECs. If PB levels do not change with MyoVa knockdown, as seen with shMYOVA-1, it suggests that MyoVa does not control PB levels in HUVECs. If MyoVa knockdown increases Hedls puncta, it suggests that MyoVa is somehow involved in mediating PB disassembly, perhaps through directing transport of PBs to the degradation machinery. These results need to be verified using alternate approaches (additional shRNAs, overexpression constructs) to confirm or refute the role of MyoVa as a regulator of PB dynamics, both in vector and KapB-expressing cells.

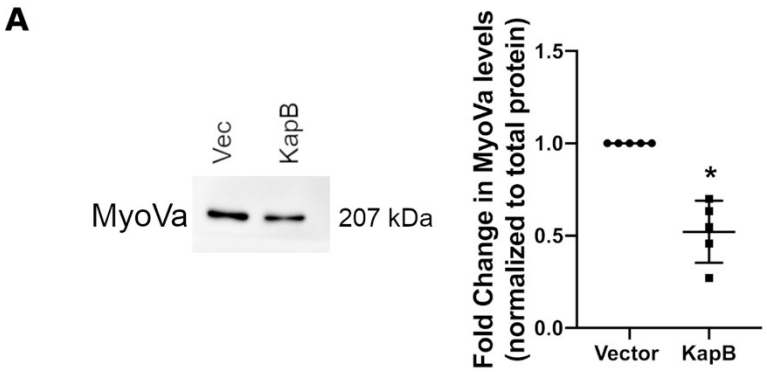


**Figure A1: Myosin Va levels decrease in KapB-expressing cells.** HUVECs were transduced with KapB-expressing and empty vector lentivirus then selected with 5 $\mu$g/mL blasticidin. Cells were lysed for immunoblotting. (A) Representative blot and quantification of lysates immunoblotted using an antibody to MyoVa. MyoVa protein levels in each condition were normalized to total protein (not shown). Error bars represent standard deviation. Statistics were determined using a ratio paired t-test, n=5, $p < 0.05$.

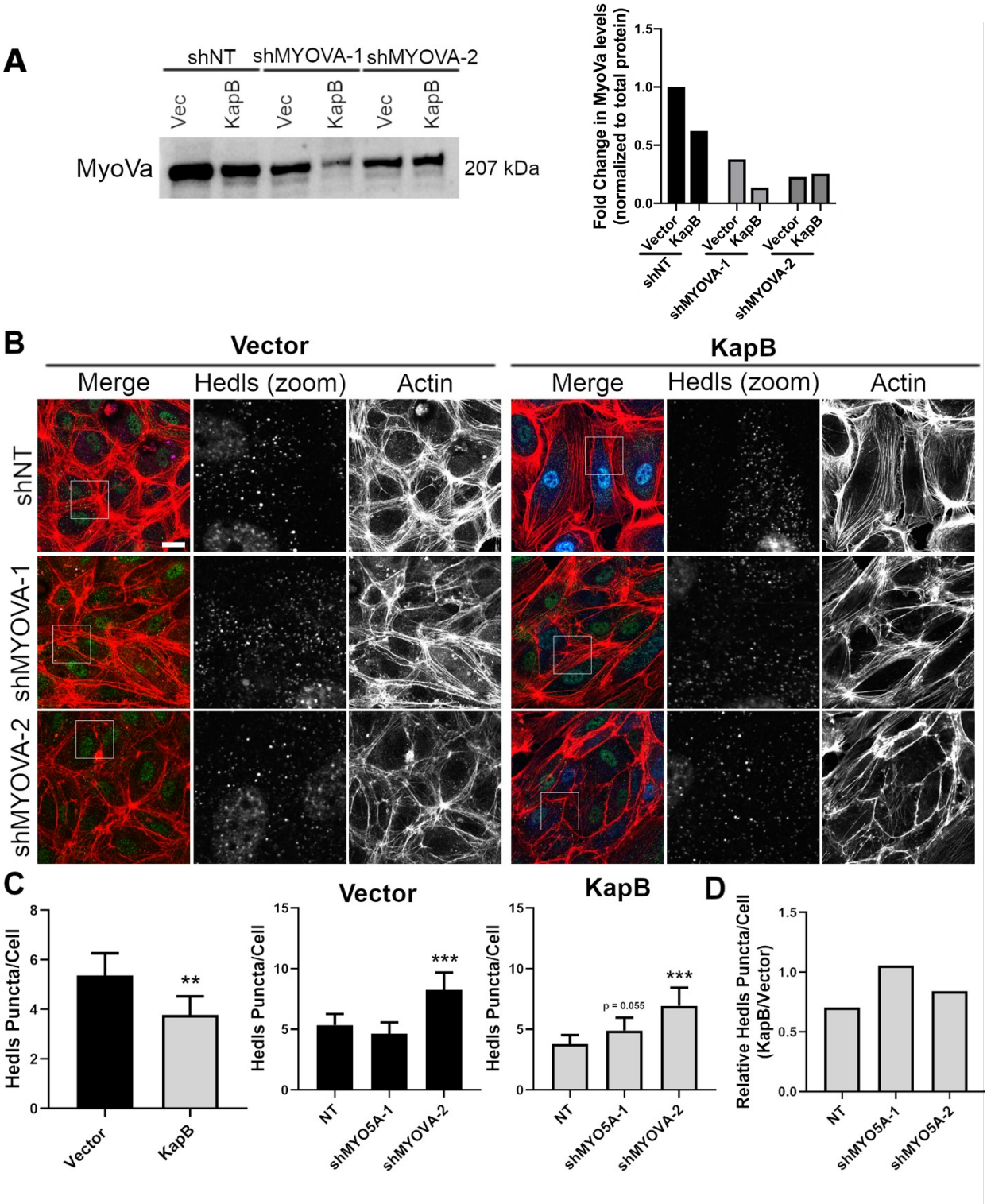


**Figure 3.11: The role of MyoVa in PB disassembly is inconclusive.** HUVECs were transduced with KapB-expressing and empty vector lentivirus and selected with 5 $\mu$g/mL blasticidin. Cells were then transduced with shRNAs targeting MyoVa (shMYOVA-1, shMYOVA-2) or with a non-targeting (shNT) control and selected with 1 $\mu$g/mL puromycin. Cells were lysed for immunoblotting of fixed for immunofluorescence. (A) Representative blot and quantification of lysates immunoblotted using an antibody to

MyoVa. MyoVa protein levels in each condition were normalized to total protein (not shown). (B) Representative images of cells stained for PB-resident protein Hedls (green), KapB (blue), and F-actin (red, phalloidin). Boxes indicate images shown in Hedls (zoom) panel. Scale bar represents 20 $\mu$m. (C, D) Fixed cells were stained for CellProfiler analysis as detailed in the methods. (C) The number of Hedls puncta per cell was quantified and normalized to the vector NT control. (D) CellProfiler data was used to calculate the ratio of Hedls puncta count in KapB-expressing cells versus the vector control for each treatment condition. Error bars represent 95% confidence interval. Statistics were determined using a negative binomial regression, $p < 0.05$. N=1.